Glycerol Acetylation to Triacetin over Solid Acid Catalysts in Liquid and Gas Phase

Dissertation
zur
Erlangung des akademischen Grades
doctor rerum naturalium (Dr. rer. nat.)
der Mathematisch-Naturwissenschaftlichen Fakultät
der Universität Rostock

vorgelegt von
M.Sc. Sumeet S. Kale
geboren am 19.07.1988 in Bhise Wagholi, Indien
Rostock: 30.06.2016

urn:nbn:de:gbv:28-diss2018-0015-0

Name: Sumeet S. Kale

Submission date: 30th June 2016

Defense date: 25th October 2016

Defense place: Hörsaal 001, Institut für Chemie, Universität Rostock

Dissertation title: Glycerol Acetylation to Triacetin over Solid Acid Catalysts in Liquid and Gas Phase

Referees:

1. PD Dr. habil. Andreas Martin
   Leibniz Institute for Catalysis
   University of Rostock
   Albert Einstein Str. 29a
   18059, Rostock
   Germany

2. Prof. Dr. Erhard Kemnitz
   Institut für Chemie
   Humboldt-Universität zu Berlin
   Brook-Taylor-Str. 2
   12489 Berlin-Adlershof
   Germany

Dedicated to my entire family

Declaration

I declare that the work presented in this thesis entitled “Glycerol Acetylation to Triacetin over Solid Acid Catalysts in Liquid and Gas phase” is original and carried out by myself to obtain the doctoral degree at Leibniz Institute for Catalysis e.V., Rostock, Germany, under the guidance of my supervisors PD Dr. habil. Andreas Martin (Head of Department of Heterogeneous Catalytic Processes) and Dr.-Ing. Udo Armbruster (Group leader). I further declare that this thesis has not been submitted, either wholly or in part, to any academic institutions for the award of any other degree or qualifications.

Rostock, 30.06.2016
Sumeet S. Kale

Acknowledgment

It has been my privilege to meet and work with a lot of nice and talented people over the course of my PhD studies at Leibniz Institute for Catalysis at the University of Rostock (LIKAT Rostock), Germany. It is my great pleasure to present the doctoral thesis on "**Glycerol Acetylation to Triacetin over Solid Acid Catalysts in Liquid and Gas phase**". I would like to acknowledge a number of people for their support during the research work for this thesis.

With great pleasure, I would like to express my deep sense of gratitude and appreciation to my supervisor, **PD Dr. habil. Andreas Martin**, for giving me an opportunity to work on this challenging topic and supported me throughout my doctoral work with his valuable suggestion, discussions, continued encouragement and inspiration. Without his guidance, motivation and immense knowledge in catalysis, this PhD work would not have been successful.

I am extremely grateful to my co-supervisor, **Dr.-Ing. Udo Armbruster**, for his outstanding help and logical discussions time to time in a friendly manner. I am greatly indebted for his patience with my flaws and believing in me and encouraging me throughout this work. His wide knowledge and personal experience added great strength to this dissertation.

My sincere thanks to **Dr. Shubhangi B. Umbarkar** (NCL, Pune) her wide knowledge and logical suggestions have provided a strong support for the present thesis. Her accurate and critical review of my work kept me on the right track. I am thankful to her for guiding me and teaching the research skills.

My special thanks to **Dr. Mohan K. Dongare** (NCL and Möjj Eng. Syst. Ltd., Pune), I deeply respect his persistent and meticulous attitude. His constant support, guidance and mentoring helped me overcome many hurdles throughout my PhD research. I am grateful for his outstanding assistance and scientific discussions.

I would like to thank, Prof. Dr. Matthias Beller (Director LIKAT) for allowing me to work in a reputed institute like LIKAT. Special thanks to my colleagues in "Heterogeneous Catalytic Processes" Department for unconditional help during my stay in LIKAT. I also would like to thanks Dr. Michael Bartoszek and Mr. Reinhard Eckelt for their help to solve the problem with experimental set-up. It is my pleasure to thank, Dr. Hanan Atia for her ready assistance and wonderful support whenever required. Her firm but gentle guidance and incredibly valuable advice helped me to achieve my goals.

Besides, within LIKAT, I would like to express my sincere thanks to Hoan, Thuan, Anna, Katharina, Diego, Markus, Amely, Andre, Quan, Christin, Daniel for sharing their views and experiences not only in research but also in cultural and social life. In addition many thanks to the Analytical staff members of LIKAT, Dr. U. Bentrup, M. Schneider, Dr. M.–M. Pohl, Dr. J.

Radnik, Mrs. Lehmann, Ms. A. Simmula for their help in the characterization of samples and detailed discussion.

I also would like to express my gratitude to all friends in Rostock who made my stay more enjoyable. I am grateful to all friends, Rahul, Jeet, Nitesh, Raymond, Prasanna, Shoubhik, Piyali, Vijay Anna, Praveen, Chandru, Bhushan, and Krish for stimulating discussions, countless parties and playing cricket at our beloved ground. I also thank my friends back home in NCL Pune, Dr. Trupti, Dr. Vaibhav, Dr. Vidhya, Dr. Swati, Dr. Samadhan, Rajesh, and Atul for their unconditional help which developed my research skills. I also acknowledge my friends from Fergusson College, Pune and S. P. College, Pune, who were just a “phone call away” at any time for their continuous support, understanding, encouragement and an immense help. I cannot list all names here, but you are always in mind.

Finally, I am especially grateful to parents and my family members for their love, encouragement and incredible support spiritually throughout my study and my life in general. They taught me to balance work and personal life together.

Sumeet S. Kale

Abstract

Glycerol is inevitably produced by 10 wt% in total biodiesel production which resulted in large surplus of low-grade glycerol in the market. Therefore, intensive efforts are undertaken to valorize raw glycerol to chemical intermediates, mostly using catalytic processes, such as hydrogenolysis, dehydration, oligomerization and oxidation. Glycerol esterification with acetic acid (acetylation) is one of processes to get useful chemicals such as glycerol monoacetate (MAG) and diacetate (DAG) that have applications in cryogenics and polymers, as well as glycerol triacetate (TAG), widely used in food industries as humectant and also act as cold flow improver and viscosity reducer for biodiesel. Glycerol acetylation is generally performed in batch operation using homogenous catalysts like sulfuric acid and p-toluene sulfonic acid, but also heterogeneous solid acid catalysts such as sulfated mesoporous silica, supported heteropolyacids, or acidic ion exchange resins like Amberlyst-15. However, the solid catalysts get deactivated due to leaching of active species. The single-stage transformation of glycerol with high triacetin selectivity is impossible, as the reaction comprises a series of consecutive esterification steps forming various intermediates, and each of them is controlled by chemical equilibrium due to the formation of water as an unavoidable by-product.

In the present work, a modified Dean-Stark apparatus and toluene as an entrainer were used to remove the water formed in the reaction via azeotropic distillation and to shift the reaction equilibrium towards the product side. Several organic ion exchange resins like Amberlyst-15 (A15) and Amberlyst-70 (A70) and inorganic materials like silica, silica-alumina and alumina-supported heteropolyacids (STA = silicotungstic acid, TPA = tungstophosphoric acid, PMA = phosphomolybdic acid) were used as catalysts. The catalysts were intensively characterized by various techniques (BET, XRD, Py-IR and others). The activity test revealed that organic catalysts A70 and A15 as well as supported inorganic catalysts STA/SiO_2 and TPA/SiO_2 showed significantly higher glycerol conversion and selectivity to TAG compared to other supported catalysts. The maximum selectivity to TAG was more than 94% with both A15 and A70 catalysts after 24 h. The inorganic STA/SiO_2 and TPA/SiO_2 catalysts showed 71.4% and 67.4% selectivity to TAG, respectively, after 24 h. The high activity of the A15 and A70 catalysts is strongly related to the specific acidity, in particular, Brønsted acidic sites, and thermal stability of the catalysts. Regarding inorganic catalysts, the activity correlated with the acidity which in turn depends on the stabilization of the respective heteropolyacid (Keggin structure).

In addition, glycerol acetylation was also performed in continuous gas phase operation as it has several advantages, especially large-scale production and application in industry. Some

selected supported heteropolyacid catalysts (like STA/SiO_2, STA/Al_2O_3 and blank support Al_2O_3) from batch operation were evaluated in continuous fixed bed quartz reactor in the temperature range of 225-325 °C using an acetic acid: glycerol feed (molar ratio 6: 1). The selected catalysts exhibited excellent activity, however, selectivity to the desired TAG was rather low (<16%). On the other hand, high selectivity to acrolein was observed (80-84%) at 325 °C at a complete conversion of glycerol. These observed catalytic results can be strongly correlated with the acidity of the catalysts. Thus, another series of low acidic SiO_2-based mixed metal oxide (SiM30 where M = TiO_2, MgO, ZrO_2, SrO and Sc_2O_3) catalysts were prepared by the sol-gel method in a molar ratio of 30:1 and tested in gas phase glycerol acetylation. Furthermore, other SiO_2-TiO_2 composites such as Ti-SiO_2 and Ti-SBA-15 (prepared by the impregnation method) and Ti-MCM-41 (prepared by sol-gel method) catalysts were also evaluated in gas phase glycerol acetylation. The prepared catalysts were characterized by several physico-chemical techniques (BET, XRD, Py-FTIR, UV-vis, ATR-IR, TEM-EDX and XPS) in order to derive structure-activity relationship. All catalysts (except blank SiO_2 support) showed excellent activity (~100% glycerol conversion) at 325 °C, but related product distribution showed remarkable differences. Among the prepared catalysts, SiO_2-TiO_2 composites (SiTi30, Ti-SiO_2, Ti-SBA-15 and Ti-MCM-41) exhibited more than 39% selectivity to desired TAG at $\leq$300 °C, whereas the other catalysts were either less selective towards TAG or selective towards undesired acrolein. In addition, the influence of space velocity and molar ratio of acetic acid to glycerol were investigated. At a high molar ratio of acetic acid to glycerol (9/1), the selectivity to TAG increased to 59% at complete conversion of glycerol at 300 °C. The SiTi30 catalyst was also stable in a long-term stability test up to 200 h with a certain decrease in TAG selectivity (from 32% to 10%). However, after regeneration (600 °C for 5 h in air) the activity and TAG selectivity dropped to 95% and 7%, respectively. The Ti-MCM-41 catalyst was evaluated in a long-term stability test at 275 °C and it showed high activity and selectivity to TAG (42%) for the first hour but then it started to deactivate rapidly mainly due to deposition of carbonaceous compounds. Regeneration at 500 °C in air could restore the same activity and selectivity, but the catalyst deactivated rapidly following the same conversion and selectivity pattern. The characterization results revealed that the high catalytic activity of SiO_2-TiO_2 composites (SiTi30, Ti-SiO_2, Ti-SBA-15 and Ti-MCM-41) should be related to the formation of Si-O-Ti bonds within the silica matrix. Among the prepared catalysts, SiTi30 produced the best yield of TAG (average 20% in 200 h) at 300 °C using a 6: 1 molar ratio of acetic acid to glycerol at 2.73 h^{-1} WHSV.

Zusammenfassung

Bei der Biodieselproduktion fällt Glycerin als Koppelprodukt mit 10 Ma-% Anteil an. Aufgrund des starken Wachstums der Biodieselproduktion steigt der Überschuß an weniger reinem Glycerin ständig an. Deshalb gibt es intensive Bemühungen, dieses Rohglycerin chemisch zu verwerten, meistens durch katalytische Prozesse, wie z.B. Dehydratisierung, Hydrogenolyse, Oxydation, Acetylierung oder Veretherung. Die Veresterung von Glycerin mit Essigsäure (Acetylierung) führt zu hochwertigen Produkten wie Glycerinmonoacetat (Monoacetin, MAG) und Glycerindiacetat (Diacetin, DAG), mit Anwendungen im Bereich Kältetechnik und Polymerchemie, und zu Glycerintriacetat (Triacetin, TAG), das vielfältige Anwendungen als Feuchthaltemittel hat und als Biodieselzusatz zur Verringerung der Viskosität verwendbar ist. Die Acetylierung von Glycerin mit Essigsäure erfolgt generell in Batchreaktoren mit homogenen Katalysatoren, wie z.B. Schwefelsäure oder p-Toluensulfonsäure, oder mit heterogenen Katalysatoren, wie z.B. sulfatiertem mesoporösem SiO_2, geträgerten Heteropolysäuren oder sauren Ionenaustauscherharzen. Problematisch ist der Aktivitätsverlust der festen Katalysatoren durch Leaching. In einer einfachen Batch-Reaktion ist es unmöglich, hohe Triacetin-Selektivitäten zu erreichen, da die Gesamtreaktion aus einer Reihe von Folgereaktionen besteht, deren jeweilige Gleichgewichte durch das in der Veresterung gebildete Reaktionswasser ungünstig liegen.

In der vorliegenden Arbeit wird mit einem modifizierten Dean-Stark-Wasserabscheider und Toluen das gebildete Reaktionswasser azeotrop entfernt und somit das chemische Gleichgewicht in Richtung TAG verschoben. Verschiedene organische Ionenaustauscherharze, wie Amberlyst-15 (A15) und Amberlyst-70 (A70), und anorganische Materialien, wie Silica, Silica-Alumina und geträgerte Heteropolysäuren (STA=Wolframatokieselsäure, TPA=Molybdatokieselsäure und PMA=Molybdato-phosphorsäure) wurden als Katalysatoren eingesetzt. Diese wurden mit verschiedenen Methoden (wie BET, XRD, Py-IR und anderen) charakterisiert. A70, A15, STA/SiO_2 und TPA/SiO_2 zeigten von allen Katalysatoren die höchsten Glycerinumsätze und TAG-Selektivitäten. Mit A15 und A70 ließ sich nach 24 h eine maximale TAG-Selektivität von 94 % erreichen, mit STA/SiO_2 und TPA/SiO_2 wurden Selektivitäten von 71,4% bzw. 67,4% erzielt. Die hohe Aktivität der Ionenaustauscherharze ist verbunden mit ihrer hohen spezifischen Acidität, insbesondere der Brønsted-Acidität, und mit ihrer thermischen Stabilität. Die Aktivität der anorganischen Katalysatoren korreliert mit der Acidität, die von der Stabilisierung der Heteropolysäure (Keggin-Struktur) abhängt.

Weiterhin wurde die Acetylierung von Glycerin auch kontinuierlich in der Gasphase durchgeführt. Ein solches Verfahren wäre insbesondere vorteilhaft für eine industrielle Produktion. Ausgewählte Katalysatoren von den Flüssigphasenexperimenten, wie STA/SiO_2, STA/Al_2O_3 und Al_2O_3, wurden in einem Quarz-Reaktor im Temperaturbereich 225-325°C mit einem Essigsäure/Glycerin-Gemisch (molares Verhältnis=6:1) getestet. Die Katalysatoren zeigten eine exzellente Aktivität. Die erreichbare Selektivität für TAG war niedrig (<16 %), aber bei 325 °C werden 80-84 % Selektivität für Acrolein bei vollem Glycerinumsatz gefunden, was mit der starken Acidität der Katalysatoren korreliert. Eine Reihe von schwach aciden SiO_2-MOx-Katalysatoren (MOx = TiO_2, MgO, ZrO_2, SrO und Sc_2O_3) wurde auf einer Sol-Gel-basierten Methode mit einem molaren Verhältnis von 30:1 hergestellt und getestet. Weiterhin wurden Ti-SiO_2 und Ti-SBA-15 Katalysatoren durch Tränkung und Ti-MCM41 durch einen Sol-Gel-Prozess hergestellt und in der Gasphasenacetylierung unter identischen Bedingungen evaluiert. Die Charakterisierung erfolgte durch verschiedene Methoden (BET, XRD, Py-IR, UV-vis, ATR-IR, TEM-EDX und XPS) um Struktur-Aktivitäts/Selektivitäts-Beziehungen abzuleiten. Alle Katalysatoren außer SiO_2 erreichten bei 325 °C vergleichbar hohe Glycerinumsätze von nahezu 100%. Die jeweilige Produktzusammensetzung unterschied sich jedoch signifikant. SiTi30, Ti-SiO_2, Ti-MCM41 und Ti-SBA-15 zeigten Selektivitäten für TAG von mehr als 39% bei 300°C, während die anderen Katalysatoren weniger TAG und mehr Acrolein lieferten. Der Einfluß von Verweilzeit und molarem Essigsäure/Glycerin-Verhältnis auf die Selektivität wurde untersucht. Bei einem Verhältnis von 9:1 wurde an SiTi30 bei 300°C eine TAG-Selektivität von 59% bei vollem Glycerinumsatz erreicht. Der gleiche Katalysator war stabil in einem 200 h-Test. Die TAG-Selektivität fiel von 32% auf 10%. Nach Regenerierung mit Luft bei 600°C wurden ein Glycerinumsatz von 95% und eine TAG-Selektivität von 7% erreicht. Der Ti-MCM-41-Katalysator wurde bei 275°C einem Stabilitätstest unterzogen und erreichte am Anfang hohe Aktivität und Selektivität zu TAG (42%). Es erfolgte aber schnelle Desaktivierung durch Ablagerung kohlenstoffhaltiger Verbindungen. Nach Regeneration bei 500°C in Luft wurden die vorherige Aktivität und Selektivität wieder hergestellt. Die Ergebnisse der Charakterisierung zeigen, dass die hohe Aktivität und Selektivität von SiTi30, Ti-SiO_2, Ti-MCM41 und Ti-SBA-15 mit dem Vorhandensein von Si-O-Ti-Bindungen in der SiO_2-Matrix verbunden sind. Von allen Katalysatoren erreichte SiTi30 die beste TAG-Ausbeute (20 Ma-% während 200 h) bei 300°C mit einem molarem Essigsäure/Glycerin-Verhältnis von 6 und bei einer WHSV von 2,73 h^{-1}.

Abbreviations

AA	Acetic acid
AAS	Atomic Absorption Spectroscopy
ATR	Attenuated total reflect
BE	Binding Energy
BET	Brunauer – Emmet – Teller model
BJH	Barret – Joyner – Halenda model
BAS	Brønsted Acid Sites
CHNS	Carbon, Hydrogen, Nitrogen, Sulfur
°C	Degree Celsius
EDX	Energy Dispersive X-ray Spectroscopy
FID	Flame Ionization Detector
FTIR	Fourier transform infrared spectroscopy
GC	Gas Chromatography
GC-MS	Gas Chromatography Mass Spectrometry
HAADF	High Angle Annular Dark Field
ICP-OES	Inductive Coupled Plasma Optical Emission Spectroscopy
py-IR	Infrared Spectroscopy of Adsorbed Pyridine
K	Kelvin
LAS	Lewis Acid Sites
NH3-TPD	Temperature Programmed Desorption of Ammonia
nm	nanometer
RT	Room Temperature
TCD	Thermal Conductivity Detector
TEM	Transmission Electron Microscopy
WHSV	Weight Hourly Space Velocity
XRD	X-ray Diffraction
XPS	X-ray Photoelectron Spectroscopy

Contents

1 Introduction

1.1 The role of biomass in the future energy and chemicals supply

Biomass valorization has become an important field of research to develop new and sustainable technologies for the production of energy and chemicals, especially in the field of transportation fuel sector which strongly depends on fossil sources. Biomass can be defined as the material formed biologically excluding the material formed geologically or being fossilized. This includes plants, animals, algae, and biological waste from households, agriculture, animals or foods. Currently, fossil coal is the main source of energy, however, with worldwide supply and depletion of fossil based fuel becoming more and more expensive. Also the use of fossil fuels and their derivatives represents the main source of greenhouse gas (mainly CO_2) emission worldwide which drives researchers to find an alternative to fossil fuels [1].

Biomass is an ideal and sustainable source of organic compounds that can replace the fossil fuels for the production of renewable fuels and chemicals. Furthermore, the usage of biomass and its derivatives will reduce the emission of greenhouse gas. In recent years, several developing countries have implemented ambitious biofuel targets or mandates, in order to achieve a high level of energy supply and the proportion of biofuel used for transport. Brazil is the world's leading user of biofuel with 19% of transport fuel currently derived mainly from biomass and in Europe, Germany is the leading consumer and producer of biofuel [2]. For long term sustainability, European commission in January 2014 within the framework of energy and climate policy has set a target to use at least 27% of EU energy from renewables by 2030 [3].

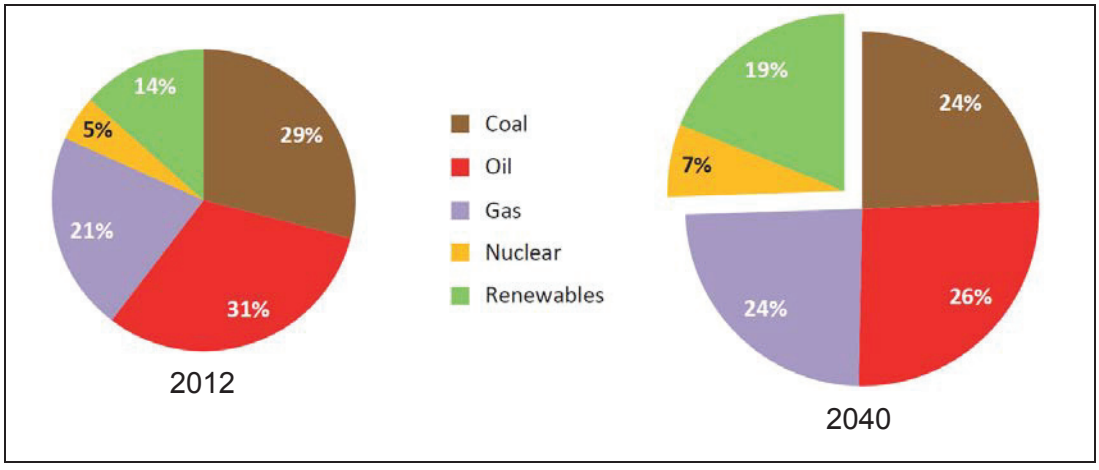

Figure 1.1. Fuel share in world-energy demand [**3**].

According to world energy outlook to 2040, the share of fossil fuel including oil, coal and gas will remain the major source of energy over the next three decades. The share of oil slowly will decrease from 31% in 2012 to 26% in 2040 and reach the level of coal and gas. The contribution of energy from renewable and nuclear sources will increase to 19% and 7% by 2040 as shown in Figure 1.1. The intention is more towards the use of carbon-free energy based on renewable and nuclear power [3].

The global consumption of biomass derived biofuel is expected to increase from 1.3 million barrels of oil equivalent per day (mboe/d) in 2012 to 2.2 mboe/d in 2020 and 4.6 mboe/d in 2040. Biofuel will contribute 8% of global transportation fuel by 2040 and the consumption will be concentrated in United States, Brazil and in the European Union as shown in Figure 1.2.

However, the use of biofuel is a controversial topic and so the European Union Energy Council agreed to reset the target defined by Renewable Energy Directive (RED) (2009/28/EC) from 10% to 7% of biofuel admixture by 2020 [3]. In order to achieve original RED 2020 target of 10%, incorporation of advanced biofuel derived from cellulosic biomass, agricultural and forestry residues and from the algae are promising [4].

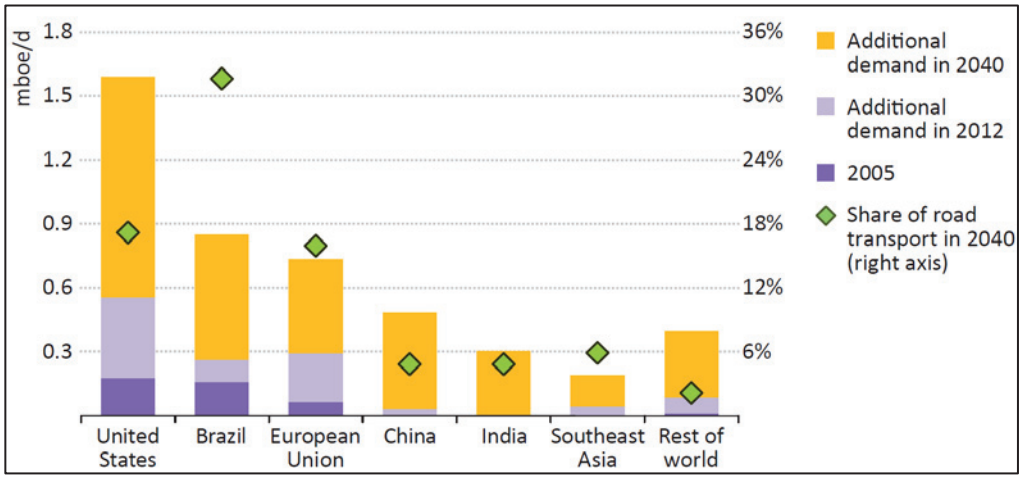

Figure 1.2. Biofuels consumption by road transport versus region [**3**].

1.2 Biomass-derived biofuels and platform chemicals

Biomass-derived feedstock can be classified into three general classes: 1) starch or sugars – from edible feedstocks like corn, sugarcane, etc., 2) lignocellulosic feedstock from agriculture residues, pulp and paper waste, etc., and 3) triglycerides from feedstocks like plant oil, animal fat, etc. [5]. Biodiesel and bioethanol are most extensively used liquid biofuels. Bioethanol is mainly produced from sugar and starch crops by fermentation processes but it can be also obtained from lignocellulosic biomass like wood and starch by hydrolysis and fermentation processes. Biodiesel is mainly produced by transesterification of

oil and fat (triglycerides) with methanol or ethanol in the presence of base as a catalyst, where oil is obtained from oilseed crops or oil based residues as shown in Figure 1.3 [6].

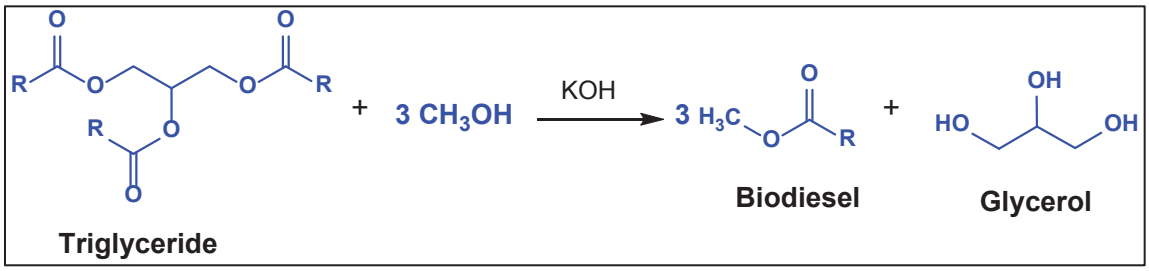

Figure 1.3. Biodiesel production from triglyceride.

Biodiesel can be used directly or in a mixture with conventional diesel in different ratios. The blending of biodiesel with conventional diesel in the ratio of 20: 80 can be used in regular diesel engines without modification. Moreover, biodiesel is less toxic, biodegradable and reduces particulate and hydrocarbon emission. Generally, all kind of plant /edible oil such as soya, palm, sunflower and rapeseed oil can be used as feedstock for biodiesel production, also known as first generation biofuels [7]. However, there are a number of social and economic problems with first generation biofuels, as the most of the land is needed to grow food crops. The most controversial issue with first generation biofuels is 'fuel vs food' [8]. To overcome this problem, second generation biofuels have been developed, in which non-edible oil such as Jatropha oil, Pongamia oil, and Jojoba oil are used. These plants require minimal cultivation and do not use the traditional agricultural land. Additionally, development of biodiesel from non-edible algae oil as a next generation feedstock is expected in the coming years. Algae can produce 80-180 times more oil per hectare annually than plants. Around 9% of total transportation fuel is expected to be made from algae by 2030 [8, 9]. Biodiesel is mostly consumed in Europe as a road transportation fuel mainly obtained from rapeseed oil. The development and the commercial growth of biodiesel have been rapidly expanding in Europe and US over last few years. According to the OECD-FAO Agriculture Outlook 2014, global production of biodiesel is expected to reach 40 bln L by 2023 and 19 bln L in Europe by 2020 [10].

1.3 Biomass-derived glycerol

As the global production of biodiesel continues to increase, this will lead to a surplus of the by-products in this process. The major byproduct is glycerol, which is inevitably produced by 10 wt% in total biodiesel production which results in a large amount of glycerol in the market [11]. In the conventional biodiesel process, high methanol to oil ratio is used (1: 6) in order to achieve complete conversion of oil. The excess methanol remains in glycerol and later it is recovered by distillation. The composition of bioglycerol (or crude glycerol) is quite variable with 65-85% (w/w) glycerol, more than 20% methanol, water, methyl esters,

inorganic salts, unreacted triglycerides, etc. Many companies like Evonik and BASF have started to use sodium methylate catalyst instead of NaOH or KOH as it produces excellent yields of biodiesel and better quality of glycerol. Similarly, glycerol is also by-product in the oleochemicals synthesis, where plant oil and animal fats are hydrolyzed to produce fatty acids. Oleochemicals are used to prepare soaps and detergents as well as they have applications in the synthesis of lubricants. In the past, glycerol was prepared by epichlorohydrin process, in which chlorination of propene (fossil feedstock) produces allyl chloride, which is further oxidized with hypochlorite in the presence of base to give epichlorohydrin. Hydrolysis of epichlorohydrin will produce glycerol [11, 12]. The world scenario of crude glycerol production is shown in Figure 1.4. The global production of crude glycerol from biodiesel is expected to be 41.9 billion liters by 2020. Thus, the utilization of crude glycerol has become a serious issue and especially to make biodiesel industry economically and environmentally liable [13].

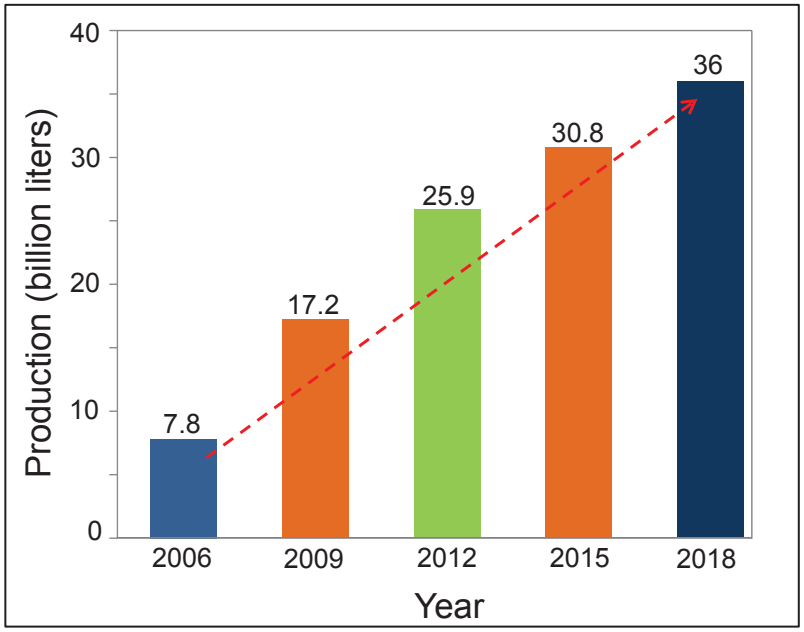

Figure 1.4. World's scenario of crude glycerol production [13].

Glycerol is a simple polyol (IUPAC name is propane-1,2,3-triol) which is a colourless, odourless and viscous liquid. The three hydroxyl groups of glycerol are responsible for its hygroscopic nature and miscibility with water. Traditionally glycerol has applications in cosmetic and pharmaceutical products (skin care, cough syrup); it also serves as additive in food industries (humectant, solvent, sweetener, preserving food, etc.), and is used as chemical intermediate in the synthesis of nitroglycerin (explosives), alkyd resin, soap, etc. [14]. Glycerol is a nontoxic, edible, sustainable and biodegradable compound. However, the technical and economic analysis shows that the demand is rather low to consume the

surplus amount of glycerol. Hence, several efforts are taken to convert low value glycerol to value added products especially for the sustainability of biodiesel industry.

1.4 Glycerol conversion into value added chemicals

The potential conversion of low cost and a surplus amount of glycerol into value-added chemicals can facilitate the replacement of fossil based products. In comparison with glycerol, most of the molecules from fossil feedstocks (e.g. propane) are unfunctionalized; glycerol is already functionalized molecule, easily to transform into valuable product via different reaction pathways. Moreover, these products can be of interest for several chemical industries because of the availability and low cost of glycerol [15]. For instance, Solvay is already producing epichlorohydrin (100,000 tons p.a.) from glycerol by Epicerol® process in Thailand and announced to start a second plant in China to produce 100,000 tons/year epichlorohydrin by the same process [16, 17]. In last few years, several catalytic processes that convert low value bioglycerol to value added products have been reported in the literature in particular oxidation, dehydration, reforming, acetalization, hydrogenation, oligomerisation, etherification and acetylation, as shown in Figure 1.5.

The oxidation of glycerol produces dihydroxyacetone, hydroxypyruvic acid, mesoxalic acid, glyceric acid, tartronic acid, oxalic acid and intermediates (glycoxylic acid, glycolic acid and glyceraldehyde). In particular, mesoxalic and tartronic acid have applications in the synthesis of fine chemicals and novel polymers, moreover, tartronic acid can act as an oxygen scavenger and anti-corrosive agent. Dihydroxyacetone is used as an ingredient in tanning agents and building blocks for polymer synthesis. Generally, supported noble metal nanoparticles such as Pd, Pt, Bi and Au are used as catalysts, mostly in an aqueous medium at acidic or basic conditions and with pure oxygen or air as oxidant either in batch, semi-batch or fixed-bed reactor [18].

The dehydration of glycerol leads to acrolein in the presence of acidic catalysts. Currently, acrolein is produced from propylene oxide by using BiMo mixed oxide catalysts. Acrolein is extensively used in the synthesis of polymers and poly-acrylates. Acrolein is also used in the synthesis of fine chemicals and feed additives like DL-methionine (an amino acid used to feed animals). Dehydration of glycerol is generally performed in gas or liquid phase using a solid acid catalyst such as zeolite and mixed metal oxides [19]. Moreover, several supported heteropolyacids and salts of heteropolyacids have been employed for glycerol dehydration reaction [19, 20].

Hydrogenation of glycerol produces 1,2-propanediol (1,2-PD), 1,3-propanediol and ethylene glycol in the presence of metallic catalysts. 1,2-PD has applications in polyester resins, pharmaceuticals, cosmetics, flavors and fragrances, as an anti-freezing agent, animal feed, etc. 1,3-PD is also used in the synthesis of special polyester fiber, films and coatings [21, 22, 15]. Catalytic hydrogenolysis of glycerol generally is carried out over heterogeneous

catalysts like Cu, Pd, Pt, Ru, Rh supported on ZnO, alumina, carbon and silica. Several commercial catalysts have been employed for these reactions such as 5% Ru/alumina (Johnson Matthey), 5%Pt/C (Degussa), Raney copper (Grace Davision) and copper chromite (Süd-Chemie). The Cu-based catalyst was found to be more selective towards PD while Ru and Pd based catalysts showed poor selectivity to PD [15]. H_2 can also be generated in situ from hydrogen donor molecule; such process is called catalytic transfer hydrogenation. Simple molecules like hydrazine, cyclohexene, formic acid, formates, alcohols like 2-propanol and methanol can be used as H_2 donors. Several research groups have used Pd, Pt, Rh, Ni and Cu supported catalyst for transfer hydrogenation of glycerol. The use of Ni-Cu/Al_2O_3 catalyst showed 82% selectivity for 1,2 PD at 90% of glycerol conversion using formic acid as a hydrogen donor [23, 24].

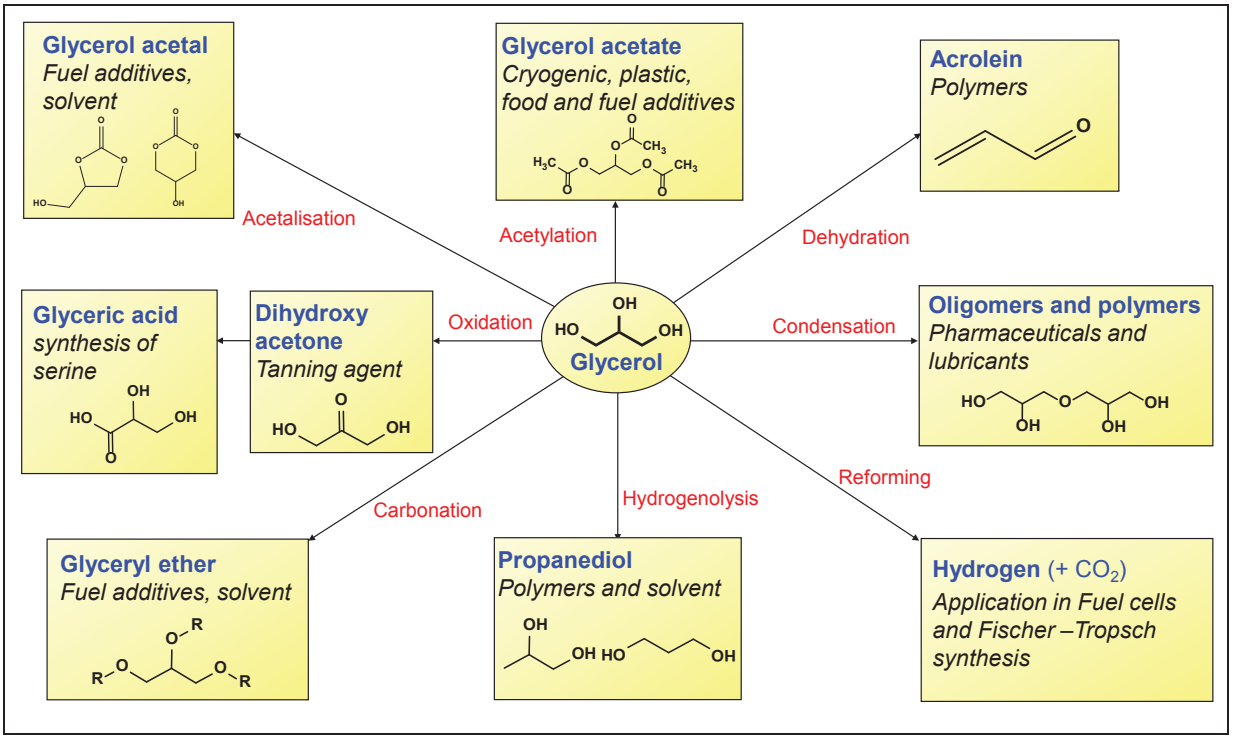

Figure 1.5. Possible ways to convert glycerol into value-added chemicals.

Glycerol was found to be an alternative to methane reforming for the production of hydrogen rich gas. It is important to note that the Dutch company BioMethanol Netherland Chemie produces syngas by reforming of glycerol and the resultant syngas is subsequently used to produce methanol [18, 19]. Generally, reforming of glycerol is performed over heterogeneous metallic catalysts such as Rh, Ru, Ni, Ir, Co, Pt and Fe. Rh was found to be the most active and coke resistant catalyst but number of reports is relatively low, probably due to higher cost of Rh. Ni and Pt are mostly used catalysts for steam reforming of glycerol [25].

Acetalization of glycerol with carbonyl compound (mainly acetone/benzaldehyde) is generally performed using homogeneous acid catalysts (like HCl, H_3PO_4, p-toluene sulfonic acid) or heterogeneous acid catalysts (ion exchange resins [26], supported heteropolyacids [27], metal oxides [28]) to form cyclic acetals such as 5-membered 1,3-dioxolan and 6-membered 1,3-dioxane. The ratio of these isomers depends on temperature, molar ratio of reactants, structure of carbonyl compound (aldehyde or ketone) and on the catalyst used. Glycerol acetals can enhance the cold flow property of biodiesel and can also be used as diesel fuel additive to reduce the emission of CO and hydrocarbons. Moreover, they are used in cosmetics, fragrance, food and beverages as additives and as pharmaceuticals and anti-knocking agent in fuels [29]. The blending of acetals with gasoline in the range of 1-5 vol% results in a significant reduction of gum formation, improving its antioxidant potential, moreover, an increment in octane number was observed [30].

Glycerol etherification with alcohols (like tert-butyl alcohol) or lower olefins (like isobutene) is an acid catalyzed and consecutive reaction to form mono tert-butyl ether (with two isomers), di- tertiary butyl ether (with two isomers) and tri-tert-butyl ether. Di and tri ethers are used as fuel additives which reduce the viscosity and improve the cold flow property of diesel; moreover, they act as octane boosters and reduce particulate, CO and hydrocarbon emission [6]. In the presence of tert-butyl alcohol as an etherifying agent, water is formed during the reaction which inhibits the formation of higher ethers, whereas isobutene can undergo oligomerization to form higher hydrocarbons (C8 or C12). Glycerol etherification was performed over Brønsted acidic heterogeneous catalysts such as ion exchange resins [31], Hyflon (perflurosulfonic isomer similar to Nafion®) [32], supported heteropolyacids [33, 34], sulfated metal oxide or carbon (SiO_2, ZrO_2) [35-37].

Besides glycerol etherification with alcohols or olefins, many researchers are also working on glycerol oligomerization or polymerization to produce diglycerol and polyglycerols. These products have potential application in cosmetic, polymer and plastic industries and can be used as a lubricant and emulsifier in the food industry [38, 39]. During glycerol dimerization in the presence of acidic or basic catalyst, three isomers of diglycerol might be formed as αα' (linear), αβ (branched), or ββ' dimer [40]. Glycerol oligomerization can be performed over acid catalyst such sulfuric acid (homogeneous) [41], zeolite (different Si/Al ratio) [42] and ion exchange resins (Amberlyst-16) [43]. Super-acidic ion exchange polymer like Nafion® foil (perfluorinated along with sulfonic groups) was used in a falling film reactor in which the foil was placed in a tube above the bulk of glycerol. The reactor was evacuated using oil pump and a dephlegmator was used to remove the condensed water. With this technique 85% selectivity to diglycerol can be reached at more than 90% glycerol conversion [40]. On the other side, homogeneous basic catalysts such as carbonates of alkali metals (Na_2CO_3,

Cs_2CO_3 and $CsHCO_3$) and heterogeneous MgO, CaO, SrO, BaO, Faujasite X and Y and Zeolite Beta catalysts have been employed for glycerol oligomerization [44-46].

From the literature, it can be noticed that the effective conversion of glycerol into value-added chemicals is still a hot topic. In cases, it is difficult to reach high selectivity towards the desired product at high glycerol conversion. Because of the two primary hydroxyl groups and one secondary hydroxyl group, it can undergo several possible reactions. Hence, it is very difficult to find optimal catalysts and reaction conditions. Comparatively, much research has been carried out on oxidation, dehydration and hydrogenation; however, few processes are established.

Some of the reactions such as etherification and oligomerization are acid catalyzed consecutive reactions. Most of the researchers have used strong Brønsted acid catalysts such as ion exchange resin and supported or non-supported heteropolyacids. However, in the presence of water both reactions are equilibrium controlled and hence selectivities to desired products are limited. Similar to this, another interesting approach to utilize glycerol is its esterification with acetic acid to form value added acetins. In addition, some other acid catalyze reactions (e.g. dehydration of glycerol) may also run during esterification of glycerol to form side products.

1.5 Glycerol esterification with acetic acid (acetylation)

Valorization of glycerol via esterification with acetic acid or acetic anhydride (acetylation) can be an attractive sustainable alternative for the utilization of low value glycerol. During this process, monoacetyl glycerol (MAG, monoacetin), diacetyl glycerol (DAG, diacetin) and triacetyl glycerol (TAG, triacetin) are formed simultaneously in three consecutive reaction steps as shown in Figure 1.6. Depending on the position of acetyl groups, monoacetin (MAG) and diacetin (DAG) exist in two different isomers. MAG and DAG have application in food industry, cryogenics and as starting monomer for the production of biodegradable polymer [47]. In particular, MAG is used in the manufacture of explosives (dynamite), tanning leather and solvent for dyes, whereas DAG can act as softening agent, plasticizer, printing ink and solvent [48]. TAG can act as viscosity reducer and cold flow improver for biodiesel, anti-knock additive and octane booster for gasoline being a sustainable and renewable alternative for trialkyl ethers (MTBE and ETBE). TAG is also widely used in food industries as a humectant, emulsifier and binder, in beverage industries as a flavor enhancer and emulsifier, in pharmaceuticals as antifungal agents and plasticizer, in cosmetics to maintain the moisture in creams/ lotions moreover, in cigarette filters to plasticize and solidify and in production of photographic films and various perfumes [49-51].

Glycerol esterification with acetic acid (acetylation) is an acid catalyzed and consecutive three-step reaction where each step is controlled by chemical equilibrium due to the formation of water as an unavoidable by-product. Traditionally, glycerol acetylation is

performed using homogeneous mineral acids such sulfuric acid, hydrofluoric acid and p-toluene sulfonic acid, however, these acid catalysts have several major drawbacks as they are toxic, corrosive and difficult to remove from the reaction mixture. Hence, to overcome these difficulties, it is desired to replace hazardous mineral acids by solid acid catalysts. Glycerol acetylation reaction has been mostly studied in batch reactors using solid acid catalysts such as ion exchange resins, supported heteropolyacids, MoO_3 and WO_3 promoted metal oxides (ZrO_2-TiO_2) [52] and magnesium fluorides [53], often with excess of acetic acid, but the observed selectivity for TAG was rather low due to the thermodynamic equilibrium limitation.

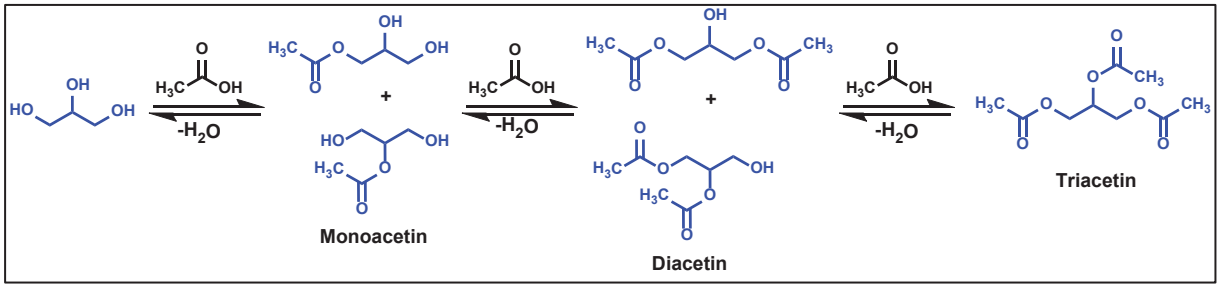

Figure 1.6. Consecutive esterification of glycerol with acetic acid.

Various types of SO_3H-functionalized oxides have been employed for this reaction, for instance, Melero et al. used an SBA-15 functionalized-SO_3H catalyst with acetic acid to glycerol molar ratio of 9 which exhibited 85% combined selectivity for DAG and TAG at 90% conversion of glycerol [54]. On the other hand, Testa et. al. reported the use of sulfated mesoporous SiO_2 showing 60% selectivity to TAG after 24 h at complete conversion of glycerol [55]. Similarly, Kim et al. used different solid acid catalysts at low temperature and found that sulfonic acid functionalized SBA-15 exhibited high selectivity to TAG at complete conversion compared to all other catalysts [56]. Activated carbon [57, 58] and carbonaceous material such as cellulose [59] and hydrothermal carbon [60] have been used for SO_3H-functionalization, which further were employed as a catalyst in glycerol acetylation. The best result reported were 57% selectivity for TAG at 98% conversion of glycerol over SO_3H-hydrothermal carbon using 9/1 acetic acid to glycerol molar ratio. Sulfated Ce-ZrO_2 and KIL-ZrO_2 (KIL=SiO_2) resulted in 16% and 20% selectivity for TAG using 9 and 6 acetic acid to glycerol molar ratio, respectively, at complete conversion of glycerol [61, 47]. Similarly, Mallesham et al. used sulfated SnO_2 giving 55% selectivity for TAG with high acetic acid to glycerol molar ratio of 9/1 [62]. However, most of these catalysts either show low selectivity towards TAG (4-10%) or undergo severe deactivation due to leaching of active sulfonic group from the surface of support.

Ion exchange resins like Amberlyst-15 and Amberlyst-36 were also used for glycerol acetylation and other esterification reactions [63, 64]. For example, Zhou et al. used

Amberlyst-15 as a catalyst and found high selectivity for TAG (44.5%) using an acetic acid to glycerol molar ratio of 9 at complete glycerol conversion [65]. Alternative concepts for reaction engineering have been studied, for instance, Rezayat et al. used Amberlyst-15 for continuous synthesis of triacetin in supercritical carbon dioxide reaction medium, giving 100% selectivity for triacetin with 41% yield at a high molar ratio of glycerol to acetic acid (1:24) and high pressure (up to 200 bar) [66]. Acetic anhydride was also used as an acetylating agent to achieve 100% selectivity for TAG using sulfated carbon, Amberlyst 15/35 and zeolite [67-70]. However, such a high excess of acetic acid, expensive acetic anhydride and high pressure are not desired for an industrial process. Hasabnis et al. performed reactive distillation of glycerol with acetic acid over Amberlyst-15 using toluene as an entrainer, however, the selectivity to TAG (39.8%) was rather low [71].

Heteropolyacid immobilized on different oxide supports such as SiO_2, zeolite, ZrO_2, Nb_2O_3, SBA-15 and MCM-41 mainly prepared by impregnation method have been employed for glycerol acetylation reaction with different acetic acid to glycerol molar ratio (varying from 5/1 to 16/1) [72-77]. Zhu et al. used silicotungstic acid supported on zirconia and showed 32.3% selectivity for TAG with 10/1 acetic acid to glycerol molar ratio at complete conversion of glycerol [78]. Very recently, Patel et al. used MCM-41 and ZrO_2 supported tungstophosphoric acid catalysts, but the selectivity for TAG was found to be rather low with 15% and 4%, respectively [48]. The same group also used 30 wt% tungstophosphoric acid impregnated on MCM-48 support to exhibit 30% selectivity for TAG using 6/1 acetic acid to glycerol molar ratio [79]. Huang et al. 2014 used the homogeneous tungstophosphoric acid supported on ionic liquid as a catalyst which showed 98% selectivity for TAG using high acetic acid to glycerol molar ratio (10/1) and toluene as an entrainer under nitrogen flow of 150 ml/h [80]. Recently, Rastegari et al. developed a continuous process using tubular reactor for glycerol acetylation over Amberlyst-36 as a catalyst in the liquid phase using acetic acid to glycerol molar ratio of 7, exhibiting high conversion (100%), but the selectivity to TAG was rather low (nearly 13%) [81].

According to the literature, limited selectivity to TAG in glycerol acetylation was observed, as all three consecutive steps remain in equilibrium in the presence of water. In addition, glycerol acetylation is an endothermic reaction and its standard reaction Gibbs free energies (ΔG) are positive which indicates that the reaction is non-spontaneous and thermodynamically resisted. The Gibbs free energies for the first ($\Delta G_{Glycerol \rightarrow MAG}$) and second ($\Delta G_{MAG \rightarrow DAG}$) steps are 19.15 and 17.80 kJ/mol, respectively, whereas for the third step ($\Delta G_{DAG \rightarrow TAG}$) is relatively high to 55.58 kJ/mol [82]. This means that third step should be the most difficult one. In order to increase selectivity of the desired TAG, it is necessary to shift the equilibrium and the best route would be the removal of water formed during the course of

reaction. The water can be removed by means of azeotropic distillation using an external component referred to as entrainer.

Moreover, solid catalysts get deactivated due to leaching of active species in the liquid phase. Thus it would be attractive to transform liquid phase batch processes into continuous flow processes, as this has several advantages, especially in the view of their implementation in the industry. Surprisingly, very few reports are available on continuous flow glycerol acetylation [81].

Table 1.1. Summary of catalysts and conditions for glycerol acetylation reported in the literature.

Catalysts	Performances X, S (TAG)	Reaction conditions T (°C), AA: glycerol molar ratio	Reference
SO_3H-SBA-15	X = 90%, S(DAG + TAG) = 85%	125, 9: 1	[54]
A15	X =100% S(TAG) = 100%	105, 3: 1, Acetic anhydride	[67]
A15	X = 41% S(TAG) = 100%	110, 24: 1, $scCO_2$ 200 bar	[66]
PMA/NaUSY	X = 60% S(TAG) = 4%	120, 16: 1	[72]
TPA/SiO_2	X = 70%, S(TAG) = 8%	120, 16: 1	[73]
A15	X = 99%, S(TAG) = 39.8%	120, 3: 1, EDC** as entrainer	[71]
Zeolite Beta, K-10, A15	X = 100%, S(TAG) = 100%	60, 4: 1, Acetic anhydride	[68]
TPA/Cs-ZrO_2	X = 94%, S(TAG) = 3%	120, 5: 1	[74]
TPA/Nb_2O_5	X = 98%, S(TAG) = 19%	120, 5: 1	[75]
MoO_3/TiO_2-ZrO_2	X = 100%, S(TAG) = 7.5%	120, 6: 1	[52]
TPA/Ac. Carbon	X = 75%, S(TAG) = 12%	120, 16: 1	[83]
$MgF_2(OH)$	X = 94%, S(DAG + TAG) = 94%	100, 3: 1	[53]
SO_3H-ionic liquid	X = 96%, S(TAG) = 15.1%	140, 5: 1	[84]

Catalysts	Performances X, S (TAG)	Reaction conditions T (°C), AA: glycerol molar ratio	Reference
SO_3H-Ac. Carbon	X = 99.6%, S(TAG) = 41%	105, 9: 1	[57]
SO_3H-Ac. Carbon	X = 92%, S(TAG) = 34%	120, 10: 1	[58]
A15, A36	X (AA*) = 95%, S(MAG) = 70%	120, 1: 8	[63]
A15	X = 97%, S(TAG) = 43.2%	110, 9: 1	[64]
PMA/SBA-15	X = 77%, S(TAG) = 15%	110, 8: 1	[76]
SO_3H-CeO_2-ZrO_2	X = 100%, S(TAG) = 16.5%	120, 6: 1	[61]
TPA	X = 96%, S(MAG) = 66%	60, 3: 1	[77]
A15	X = 97%, S(TAG) = 44%	110, 9: 1	[65]
Ag-TPA	X = 96%, S(TAG) = 5.2%	120, 10: 1	[85]
SO_3H-SiO_2	X = 100%, S(TAG) = 49%	105, 3: 1	[55]
STA/SiO_2	X = 100%, S(TAG) = 32.3%	120, 10: 1	[78]
SO_3H-SBA-15	X = 100%, S(TAG) = 27%	80, 6: 1	[56]
SO_3H-cellulose carbon	X = 100%, S(TAG) = 10%	80, 6: 1	[59]
SO_3H-ZrKIL-2 KIL-2 = SiO_2	X = 100%, S(TAG) = 20%	100, 10: 1	[47]
Y/SBA-3	X = 97%, S(TAG) = 56%	110, 8: 1	[86]
TPA/MCM-41	X = 92%, S(TAG) = 10%	100, 6: 1	[48]
TPA/MCM-48	X = 99%, S(TAG) = 13%	100, 6: 1	[79]
SO_3H-SnO_2	X = 99%, S(TAG) = 56%	100, 9: 1	[62]

Catalysts	Performances X, S (TAG)	Reaction conditions T (°C), AA: glycerol molar ratio	Reference
SO_3H-Carbon	X = 100%, S(TAG) = 100%	115, 4: 1 Acetic anhydride	[70]
TPA-Ionic liquid	X = 100%, S(TAG) = 98%	100, 10: 1, N_2 = 150 ml/h, Toluene as entrainer,	[80]
SO_3H-Hydrothermal Carbon	X = 98%, S(TAG) = 57%	115, 5: 1	[60]
A15	X = 100%, S(TAG) = 14%	100, 7: 1, Continuous fixed bed reactor	[81]
SO_3H-Act Carbon, H-Y	X = 100%, S(TAG) = 100%	80, 4: 1 Acetic anhydride	[69]
Ac. Carbon (Karanja seeds)	X = 88.5%, S(TAG) = 4%	120, 5: 1	[87]
A15: Amberlyst-15, A36: Amberlyst-36 AA*: Acetic acid conversion, EDC**: Ethylene dichloride (entrainer)			

1.6 Heteropolyacids as catalysts

Heteropolyacids (HPAs) are a class of solid acids made up of a particular combination of hydrogen and oxygen with certain metals and non-metals. These materials have metal-oxygen octahedra as their basic structural units and are able to release protons, thereby forming polyoxometalate anions (heteropolyanions). Depending upon the composition and combination of metal atom and non-metal hetero-atom, various structures of heteropolyacids are formed such as Keggin, Silverton, Dawson, Anderson, etc. Among all the HPA structures, Keggin-type polyoxometalates are the most stable, acidic and thus most prominent structure [7]. The chemical composition of Keggin structure can be represented as $XM_{12}O_{40}^{x-8}$ (with X is a central hetero-atom, generally the main group element such as Si^{4+}, P^{5+}, x is its oxidation state and M is a metal ion, generally d-block element Mo^{6+}, W^{6+}, V^{5+}). The Keggin type heteropolyanions are generally prepared under acidic pH by simple inorganic reactions as shown in the following equations.

$$[PO_4]^{3-} + 12[MoO_4]^{2-} + 24[H]^{+} \rightarrow [PMo_{12}O_{40}]^{3-} + 12H_2O \quad \text{(eq. 1.1)}$$

$$[SiO_4]^{4-} + 12[WO_4]^{2-} + 24[H]^{+} \rightarrow [SiW_{12}O_{40}]^{4-} + 12H_2O \quad \text{(eq. 1.2)}$$

The Keggin structure consists of a central XO_4 tetrahedron surrounded by twelve MO_6 octahedra arranged in the four M_3O_{13} groups sharing edges and connected to the central X heteroatom through an oxygen atom (see Figure 1.7). Generally, Keggin heteropolyanions are linked together through protonated water species (H_3O^+, $H_5O_2^+$, etc.) and hydration water

to form the ionic crystal. The crystal structure of HPAs depends on the amount of hydration water. The water can be released on heating; then the linked protons are available which ultimately form the Brønsted acid sites and also increase the acidity of the catalyst [20].

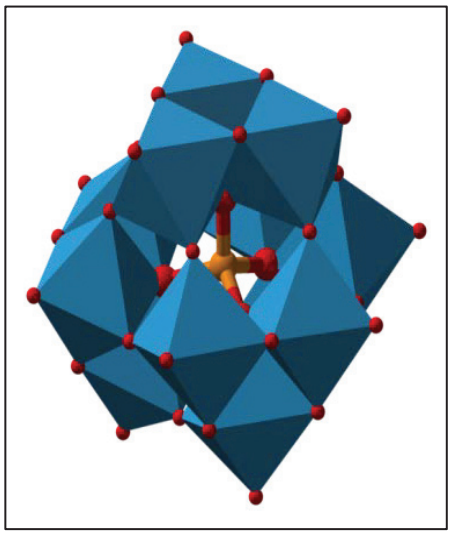

Figure 1.7. Keggin structure, $XM_{12}O_{40}^{n-}$ [88].

HPA with Keggin structure such as silicotungstic acid ($H_4[SiW_{12}O_{40}]$ = STA), phosphotungstic acid ($H_3[PW_{12}O_{40}]$ = TPA), phosphomolybdic acid ($H_3[PMo_{12}O_{40}]$ = PMA) and silicomolybdic acid ($H_4[SiMo_{12}O_{40}]$) are strong Brønsted acids and have the ability to catalyze a wide variety of reactions in both homogeneous and heterogeneous systems. Due to their special structure, HPA has large number of advantages over traditional mineral acids like H_2SO_4, HCl, or HNO_3. The Brønsted acidity of HPA is comparable with mineral acids and hence catalyzes liquid homogeneous phase reaction environmental friendly and efficiently. Moreover, due their strong Brønsted acidities, they show higher catalytic activity (100-1000 times) than the traditional mineral acids. Hence, reaction can also perform at mild conditions (lower catalyst concentration and/or temperature) [7]. The use of HPA will also avoid side reactions like sulfonation, chlorination nitration, etc., which might occur with H_2SO_4, HCl, or HNO_3, respectively. The HPAs are highly soluble in polar solvents such as water or alcohol and insoluble in non-polar solvents like hydrocarbons. They dissociate in aqueous phase into their respective anions and protons. The Brønsted acidities of these heteropolyacids are also much stronger than those of known solid acids such as SiO_2-Al_2O_3, H_3PO_4/SiO_2 and zeolites (HX and HY). The acid strength of Keggin heteropolyanions increases in the order PMA < SMA < STA < TPA [89]. Interestingly, the acidity of the heteropolyacids can be tuned by replacement of H^+ by metal ion such as Li^+, Na^+, Cs^{2+}, Mg^{2+}, NH_4^+ and K^+ [90, 91]. However, the major disadvantages of HPAs are their low specific surface area and limited thermal stability. To overcome these problems, HPAs can be supported over acidic supports (Al_2O_3), neutral supports (SiO_2) or activated carbon in order to increase the surface area and to make them thermally stable [7, 20].

1.7 Ion exchange resins as catalysts

Ion exchange resins are ionic and covalently bond cross-linked insoluble polymeric materials provided in the form of beads. These beads have either compact internal structure with narrow pores, also called microporous resins or multichannel structure with large pores called as macroporous or macroreticular resins (Figure 1.8). Generally, such resins are prepared by polymerization of styrene along with structure directing agent divinyl benzene, also known as a cross-linking agent. Porosity in the resins is controlled by cross-linkage (typical range is 0.5 to 20%). Low cross-linked resins are microporous whereas highly cross-linked polymer are macroporous in nature [92, 93]. The ion exchange resins contain ions which are electrostatically bound to the polymeric matrix and are capable to exchanging with other ions of the same charge in a solution. Depending on the functional group attached to the polymeric support, they are classified into acidic-cation exchange resins and basic-anion exchange resins.

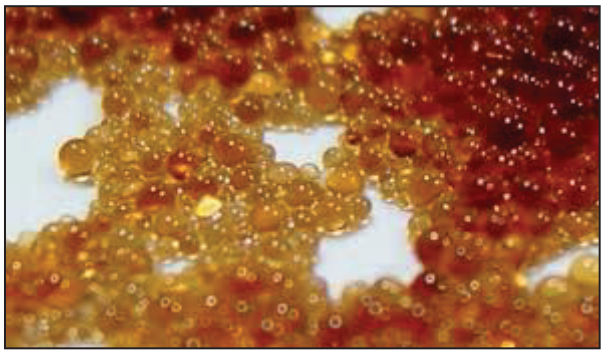

Figure 1.8. Ion-exchanged resin beads [94].

When the polymeric support are functionalized with sulfonic groups (sodium polystyrene sulfonate), then the resin is strongly acidic whereas and when supported with carboxylic acids then the resin is weakly acidic. Similarly, when the polymeric support is functionalized with a quaternary amino group (trimethylammonium group) then the resin is strongly basic. With primary, secondary or tertiary amino group (polyethylene amine), the resin is weakly basic. The extent of exchange depends on the concentration of ions in the solution and affinity of the ions to the polymer matrix. Macroporous resins possess high surface area which provides a high number of exchange sites, in particular for larger ions. Moreover they are more rigid and this makes them facile to use and remove from the reaction system [92]. The main advantage of ion exchange resin is that they are insoluble in an aqueous phase. Therefore after the exchange of ions in solution, the resins can be easily removed by simple filtration. This also makes them easy to use in a continuous process where columns and chromatographic separations are involved. They are used in water softening, water purification, toxic metal separation (uranium from plutonium or other metals like thorium ad

lanthanum), wastewater treatment, hydrometallurgy, sensors, chromatography, biomolecular separations and pharmaceutical operations as purifying and isolating agent [93-96].

Ion-exchange resins, in particular, acidic resins were reported as catalysts in several reactions such as carbonylation, hydroformylation, oxidation, hydrogenation, esterification and transesterification. The catalytic performance depends on structure and properties of resins such as porosity, cross-linking percentage in the polymer matrix and the bulk properties (swelling, loading capacity, equilibrium rate). Generally, microporous resins have high moisture content, high loading capacity (total number of chemical equivalents available for exchange per unit weight or volume) and high equilibration rate (time required to reach equilibrium in ion exchange reversible reaction). Swelling volume of resins in the solvent can increase up to 800% by decreasing the cross-linking percentage. Ion exchange resins with different precursor such as Nafion® (with perfluorinated sulfonic acid groups) and acrylic based resins are well known for organic transformation and ion exchange [93, 97].

1.8 Metal Oxides as catalysts

Large numbers of solid acidic catalysts such as ion exchange resins, zeolites and supported heteropolyacids are used in the liquid phase esterification reaction. However, the catalysts to be used in gas phase process must be thermally and structurally stable [98]. The Amberlyst resins cannot be used in gas phase process due to their limited thermal stability. On the other side, supported heteropolyacids are widely studied in catalysis and can be used as heterogeneous catalyst especially under gas phase reaction conditions. Supporting heteropolyacid on different oxides increases its thermal stability and hence it can be used in gas phase reaction at elevated temperature. Interactions with supports i.e. metal oxide (like Al_2O_3, SiO_2) also controls the physical properties such as primary structure (Keggin structure), pore size, particle size, etc., which in turn influence the catalytic performance.

Bulk metal oxides can act as a catalytically active material due to their surface properties, composition, morphology, coordination structure and the hydroxyl groups which can produce surface acid-base properties. Oxides of metal are generally solids and their properties mainly depend on the bonding character of metal with oxygen. Mixed metal oxides are multi-metal multi-phase oxides and generally composed of transition metal oxides which control the chemical and physical properties of the final solid. Generally these materials have complex chemical structure and hence are difficult to characterize. They are widely used as catalysts in selective oxidation, ammoxidation, oxydehydration, redox reaction, etc. [99]. Acidic properties of these materials can be varied by using different transition metal oxides or by adding alkaline (earth) metal oxides. In this work, highly acidic supported heteropolyacids and low acidic SiO_2 modified with transition metal oxides and alkaline (earth) metal oxides as a reference material were studied for gas phase glycerol acetylation.

1.9 Objective of the thesis

The main objective of this work is to improve the yield of TAG using solid acid catalysts for glycerol acetylation. In order to achieve this objective, an innovative concept of reaction engineering is chosen to shift the chemical equilibrium towards the product side by continuous removal of water during the course of reaction. The use of toluene as an entrainer can remove water permanently by azeotropic distillation. In addition, it is planned to use two series of strong acidic catalysts as: organic ion exchange resins and inorganic supported heteropolyacids. The selected catalysts should be tested in glycerol acetylation under water-free conditions, to gain knowledge of the structure and the nature of acid sites to develop a selective catalyst and to study the impact of the reaction parameters such as catalyst/feed ratio, reaction time and feed ratio (acetic acid: glycerol molar ratio).

Another objective is to transform the liquid phase batch process into a continuous flow process which can make TAG synthesis more sustainable and greener in practice. The best performing supported heteropolyacid catalysts from the batch operation should be used in gas phase operation. For comparison, another series of low acidic catalysts (mixed metal oxides) should be tested in gas phase acetylation.

To understand, illustrate and to derive structure-activity/selectivity relationship, the fresh and spent catalysts have to be characterized by various techniques such as ICP-OES, AAS, CHN analyzer, N_2 physisorption, XRD, Raman, ATR-IR, TEM, NH_3-TPD and Pyridine-IR.

2 Experimental procedures

2.1 Catalyst preparation

The catalytic properties of heterogeneous catalysts strongly depend on structure and method of synthesis. Depending on the structure, the catalysts can be divided into two main groups: A) Supported catalysts – catalytically active species are immobilized on the solid support mainly by impregnation, deposition- precipitation and ion exchange methods. B) Bulk catalysts – catalytically active species are formed during synthesis mainly by sol-gel, precipitation and co-precipitation method [100-102]. In the presented work, the impregnation and sol-gel methods were used for the synthesis of catalysts and hence will be discussed in details.

2.1.1 Materials

The organic compounds glycerol (Alfa Aesar, >99%), acetic acid (Fisher chemicals, Analytical reagent grade), toluene (Acros Organics, analytical reagent grade) and the heteropolyacids silicotungstic acid (STA, Fluka), tungstophosphoric acid (TPA, Fluka), phosphomolybdic acid (PMA, Merck) and the supports silica-alumina (SIRAL® 40, Sasol; SiO_2/Al_2O_3 = 40: 60), dispersible alumina (Disperal P2®, Sasol) as precursor for γ-alumina (γ-Al_2O_3) and silica (SS61138, Chempur) were used. Other inorganic chemicals tetraethyl orthosilicate (TEOS), ammonium titanyl oxalate (Merck), magnesium acetate (Merck), zirconium oxychloride (Merck) and strontium nitrate (Alfa Aesar) were used as received. Scandium nitrate was prepared from Scandium (Sc: procured from Smart elements) by precipitation method. In typical procedure, Sc metal was dissolved in conc. HCl to get $ScCl_3$ which was first treated with aq. NH_3 (pH = 9) and then with conc. HNO_3 to Scandium nitrate ($Sc(NO_3)_3$) solution. Furthermore, trimethylchlorosilane and hexamethyl disilazane (Aldrich), dodecane (TCI Europe), hexadecane (Aldrich) and pyridine (ACROS) were used for analytical purposes.

2.1.2 Preparation of γ-Al_2O_3

Dispersible alumina (Disperal P2®) was used as a precursor to prepare mesoporous γ-Al_2O_3 with tailor-made properties. In a typical procedure, 70 g of Disperal P2® were added to 350 g of distilled water and stirred for 1 h; to this solution, 78 g of Triton X 100 (Roth) template and 30 g of an aqueous ammonium acetate (Aldrich) solution (33 wt%) were added to form a white gel. This gel was further dried in air at 110 °C and calcined in air at 600 °C for 4 h. The other supports SiO_2 and SiO_2-Al_2O_3 were calcined in air at 500 °C for 5 h before impregnation.

2.1.3 Preparation of supported heteropolyacid catalysts

The heteropolyacids STA, TPA, and PMA were immobilized onto the three supports by wetness impregnation method with a nominal HPA load of 20 wt%. In the typical procedure for STA/SiO_2, an aqueous solution (10 ml) of STA (2 g) was added to the silica (8 g) under constant stirring overnight. Excess water was removed using a rotary evaporator. The obtained solid was dried at 120 °C for 2 h and then calcined at 300 °C with air in a muffle furnace for 4 h to obtain the powdery catalyst.

2.1.4 Ion exchange resins

Commercial ion exchange resins Amberlyst-70 (A70, moisture holding capacity 51-59%, Dow Chemicals) and Amberlyst-15 (A15, Dry, Aldrich) were purchased. Amberlyst-70 was kept in a fume hood to remove moisture for 24 h at RT.

2.1.5 Preparation of SiO_2-MO_x catalysts

The SiO_2-MO_x catalysts (MO_x = TiO_2, MgO, ZrO_2, SrO and Sc_2O_3 using precursor ammonium titanyl oxalate (ATO), magnesium acetate, zirconium oxychloride, strontium nitrate, and scandium nitrate, respectively) were prepared by the sol-gel method and SiO_2 to MO_x molar ratio was set to 30/1. In a typical procedure, SiO_2-TiO_2 catalyst was synthesized by dissolving 5.7 g of ATO in 30 g of distilled water. This solution was added to the 50 wt% aqueous solution of 120 g of TEOS (tetraethyl orthosilicate precursor for SiO_2) and conc. HCl (0.4 ml). Under stirring, an aqueous ammonium acetate (buffer) solution was added to the above solution to form a transparent colourless gel (yellow colour in case of TiO_2), which was further aged for 12 h at 70 °C. To this gel, 110 g of aqueous ammonia solution (2.5 wt%) were added and the sample was again aged for 12 h at 70 °C, further dried (110 °C for 12 h) and calcined at 500 °C for 5 h. Similarly, SiO_2 catalysts with MgO, ZrO_2, SrO and Sc_2O_3 were prepared. They are denoted as SiM30 where M is MO_x.

Furthermore, pure TiO_2 was prepared by calcining ammonium titanyl oxalate (ATO) at 500 °C for 5 h and pure SiO_2 was prepared following the same method without metal oxide (MO_x) precursor for comparison. In addition, SiO_2-TiO_2 (SiTi60) with the molar ratio of 60/1 and SiTi30 (calcined at 700 and 800 °C) samples were prepared for comparison.

2.1.6 Preparation of TiO_2/SiO_2 (Ti-SiO_2)

The Ti-SiO_2 was prepared by incipient wetness impregnation method. The required volume of aqueous solution of ammonium titanyl oxalate (ATO) was added to the SiO_2 (prepared by the sol-gel method as described above). The resultant solid was dried at 110 °C for 12 h and calcined at 500 °C for 5 h.

2.1.7 Preparation of TiO_2/SBA-15 (Ti-SBA-15)

Initially, SBA-15 was synthesized as support by mixing 100 g of conc. HCl (37%), 500 g of distilled water and 17 g of Pluronic 123 ($(EO)_{20}(PO)_{70}(EO)_{20}$ Aldrich) as a template and stirred for 30 minutes at room temperature until homogenization. To this solution, 37 g of TEOS (tetraethylorthosilicate) were added with constant stirring. This resultant white solution was stirred at 40 °C for 24 h and then heated at 90 °C for another 24 h under static condition. The solid was recovered by filtration, washed with water and dried at room temperature for 24 h. The obtained white solid was further dried at 100 °C for 4 h and finally calcined at 550 °C for 5 h. The Ti-SBA-15 was prepared by incipient wetness impregnation method. The required volume of aqueous solution of ammonium titanyl oxalate (ATO) was added to the SBA-15. The resultant solid was dried at 110 °C for 12 h and calcined at 500 °C for 5 h.

2.1.8 Preparation of TiO_2/MCM-41 (Ti-MCM-41)

In typical synthesis procedure, Ti-MCM-41 was prepared by mixing 200 g of ethanol, 500 g of distilled water, 32 g of cetyltrimethylammonium bromide (CTAB), 74 g of TEOS (tetraethylorthosilicate) and 0.4 ml of concentrated HCl (pH nearly 2) in a 1 litre plastic bottle with constant stirring at room temperature. To the resultant solution, an appropriate amount of titanyl ammonium aqueous solution (3.5 g in 10 g H_2O) was added dropwise and stirred for 30 minutes. A 20 ml glass vial filled with aqueous ammonia solution (25 wt%) was hanged inside the plastic bottle with the help of thin wire above the solution with constant stirring for 24 h. The cap of the bottle is closed while stirring for 24 h. The white solid was recovered by filtration, washed 3 times with water and dried at room temperature for 24 h. The obtained solid was dried at 100 °C for 4 h and finally calcined at 550 °C for 5 h.

2.2 Techniques used for catalyst characterization

The interpretation of structure, composition and chemical properties of fresh and spent catalysts is important to understand the relationship between catalysts property and catalytic performance. The knowledge from the catalysts characterization is also necessary to develop highly active, selective and long-lasting catalysts. Physical and chemical properties of fresh and spent catalyst were studied by following techniques.

2.2.1 N_2 physisorption

Gas adsorption analysis is most commonly used to determine the surface area and porosity of various materials. The gas molecules are allowed to adsorb on the surface of the solid at a specified pressure to form a thin and uniform monolayer, which is used to calculate the specific surface area. As the pressure of the gas increases, additional molecules are adsorbing which leads to the formation of multilayer, also referred to as capillary condensation. Brunauer, Emmett and Teller (BET) technique is most widely used to

determine the surface area of the solid material. Generally, nitrogen is used as a probe molecule and it is adsorbed on the surface of material at liquid nitrogen condition (- 196 °C).

BET surface area, pore volume and pore diameter of the catalysts were determined from the nitrogen adsorption/desorption isotherms at -196 °C on a Micromeritics ASAP 2010 instrument. Before the measurement, each sample was evacuated at 200 °C for 4 h. The pore size distribution was calculated from the desorption isotherm using BJH (Barrett-Joyner-Halenda) method which is the corrected form of Kelvin equation.

2.2.2 X-ray diffraction (XRD)

X-ray powder diffraction is an analytical technique primarily used to study the crystal structure (phase identification of crystalline material) and can also give information on unit cell dimension (atomic spacing). X-ray diffraction is based on the interaction of X-rays with atomic planes in a sample where each interaction produces specific reflection with incident X-rays. All the reflected rays from planes interfere and in case of positive interference it gives rise to diffraction, which occurs only when conditions satisfy Bragg's law,

$$n\lambda = 2dsin\theta \qquad \text{(eq. 2.1)}$$

where n (an integer) is the "order" of reflection, λ is the wavelength of electromagnetic radiation, d is the spacing between the planes in the atomic lattice, and θ is the angle between the incident ray and the scattering planes.

Powder X-ray diffraction (XRD) patterns were measured on a theta/theta diffractometer (X'Pert Pro from Panalytical, Almelo, Netherlands) with CuKα radiation (λ = 0.015418 nm, 40 kV, 40 mA) and a X'Celerator RTMS detector. The alignment was checked by means of silicon standard. The data were collected in the 2 theta range from 5-70°. The phase composition of the samples was determined using the program suite WinXPOW by STOE&CIE with the inclusion of the Powder Diffraction File (PDF) database of the ICDD (International Centre for Diffraction Data).

2.2.3 Infrared Spectroscopy

The fundamental principle of infrared spectroscopy is the absorption of infrared radiation which causes a vibrational transition in the molecule. Hence, IR spectroscopy is also called as vibrational spectroscopy. The infrared portion of the electromagnetic spectrum is generally classified into three regions; the near- (14000-4000 cm^{-1}), mid- (4000-400 cm^{-1}) and far- (400 - 10 cm^{-1}) infrared regions, named after their relation to the visible spectrum. The energy in the form of infrared radiation is applied over a sample which causes vibration between the atoms of a molecule. When the applied radiation frequency matches the vibrational frequency of the molecule, then absorption takes place and peak is observed with

the help of suited detectors. IR spectroscopy is mainly used to investigate structures and to determine functional groups within the molecule.

Different functional groups absorb characteristic frequency of IR radiation. A molecule can absorb IR radiation only when absorption causes a change in its electric dipole moment. Attenuated total reflection (ATR) is a sampling technique used in combination with infrared spectroscopy which allows samples to be analyzed directly in the solid or liquid state without modification. The ATR-IR spectra of the solid samples were recorded using a Bruker Alpha FTIR spectrometer equipped with a diamond ATR accessory.

2.2.4 X-ray photoelectron spectroscopy (XPS)

X-ray photoelectron spectroscopy is a surface technique used to determine the elemental composition of the near-surfacet layer of the solid (1-10 nm). XPS can also determine chemical and electronic state of the elements within this layer. The fundamental principle is based on the photoelectric effect, the ejection of electrons from the material as a consequence of the absorption of very short wavelength radiation. Electrons of each element have characteristic binding energy. XP spectra are measured by irradiating a solid surface with a beam of X-rays while simultaneously measuring the kinetic energy of electrons that are emitted from the surface region. The ejected electrons of particular energies are detected and counted which is then further recorded in the form of spectra. Peaks detected in spectra represent characteristic energy called binding energy. The energies and intensities of the photoelectron peaks enable identification and quantification of all surface elements.

Energy of X-rays is known (E_{photon}) and the kinetic energy of the ejected electron is measured by the instrument ($E_{kinetic}$), thus the binding energy ($E_{binding}$) of ejected electron can be calculated using following equation:

$$E_{binding} = E_{photon} - E_{kinetic} - \varphi \qquad \text{(eq. 2.2)}$$

Where, φ is the work function of the XP spectrometer.

Each peak area is proportional to the number of atoms being present in the studied sample. By calculating the respective contribution of each peak area, one can determine surface chemical composition within the sample.

XPS measurement was performed with a VG ESCALAB 220iXL instrument with a monochromatic Al K(alpha) radiation (E = 1486.6 eV). The peak areas were determined after background subtraction and fitting with Gaussian-Lorentzian curves. From these peak areas, the amount of each component in the near surface region was calculated by division by the element-specific Scofield factor and the transmission function of the spectrometer.

2.2.5 Transmission electron microscopy (TEM)

The transmission electron microscope is mainly used to study the dispersion of metal or metal oxide and their composition and particle size on the catalysts can be determined by the implementation of additional techniques like EDX. In this technique, a high energetic electron beam is sent through a very thin sample (<50 nm) and the transmitted portion is focused by the objective lens into an image. The interactions between the electrons and the atoms can be used to observe features such as the crystal structure and can provide morphological information. In this study, TEM measurements were performed at 200kV with an aberration-corrected JEM-ARM200F (JEOL, Corrector: CEOS). The microscope was equipped with a JED-2300 (JEOL) energy-dispersive X-ray-spectrometer (EDXS) for chemical analysis. The aberration corrected STEM imaging (High-Angle Annular Dark Field (HAADF) and Annular Bright Field (ABF)) were performed under the following conditions. HAADF and ABF both were done with a spot size of approximately 0.13 nm, a convergence angle of 30-36° and collection of semi-angles for HAADF and ABF of 90-170 mrad and 11-22 mrad respectively. Preparation of the TEM sample: The solid samples were deposited without any pretreatment on a holey carbon supported Cu-Grid (300 mesh) and transferred to the microscope.

2.2.6 Raman spectroscopy

The fundamental principle of Raman spectroscopy is the inelastic scattering of electromagnetic radiation (photons) by molecules. Monochromatic radiation is used in the region of UV, VIS or NIR light. The interaction of monochromatic radiation causes an excitation of an electron from ground state and while returning to the original state they emit photons. In Raman scattering, the frequency of emitted photons is different from that of the initial monochromatic frequency. This difference in frequency provides the information about vibrational, rotational and other low frequency transitions in the molecules. In order for a sample to be Raman active, the vibrations in the molecule must be accompanied by a change in the polarizability of the molecule.

The Raman spectra were recorded using a fiber optical RXN-Spectrometer (Kaiser Optical System) equipped with a 10-400 mW diode laser for excitation at a wavelength of 785 nm and a Mk II Filtered Probe Head with a non-contact optics. The measurements were performed with 70 mW. The spectra were recorded with 3 accumulations and 3 s exposure time.

2.2.7 Ultraviolet-visible (UV-vis) spectroscopy

UV-vis spectroscopy is used to determine the absorbance spectra of a compound in solution or as a solid material. Basically, electromagnetic radiation in the form of light energy is absorbed by the sample, which excites electrons from ground state to the first singlet excited state. Interaction with incident light causes molecules to undergo vibrational

transitions and the shorter wavelength radiation with higher energy in the UV (200-400 nm) and visible (400-700 nm) range of the electromagnetic spectrum causes many atoms/molecules to undergo electronic transitions. UV-vis spectroscopy is also used to determine the coordination state of metal atoms. The UV-vis spectra of the solid samples were recorded using an AvaSpec 2048 fiber optic spectrometer (Avantes) equipped with an AvaLight-DHS light source and a FCR-7UV400-2-ME reflection probe.

2.2.8 Temperature-programmed desorption of ammonia (NH_3-TPD)

NH_3-TPD is a characterization technique used to determine the total number and strength of acid sites in solid material. In a typical procedure, the surface is saturated with ammonia at 100-120 °C, followed by removal of physisorbed ammonia and temperature programmed desorption at a specific heating rate and measuring the concentration of desorbed NH_3.

For the TPD experiments, the measurement was done using a Micromeritics Autochem II 2920 instrument. A 100 mg sample was loaded into a U-shaped quartz reactor and heated from room temperature to 400 °C with 10 K/min in He (50 ml/min) and held for 30 min at 400 °C (for the removal of adsorbed water), then cooled to 100 °C in a flow of He (50 ml/min). Then, the sample was exposed to an NH_3 (1% NH_3 in He) flow of 50 ml/min for 120 min at 100 °C, followed by removal of physisorbed NH_3 by means of helium flushing (50 ml/min) for 120 min at 100 °C. The sample was then heated to 800 °C at a heating rate of 10 K/min in flowing of He (50 mL/min). The temperature was held at 800 °C for 30 min. The analysis of the effluent gases was performed with Quadrupol mass spectrometer (Balzers Omnistar).

2.2.9 Pyridine Fourier transform infrared spectroscopy (Py-FTIR)

Pyridine-FTIR spectroscopy was used to distinguish Brønsted and Lewis acid sites on the surface of the solid material. Pyridine is used as probe molecule for adsorption because the vibrational bands for pyridinium ions formed at Brønsted acid sites and coordination complex at Lewis acid sites are well known. Quantification of acid site concentration can be obtained from band intensities in the spectrum and use of absorption coefficients [103].

The measurements in transmission mode were carried out on a Bruker Tensor 27 spectrometer equipped with a heatable homemade reaction cell with CaF_2 windows connected to a gas-dosing and evacuation system. The sample powders were pressed into self-supporting wafers with a diameter of 20 mm and a weight of 50 mg. Before pyridine adsorption, the samples were pretreated by heating in synthetic air to 300 °C for 10 min, subsequent cooling to room temperature and evacuation. Pyridine was adsorbed at room temperature by means of a carrier gas passing through a saturator filled with pyridine until saturation of sample surface. Then the reaction cell was evacuated to remove physisorbed

pyridine. The desorption of pyridine chemisorbed on acid sites was followed by heating the sample in vacuum to 300 °C and recording spectra every 50 ºC.

2.2.10 Inductively coupled plasma-optical emission spectroscopy (ICP-OES)

ICP-OES is a commonly used technique for the analysis of metals in various fields. It is a type of Atomic Emission Spectroscopy, where the sample at high temperature using inductively coupled plasma up to 8000-10000 Kelvin produces excited atoms or ionized ions. The excited atom emits a radiation when it goes back to ground state. The emitted characteristic electromagnetic radiation and intensities are measured optically by detectors. The intensity of the emission is used to evaluate the concentration of element within the sample.

For the determination of the elemental composition by means of ICP-OES technique, a Varian 715-ES ICP-Emission-Spectrometer was used. Approximately 20 mg of the sample were mixed with 8 ml of aqua regia and 2 ml of hydrofluoric acid. The digestion was performed in a microwave-assisted sample preparation system "MULTIWAVE" from Anton Paar/Perkin-Elmer at ~200 °C and ~65 bar pressure. The digested solution was filled up to 100 ml and analyzed. The data analysis was performed with the Varian 715-ES software "ICP Expert".

2.3 Experimental setup for catalytic activity test

Tests for glycerol acetylation were performed in the liquid phase using a batch stirred reactor and in the gas phase using a continuous fixed bed reactor. The experimental setups are described in this section.

2.3.1 Liquid phase setup

Liquid phase glycerol acetylation was performed in a three-necked 250 ml glass flask equipped with a fractionating Vigreux column, a modified Dean-Stark apparatus installed with thermometer (TI3) to measure the temperature of the boiling azeotropic mixture and a reflux condenser. The flask is also coupled with a glass tube with a thermocouple to monitor directly the temperature of the bulk reaction mixture (TI2). The reaction mixture was heated using an oil bath (150 °C, TI1) and both reaction mixture and oil bath was stirred using a magnetic stirrer (1200 rpm) for intensive mixing and to improve heat transfer. Typically the flask was charged with 10 g of glycerol (0.108 mol) and 39.16 g of acetic acid (0.652 mol), representing an acetic acid to glycerol ratio of 6/1, 60 g of toluene (0.652 mol) and 1 g of dodecane (internal standard to evaluate liquid volume change during the course of reaction). After heating the reaction mixture up to desired temperature, 500 mg of catalyst (ion exchange resin or supported HPA) were added. This is defined as starting time of the reaction. During the running test, samples of 100 µl volume were withdrawn periodically.

Moreover, homogeneous reaction with dissolved STA, TPA and PMA as well as a blank test in absence of any catalyst were carried out under similar reaction conditions. The total catalyst weight used in latter tests with pure HPA (0.1 g) was equal to the HPA load (20 wt%) in the supported catalysts to allow comparison of the results.

For proper quantification, highly polar compounds such as glycerol, MAG and DAG needed to be derivatized before their GC analysis. Derivatization of these compounds improves volatility and thus peak shape and sensitivity in the gas chromatographic analysis. In the present work, hydroxyl groups of glycerol and products MAG and DAG were derivatized using silylation procedure. In the typical procedure, 100 µl of product sample were silylated using hexamethyl disilazane (200 µl), trimethylchlorosilane (200 µl) and then mixed with pyridine as solvent and hexadecane as an internal standard (5wt% of hexadecane in pyridine) for GC analysis (2 ml). This means that two internal standards were used to cover the complete analysis procedure. The resultant product samples were kept at 70 °C in a drying oven for 45 min and then analyzed using a gas chromatograph (HP 5890 series II) equipped with a CP-Sil 13 CB column (25 m × 0.32 mm). The temperature program was as follows: 50 °C for 1 min hold, heating at 20 K/min to 310 °C, 2 min hold at 310 °C.

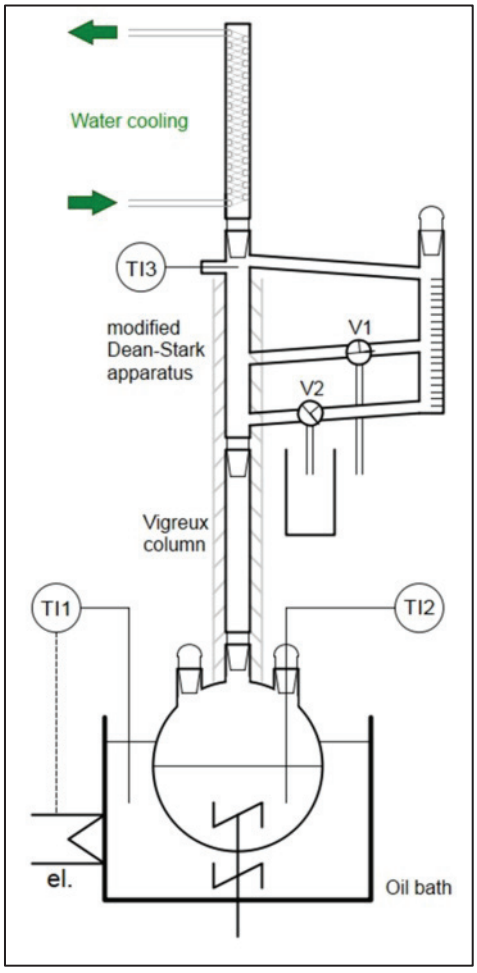

Figure 2.1. Scheme of reaction setup.

The feed glycerol and acetic acid along with the silylated products MAG, DAG and TAG were clearly eluted. Peak assignment and calibration of GC detector were carried out by means of authentic compounds that were prepared at high purity by fractionated distillation. For DAG, two isomers were detected in the chromatograms, but separation was incomplete and hence individual quantification was impossible. Diglycerol tetraacetate (DGTA) was prepared from linear diglycerol and acetic anhydride and product formation was confirmed by GC-MS combination equipped with HP-5 column (HP G1800 C, GCD Series II). The relative error of this analytical procedure was below 1%. All reported conversion data refer to glycerol. The conversion and selectivity (product distribution) were calculated based on the number of carbon moles with the following equations:

$$\text{Conversion} = \frac{\text{mole of glycerol consumed}}{\text{mole of glycerol fed}} \times 100\% \qquad \text{(eq. 2.3)}$$

$$\text{Selectivity} = \frac{\text{mole of C atoms in product}}{\text{total mole of C atoms in products}} \times 100\% \qquad \text{(eq. 2.4)}$$

2.3.2 Gas Phase setup

The glycerol acetylation tests were performed in a continuous flow system with a fixed-bed quartz reactor (length 15.5 cm, inside diameter 9.5 mm, volume 12.17 cm³) equipped with an internal guide tube (1 mm inner diameter) for a thermocouple to measure the axial temperature profile in the catalyst bed. The reactor was heated using an electrical furnace. The particle sizes of the catalysts were in the range of 315 to 500 µm. The reactor was filled sequentially with 2 g of quartz split, 0.5 cm quartz wool, catalyst bed, 0.5 cm quartz wool, 3 g of quartz split and finally 1 cm of quartz wool.

The acetic acid and glycerol solution of desired molar ratio was fed directly into the reactor using an HPLC pump (Gilson) with a flow rate of 0.025 ml/min together with N_2 inert gas (30 ml/min) and methane (1 ml/min). Nitrogen served as a carrier gas and dilutant for reactant and methane was used as internal standard to determine the volume change during the reaction in reactor passage. Methane remains inert at given reaction conditions. The flow rates of these gases were controlled by a mass flow controller (MFC, Bronkhorst). Due to high corrosiveness of hot acetic acid, most of the tubing were procured from corrosion-resistant material such as Teflon or Hastelloy C. In addition, due to high boiling point of glycerol and products, all downstream lines, including pressure regulator and sampling valve, were placed in a heated box (225 °C) to avoid condensation or polymerization. Experiments were performed at three different catalyst loads, i.e. 0.3 g, 0.6 g and 0.9 g and a standard reaction temperature program was used with five consecutive set-points at 225 °C, 250 °C, 255 °C, 300 °C and 325 °C.

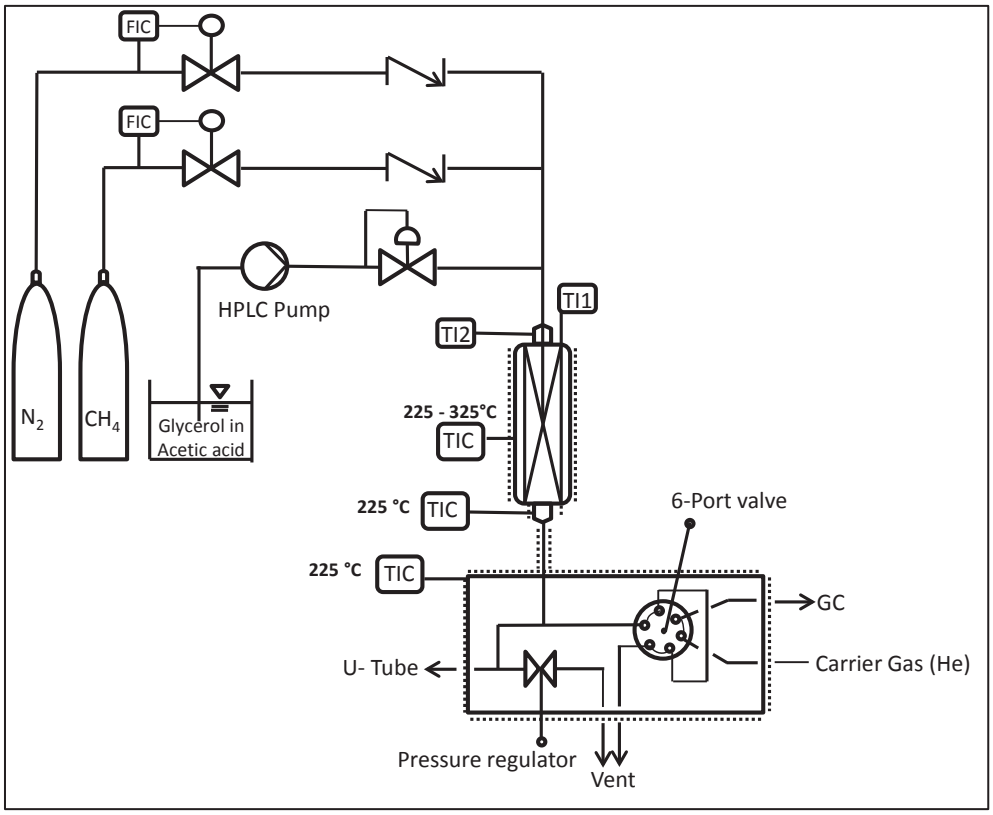

Figure 2.2. Scheme of gas-phase reaction setup.

Before the reaction, the catalyst was activated in N_2 flow at 225 °C for 1 h to remove physically adsorbed water and later the system was run underflow of reactant for 1 h to attain steady-state operation. The product gases were analyzed with an online GC (Shimadzu 17A) equipped with a switchable 6-port sampling valve (sampling loop volume = 58.54 µl), capillary column (Hewlett Packard HP-1, 30 m x 0.53 mm x 2.65 µm) and flame ionization detector (FID). The temperature of the column was held at 50 °C for 2 min, then increased to 290 °C with a rate of 15 K/min and held for 5 min. In selected case, gaseous samples were collected to check CO_x formation with another GC (Shimadzu GC 2010 Plus) equipped with thermal conductivity detector (TCD) and molecular sieve-capillary column. Moreover, the products were collected in a cold trap and the mass balance for every experiment was determined to check the performance of the system. In addition total organic carbon (TOC) analyzer (Shimadzu VCPN) was used to quantify total carbon content in liquid products. The conversion and selectivity (product distribution) were calculated based on the number of carbon moles in inlet and outlet stream with the following equations:

$$\text{Conversion} = \frac{\dot{\text{mole stream of glycerol consumed}}}{\dot{\text{mole stream of glycerol fed}}} \times 100\% \qquad \text{(eq. 2.5)}$$

$$\text{Selectivity} = \frac{\dot{\text{mole stream of C atoms in product}}}{\dot{\text{total mole stream of C atoms in products}}} \times 100\% \qquad \text{(eq. 2.6)}$$

3 Liquid phase glycerol acetylation

This chapter is divided into two sub-sections: the first sub-section shows the data obtained by using Amberlyst-15 (A15) and Amberlyst-70 (A70). In addition, the influence of reaction conditions such as acetic acid/glycerol molar ratio and catalyst nature has been studied. The fresh and spent catalysts were characterized by CHS elemental analysis. In the second sub-section, the performance of Keggin type heteropolyacid catalyst in glycerol acetylation with respect to structure and nature of acid sites was investigated. The fresh catalysts are characterized by BET surface area, XRD, Raman and py-FTIR spectroscopy and ICP-OES techniques. The spent catalysts were characterized by ICP-OES analysis and compared with fresh samples.

3.1 Batch operation - Ion exchange resins

3.1.1 Physical properties of the Amberlysts

The physical properties of the A15 and A70 are shown in Table 3.1. The thermal stability of A70 (190 °C) is higher than of A15 (120 °C), whereas, on the other side, the acidity and the surface area of A15 are higher than of A70. The acidity of the A70 was also measured by NaOH titration and confirmed the data from the supplier. The polymer matrix of A70 is chlorinated which makes it more thermally stable.

Table 3.1. Physical properties of the Amberlyst catalysts*.

Catalysts	Acidity (eq./kg)	Cross-linkage (%)	Particle size (mm)	Surface area (m²/g)	Average pore diameter (nm)	Thermal stability (°C)
A15	4.7	20	0.297-0.841	53	30	120
A70	2.55 2.80**	n.a.	0.500	36	22	190

* data were taken from the supplier and from data reported in [104].
**determined by titration with NaOH.

3.1.2 Catalytic activity of Amberlysts

3.1.2.1 Glycerol acetylation without water removal

Glycerol acetylation is a consecutive reaction with stepwise formation of MAG, DAG and TAG and their respective isomers wherein at each step, water is formed as an unavoidable by-product. In the presence of water, each reaction step is equilibrium controlled, which limits the maximum selectivity for TAG. This was observed when an experiment was performed with A70 without removal of water (simple reflux system) using toluene as an entrainer. The conversion of glycerol was almost complete (97.9%) after 10 h with maximum selectivity to DAG (58.8%), however, selectivity to MAG and desired TAG were rather low with 23.6% and 18.3%, respectively. After 24 h, selectivity for TAG increased to 29.2% with a decrease in selectivity of MAG as 15.7%, whereas DAG selectivity remained nearly the same (54.5%). This proved that presence of water in the reaction mixture inhibits the formation of TAG (See Figure 3.1).

It is important to understand that the reaction mixture of glycerol, acetic acid and toluene is biphasic at room temperature. However, good homogenization of the mixture at the beginning of reaction was achieved when the stirring speed was set to 1200 rpm. As the temperature of the mixture enhanced up to 100 °C, the reaction mixture became clearly homogeneous.

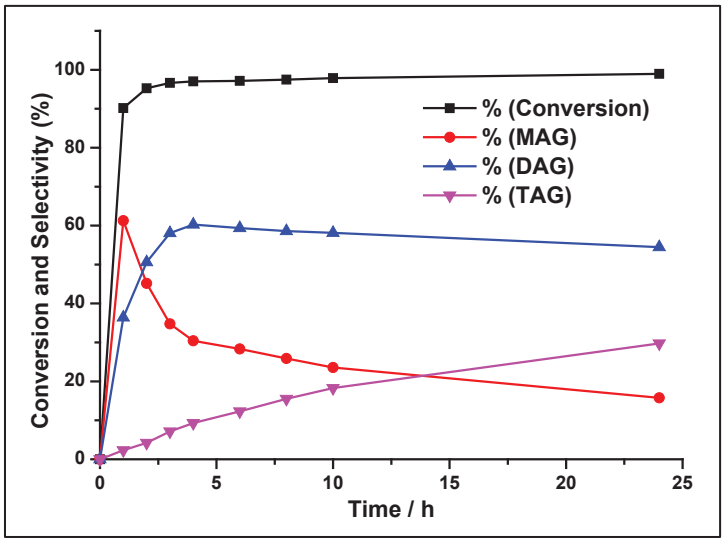

Figure 3.1. Glycerol conversion and selectivity to MAG, DAG and TAG without water removal over A70, i.e., reflux conditions (glycerol = 10 g, acetic acid = 39.16 g, catalyst = 0.5 g, molar ratio acetic acid: glycerol = 6:1, toluene = 60 g, T = 105 °C).

3.1.2.2 Glycerol acetylation with water removal

The selectivity of TAG can be increased by shifting the chemical equilibrium towards the products either by using one reactant in excess or by removing one of the products during the reaction. Hence, continuous removal of water can force the chemical equilibrium towards the desired product. In addition, an excess of acetic acid helps to enhance TAG selectivity, as the glycerol becomes the limiting reactant which can be consumed completely at end of reaction. This might be beneficial for work-up; however, too large excess makes the process less economic.

When the reaction was carried out in the absence of a catalyst (blank test Fig 3.2) under the mentioned reaction conditions, glycerol conversion was more than 50% within 4 h and MAG was the dominant product with a selectivity of 85%. DAG formed in small quantity with a selectivity of 15%. This conversion is most likely due to the presence of an acetic acid which acts as a homogeneous acid catalyst. Table 3.2 shows the glycerol conversion and product selectivities for the reaction time of 4 h.

In the first hour, selectivity of MAG is almost 100% at nearly 25% glycerol conversion. But with time, the selectivity of MAG drops and selectivity of DAG as the consecutive product increases whereas TAG formation was not observed. The use of A15 and A70 resulted in complete conversion of glycerol after 4 h with selectivity for TAG of 44.3% and 45.8%, respectively (see Table 3.2). However, still the DAG was the major product with selectivities of 54.2% and 51.7% over A15 and A70, respectively, whereas selectivities to MAG were rather low (1.5% and 2.5%, respectively).

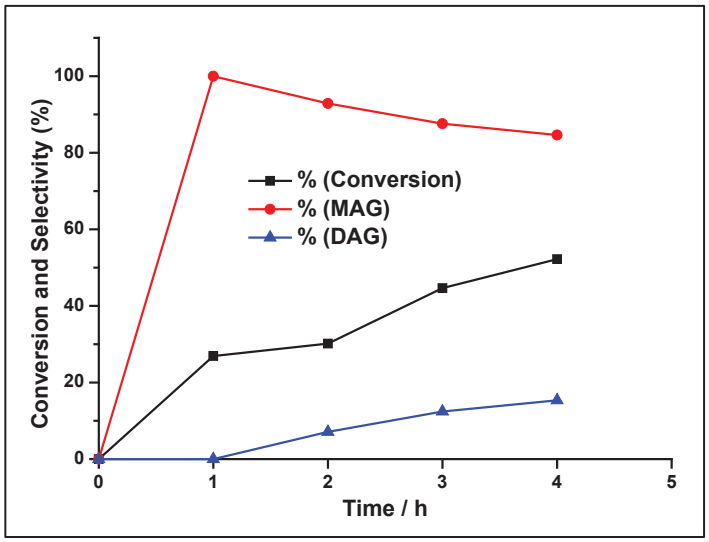

Figure 3.2. Glycerol conversion and selectivity to MAG and DAG in blank test with water removal glycerol =10 g, acetic acid = 39.16 g, molar ratio acetic acid: glycerol = 6:1, toluene = 60 g, T = 105 °C)

Table 3.2. Catalytic activity of Amberlyst catalysts in glycerol acetylation using toluene as an entrainer.

Catalysts	Reaction time (h)	Conversion (%)	Selectivity (%)		
			MAG	DAG	TAG
Blank test	4	52	85	15	0
A15	4	100	1.5	54.2	44.3
A70	4	100	2.5	51.7	45.8

(glycerol = 10 g, acetic acid = 39.16 g, toluene = 60 g, catalyst = 0.5 g, T = 105 °C)

Glycerol acetylation is an acid catalyzed reaction and acid strength of the catalyst plays an important role for the catalytic activity and selectivity. Theoretically, one can consider a Fischer esterification mechanism running in this reaction (see Figure 3.3) [64]. In the first step, a proton is added to the carbonyl carbon of acetic acid which creates positive charge on the carbonyl carbon. This facilitates the nucleophilic attack of hydroxyl group from glycerol to produce MAG and thereby eliminating water as a by-product. In a similar way DAG and TAG are formed in consecutive steps. In this work, formed water was continuously removed from the reaction mixture using toluene as entrainer by means of azeotropic distillation. Toluene can form an azeotropic mixture with water at 84 °C as well as with acetic acid at 104 °C, thus, the two azeotropic mixtures indicate the boiling point of the reaction mixture during the course of reaction due to their proportions [105]. Toluene as an entrainer is very efficient as its azeotropic mixture contains up to 20% of water. Karl Fischer-titration technique was used to determine the water concentration in the reaction mixture and after 2 h water concentration was less than 0.05% (almost negligible). The fast glycerol conversion and high selectivity to TAG is ascribed to the acidity of the catalysts as well as continuous removal of water (kinetic and thermodynamic effect).

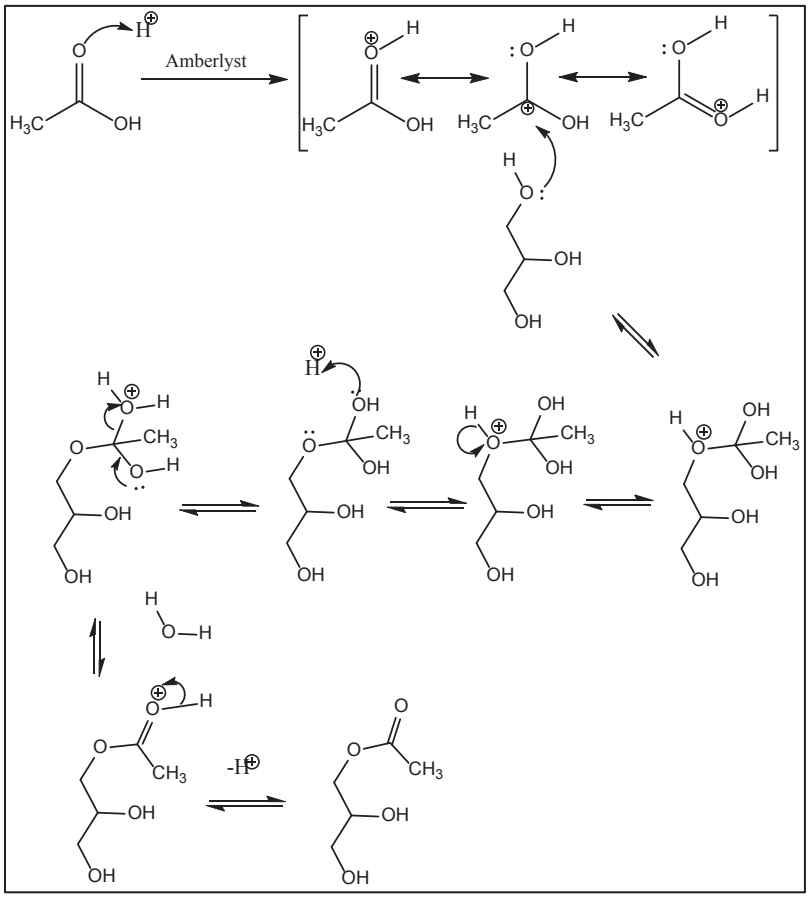

Figure 3.3. Fischer esterification mechanism of glycerol with acetic acid to produce MAG [65].

3.1.2.3 Reaction progress monitoring

The reaction was monitored for 24 h with both catalysts A15 and A70 under identical reaction conditions to study the change in selectivity pattern with time under continuous water removal (See Figure 3.4). As expected, the reaction proceeded in a consecutive manner, as the desired TAG selectivity increased continuously together with a decrease in DAG and MAG selectivities with time. The complete conversion of glycerol on both catalysts was observed within first 2 h of reaction; both the conversion curves look very similar (see Figure 3.4). After 2 h, MAG and DAG were main products. After 10 h, the selectivity of TAG increased to 83.9% and 87.6% and after 24 h it reached 94.1% and 95.3% using A70 and A15, respectively. The use of toluene as an entrainer successfully enhances more or less quantitative formation of the desired TAG. Interestingly, during the course of reaction (i.e. after 4 h) a new by-product diglycerol tetraacetate (DGTA) was observed. The formation of DGTA was confirmed by GC-MS using authentic compound prepared from diglycerol and acetic acid. DGTA can be formed by two different reaction pathways, etherification (oligomerization) and esterification, both forming water and being controlled by chemical equilibrium as shown in Figure 3.5.

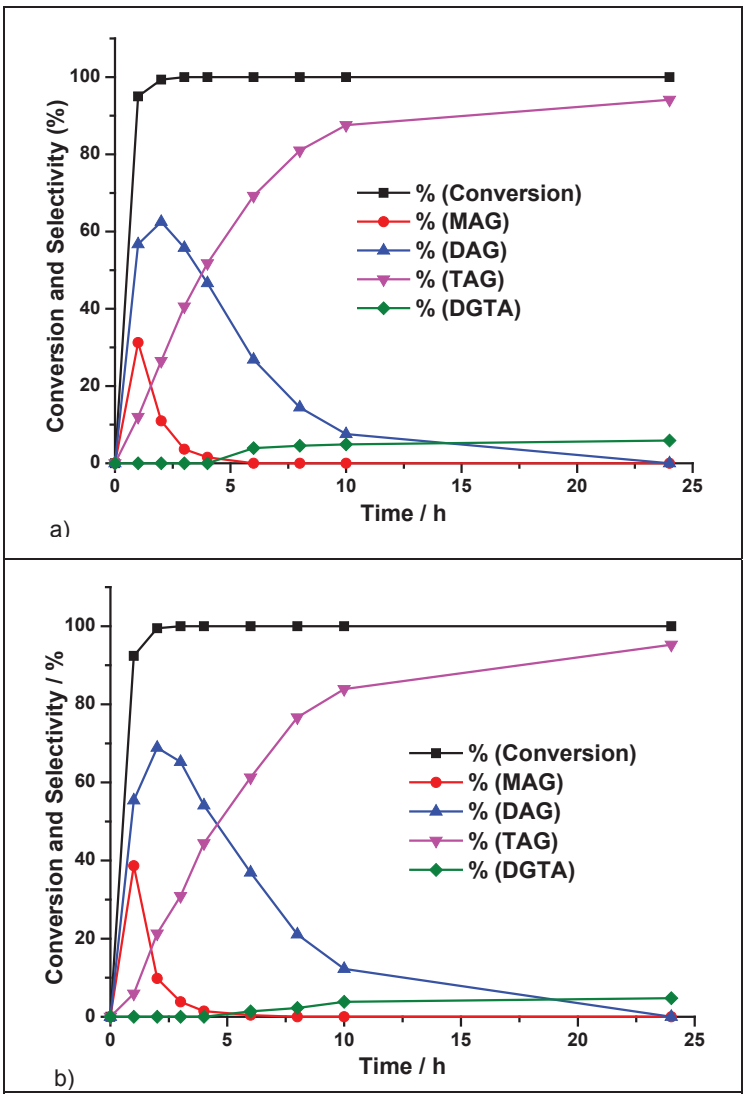

Figure 3.4. Conversion of glycerol and selectivities to products with (a) A70 and (b) A15 during 24 h of reaction (glycerol = 10 g, acetic acid = 39.16 g, molar ratio acetic acid: glycerol = 6:1, toluene = 60 g, catalyst = 0.5 g, T = 105 °C).

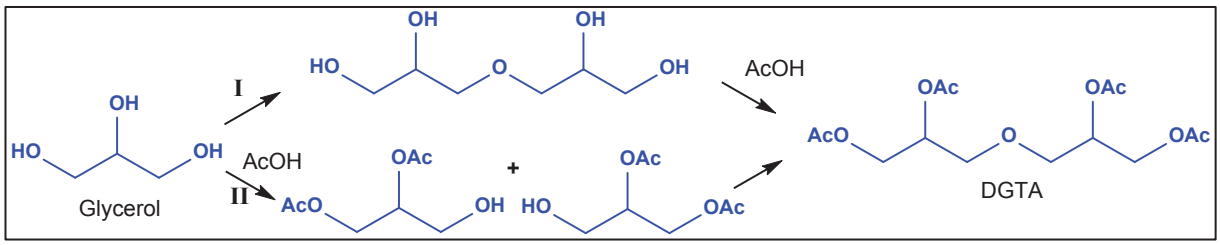

Figure 3.5. Possible ways to form diglycerol tetraacetate (DGTA).

Generally, etherification of glycerol is performed at a much higher temperature in the presence of strong acid catalyst [40]. Due to the rather low reaction temperature (ca. 100 °C), it is unlikely to transform glycerol into its dimers in parallel. Moreover, diglycerol formation was not observed in GC analysis. According to the esterification reaction sequence, first significant amount of MAG will form from glycerol and acetic acid (while water

is continuously removed by azeotropic distillation). Later, DAG is produced immediately as a consecutive product of MAG and acetic acid. However, it can be clearly seen from Figure 3.4 that formation DGTA is significant only when DAG is available in high concentration in the reaction mixture. Therefore, DAG is the most probable precursor for DGTA formation. Moreover, two different oligomerization experiments under identical conditions at 140 °C in the absence of water proved that the rate of reaction of DAG towards DGTA was higher than that of glycerol to diglycerol. However, during glycerol acetylation in the presence of water at high glycerol conversion, the formation of DGTA is not observed, suggesting that DGTA is favourably formed in the water-free process. According to the literature, this is the first report on the formation of DGTA under water-free reaction conditions. DGTA has applications in cosmetics, food industries [106] and is used in the preparation of filter material [107].

At the beginning of reaction monitoring experiments, the temperature of the reaction mixture was 100 °C for the first hour as measured on the top of the modified Dean-stark apparatus (Figure 2.1 TI3). As the reaction proceeded, the temperature of the reaction mixture increased to 105 °C which remained nearly constant for the longest period of reaction time. The maximum temperature of 110 °C (boiling point of toluene) was reached when the overall rate of esterification declined (due to low residual glycerol concentration) and little water was available to establish the first azeotropic mixture. Thus, the large fraction of acetic acid is utilized to form the second azeotropic mixture with toluene.

Interestingly, the different solid properties of A15 and A70 did not lead to a significantly different catalytic performance in glycerol acetylation. This was confirmed by repeated experiments. The surface area and the acid sites concentration of A15 are higher; one can conclude that the strength of the acid sites on A70 must be higher to obtain same activity as A15. Furthermore, one has to consider that the Amberlyst resins might swell during reaction in the presence of polar solvent, especially acetic acid and water. The swelling of resins will change the accessibility of acid sites [108, 109]. In addition, the non-polar interaction of toluene with acetic acid and glycerol can affect the catalysts reactivity. As a result, not only the acid properties influence the reaction but also the accessibility of acid sites to reactants is an important factor [110]. An additional experiment was performed with lower catalyst amount of 50 mg (10 times lower than before) to evaluate the catalytic activity of A15 and A70 at lower reaction rate under identical reaction conditions with removal of water during the course of reaction. As expected, conversion of glycerol did not achieve complete conversion even after 10 h. However, even at lower reaction rate far away from equilibrium, there was no significant difference between conversion curves of A15 and A70 as shown in Figure 3.6. Regarding the fact that the reaction mixture was homogeneous and the mesoporous nature of the catalyst, the impact of external or internal mass transfer should be negligible.

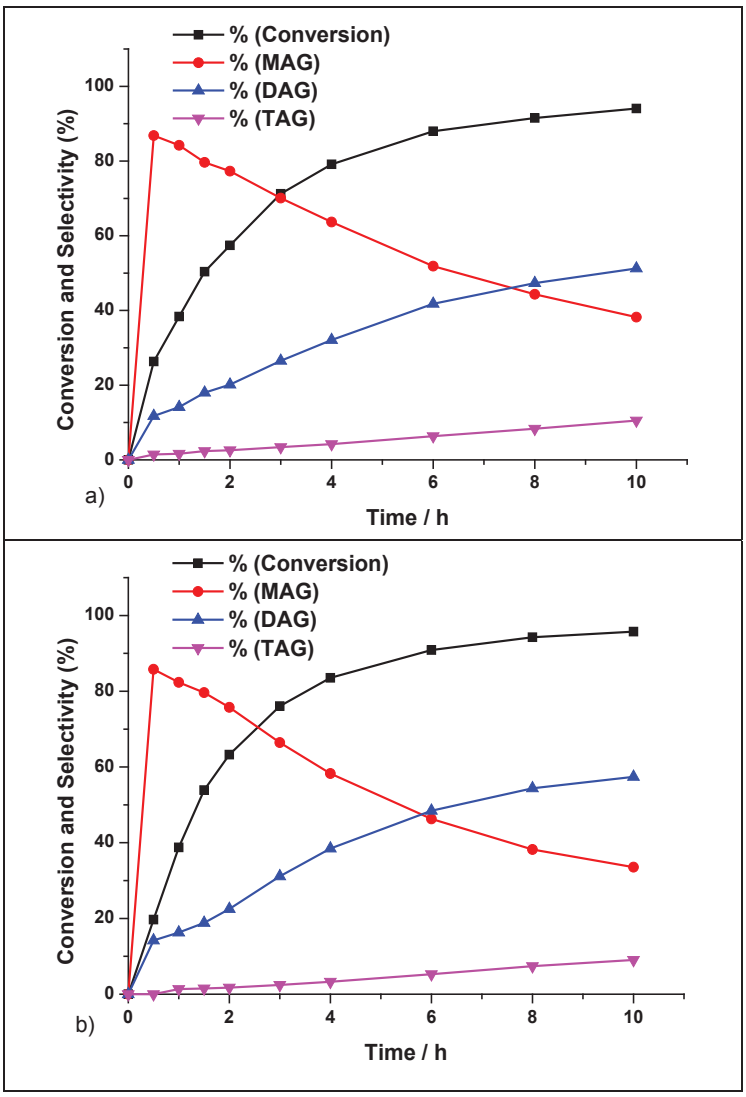

Figure 3.6. Conversion of glycerol and selectivities to products with (a) A70 and (b) A15 during 10 h of reaction at low catalyst loading (glycerol = 10 g, acetic acid = 39.16 g, molar ratio acetic acid: glycerol = 6:1, toluene = 60 g, catalyst = 50 mg, T = 105 ˚C).

3.1.2.4 Catalyst stability, reusability and homogeneous catalysis test

Reusability experiments were performed with A15 and A70 catalysts. After the reaction (10 h), the catalyst was recovered by filtration, washed thoroughly with toluene, dried at 110 °C and reused with fresh reactants. As shown in Figure 3.7, it is evident that conversion of glycerol was maintained at 100% in all recycling tests. However, a decrease in selectivity was observed for both the catalysts. There was a significant decrease in TAG selectivity from 85.4% to 54.7% after the 3rd run for A70 and from 83.9% to 38.4% after the 2nd run for A15, indicating catalyst deactivation under reaction conditions. Moreover, after 1st run A15 started to break down into fine particles, may be due to low thermal stability (120 °C) even though reaction temperature was below the thermal stability limit; another possibility is mechanical

stress on the catalyst during stirring, as the reaction mixture was slurry of the catalyst. In contrast, the observed extent of catalyst swelling is comparatively small. Dumesic and co-worker reported that polymer resin in the presence of water suffered from swelling which ultimately deactivated the catalysts [111]. However, in the present water-free process, the use of toluene lowered the overall polarity of the reaction mixture and suppressed the effect of swelling. Apart from mechanical breakdown and swelling, the catalysts may also deactivate due to the leaching of active surface species (sulfonic acid group) and/or due to the blockage of active surface species by carbonaceous compounds.

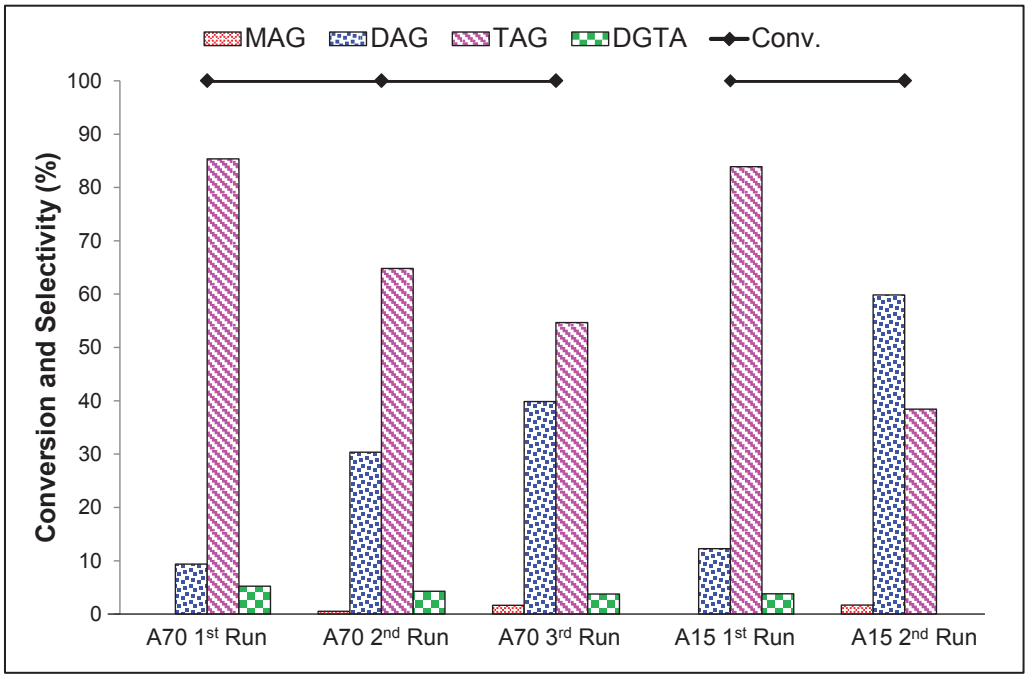

Figure 3.7. Conversion of glycerol and selectivities to products with (a) A70 and (b) A15 after 10 h of reaction in reusability tests (glycerol = 10 g, acetic acid = 39.16 g, molar ratio acetic acid: glycerol = 6:1, toluene = 60 g, catalyst = 50 mg, T = 105 ˚C).

To confirm this, carbon, hydrogen and sulfur content in the fresh and spent catalysts were determined (Table 3.3). The sulfur content of the catalysts decreased from 14.0% to 10.7% in case of A15 (after 2nd run) and from 8.2% to 6.6% in case of A70 (after 3rd run). This might be due to the hydrolysis of sulfonic groups of the polymer support by traces of water or due to the low thermal stabilities [112]. Moreover, titration of fresh and spent A70 with NaOH from regular experiment after 4 h exhibited a loss of acidity from 2.80 to 2.52 mmol/g. Consequently, sulfur was also found in the liquid reaction mixture. The loss in sulfur from A15 is more than from A70 because the latter is chlorinated which increases the bond strength between polymer and sulfonic acid group which in further increases acid strength and stability [113].

Table 3.3. Elemental CHS analysis of fresh and spent A15 and A70 catalysts.

Catalysts	Element fractions		
	C (wt%)	H (wt%)	S (wt%)
A15-fresh	41.5	5.7	14.0
A15-2nd run	44.4	5.7	10.7
A70-fresh	36.8	4.3	8.2
A70-3rd run	41.9	5.2	6.6

Moreover, chlorine analysis by potentiometric titration of liquid product showed that there was no leaching of chlorine from A70. As a consequence, the possible contribution of leached sulfur species to homogeneous catalysis had to be checked. For this, a separate stop experiment was performed at identical conditions. In a regular experiment after 2 h, selectivities to MAG, DAG and TAG were 14%, 63% and 23%, respectively, at complete conversion of glycerol. At this point, the catalyst was removed from the reaction mixture and the run was continued for another 8 h without any catalyst; meanwhile the selectivities to MAG, DAG and TAG did not change significantly. After 8 h, selectivities to MAG, DAG and TAG were 10%, 62% and 28%, respectively, which proved that leached sulfur species are not able to catalyze the consecutive reaction towards TAG.

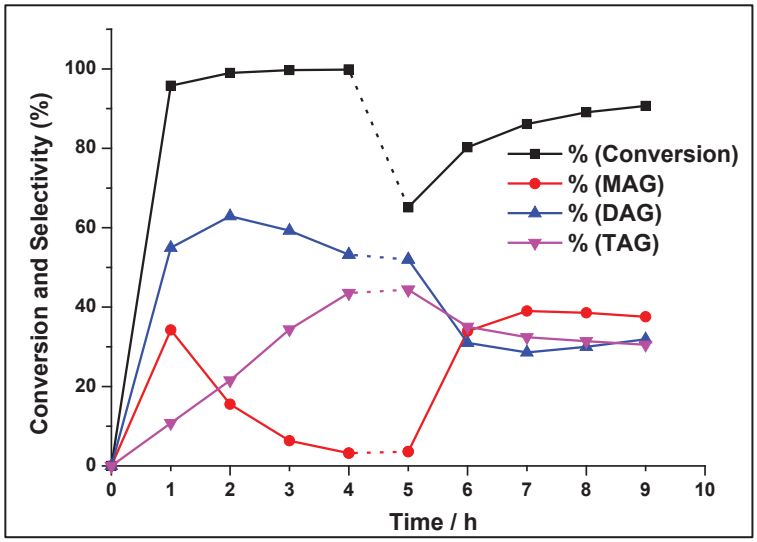

Figure 3.8. Conversion of glycerol and selectivities to products over 0.5 g A70 in a stop-experiment (reaction conditions as described in Figure 3.7; catalyst was removed after 4 h and the run was continued for further 4 h without catalyst; the dotted lines mark the time span for catalyst removal and addition of fresh feed (glycerol = 5 g, acetic acid = 19.56 g)).

Another stop experiment was performed under identical conditions where the catalyst was removed after 4 h, followed by addition of fresh acetic acid/glycerol to the reaction mixture. The reaction was run for additional 4 h under the same reaction conditions without a catalyst. Interestingly, the conversion of glycerol and product selectivities (DAG and MAG) increased

slowly. However, the slopes of the glycerol conversion and selectivity curves resemble those obtained in blank test (Figures 3.8 and 3.1). From these experiments, one can presume that the leached sulfur species do not contribute to the reaction in a homogeneously catalyzed way. Dosuna-Rodriguez and Gaigneaux observed the same feature that the leached species do not show any catalytic activity in a homogeneous way [63]. Besides leaching of sulfur, adsorption of some carbonaceous material on the surface of catalysts was also observed. The spent Amberlyst resins were analyzed and the amount of carbon in solid material increased from 41.6% to 44.3% in case of A15 (after the 2nd run) and from 36.9% to 41.9% in case of A70 (after the 3rd run) (sees Table 3.3). This relative increase outnumbers the theoretical increase of carbon content related to sulfur loss and clearly indicates surface deposits. The deposited carbonaceous material may be in the form of esters, oligomers or polymers which probably block the surface acid sites, i.e. the sulfonic acid groups. Similar behaviour was also recognized by Cara et al. for xylane (hemicellulose) hydrolysis using A70 as catalyst [114].

3.1.2.5 Influence of reaction conditions

The A70 catalyst was found to be more stable than A15 in the reusability test and moreover, showed the best efficiency in glycerol acetylation with 100% conversion and almost 94% selectivity to TAG in 24 h. Hence, the influence of reaction conditions such as acetic acid: glycerol molar ratio and catalyst: glycerol weight ratio were studied with A70 and the results are shown in Figure 3.9 (always with fresh samples).

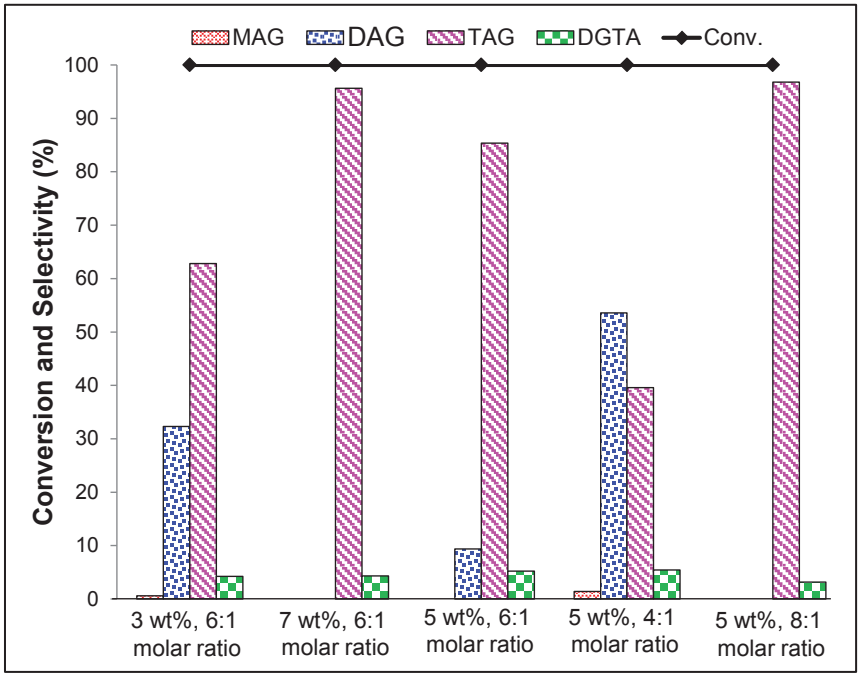

Figure 3.9. Conversion of glycerol and selectivities to products over A70 and after 10 h at named reaction conditions (glycerol = 10 g, acetic acid = 39.16 g, molar ratio acetic acid: glycerol = 4:1-8:1, toluene = 60 g, catalyst = 0.3-0.9 g, T = 105 ˚C).

The conversion of glycerol reached 100% within 3 h at every defined reaction condition, even though the acetic acid: glycerol ratio was lowered to 4:1. When acetic acid to glycerol molar ratio increased from 4: 1 to 8: 1 at a constant catalyst: glycerol ratio of 5 wt%, TAG selectivity rose from 40% to 97% after 10 h. Maximum selectivity to TAG after 10 h was 96.8% along with 3.2% DGTA using 8: 1 acetic acid: glycerol molar ratio and 5 wt% catalyst with respect to glycerol. Similarly, increasing the catalyst loading gradually from 3 wt% to 7 wt% (0.3 g, 0.5 g and 0.7 g) with respect to the weight of glycerol at constant acetic acid to glycerol molar ratio (6: 1), the TAG selectivity increased considerably. At 3 wt% catalyst loading, TAG and DGTA selectivities were 62.8% and 4.2% which rose to 95.6% and 4.3% with 7% catalyst loading after 10 h. The influence of reaction conditions showed a significant effect on TAG selectivity, but the DGTA selectivity was not affected. However, the formation of DGTA is significant when DAG is present in high concentration in the reaction mixture, as observed in the long term test (Figure 3.4).

3.1.3 Kinetic consideration about TAG production

3.1.3.1 Models for liquid phase glycerol acetylation

Model A – pseudo-homogeneous with no side reactions:

Acetylation of glycerol is a consecutive reaction, and the difference between these models regard parallel reactions that also take place as glycerol is converted.

A first model for the kinetics of triacetin formation may be described as follows:

$$G + AA \xrightarrow{k_1} MAG + H_2O \quad \text{(eq. 3.1)}$$

$$MAG + AA \xrightarrow{k_2} DAG + H_2O \quad \text{(eq. 3.1)}$$

$$DAG + AA \xrightarrow{k_3} TAG + H_2O \quad \text{(eq. 3.1)}$$

Where, G is glycerol, AA is acetic acid, MAG is monoacetyl glycerol, DAG is diacetyl glycerol, TAG is triacetyl glycerol, and k_1, k_2, and k_3 are the rate constants of the forward reactions.

This model was first proposed in detail by Gelosa et al. [115] and was applied with little modification by Hasabnis and Mahajani [71] and Hung et al. [116]. The model presented by Gelosa et al. is a LHHW (Langmuir-Hinshelwood-Hougen-Watson) kinetic model based on multicomponent adsorption equilibria, and relies on parameters that are estimated from equilibrium experiments. Nonetheless, this approach offers some limitations, provided that only the parameters relative to water, glycerol, acetic acid and TAG can be estimated by fitting the equilibrium data, leaving aside MAG and DAG, which have to be guessed [115].

Fortunately, based on the number of hydroxyl groups, estimated parameters for MAG and DAG adsorption should lie between glycerol and TAG. It is also known that mass transfer and equilibrium greatly hamper the kinetic evaluation, since the selectivity towards TAG is very low in the works using this approach [71, 115, 116].

By changing the conditions of the reaction, mass transfer and equilibrium limitations in the formation of TAG may be greatly overcome, and a straightforward homogeneous consecutive kinetic model can be advanced [64]. This entails that apparent k_1, k_2, and k_3 will suffice to describe the reaction behavior, leaving adsorption equilibria out of the model. Although it may firstly seem that there are too many approximations, the final model perfectly describes the reaction dynamics for conditions away from equilibrium. Moreover, there is no estimation of thermodynamic parameters necessary for the kinetic model, but only the number of constants sufficient for describing the concentrations of the products. From the recent catalytic results (section 3.1.2) [117], it is observed that glycerol esterification can be undertaken in conditions that shift the equilibrium in the direction of the formation of TAG, with total conversion of glycerol and high TAG selectivity (95%). To guarantee that the reaction conditions are far from equilibrium, at total glycerol conversion, two experimental conditions have to be assured: 1) water must be stripped from the reaction medium by use of an adequate solvent entrainer that does not interfere with the reaction; and 2) acetic acid must be present in abundance, in order to consider glycerol the limiting reagent. Thus, the apparent kinetic rates $k'_{a,k}$ can be expressed as a function of the consumption of glycerol, MAG, and DAG. Through these considerations, Zhou et al. [64] have neglected backward reaction and proposed the following set of differential equations:

$$\frac{dc_G}{dt} = -k_{a,1}c_G \qquad \text{(eq. 3.4)}$$

$$\frac{dc_{MAG}}{dt} = k_{a,1}c_G - k_{a,2}c_{MAG} \qquad \text{(eq. 3.5)}$$

$$\frac{dc_{DAG}}{dt} = k_{a,2}c_{MAG} - k_{a,3}c_{DAG} \qquad \text{(eq. 3.6)}$$

where $k_{a,k}$ is the apparent kinetic rate constant for compound k. The consideration of less parameter simplifies the problem and gives robustness to the model. Considering the initial condition that only glycerol is present with a concentration $c_{G,0}$ at t_0, exact solutions to the differential equations are the following:

$$c_G = c_{G,0}e^{-k_{a,1}t} \qquad \text{(eq. 3.7)}$$

$$c_{MAG} = \frac{k_{a,1}c_{G,0}}{k_{a,2} - k_{a,1}}(e^{-k_{a,1}t} - e^{-k_{a,2}t}) \qquad \text{(eq. 3.8)}$$

$$c_{DAG} = \frac{k_{a,1}k_{a,2}c_{G,0}}{k_{a,2} - k_{a,1}}\left(\frac{e^{-k_1 t} - e^{-k_3 t}}{k_{a,3} - k_{a,1}} - \frac{e^{-k_{a,2}t} - e^{-k_{a,3}t}}{k_{a,3} - k_{a,2}}\right) \quad \text{(eq. 3.9)}$$

The expression for C_{TAG} may be obtained by considering the total molar balance to be:

$$c_{TAG} = c_{G,0} - (c_G + c_{MAG} + c_{DAG}) \quad \text{(eq. 3.10)}$$

Model B – pseudo-homogeneous considering dimerization as side reaction:

The previously presented model A is very useful and clear. However, as reported in the previous section (section 3.1.3.3) and reported work [117], DGTA is formed through etherification of DAG, and its production competes with esterification. Thus, the model of consecutive reactions for TAG production must be changed to accommodate the competing reactions forming of DGTA and TAG. Therefore, a second model (B) can be presented as mere introduction of side reaction (eq. 3.11).

$$2DAG \xrightarrow{k_4} DGTA + H_2O \quad \text{(eq. 3.11)}$$

The equations describing glycerol conversion and MAG concentrations are the same as eq. 3.4 and 3.5, plus the later one describing the DAG concentration regarding the dimer formation.

$$\frac{dc_{DAG}}{dt} = k_{a,2}c_{MAG} - k_{a,4}{c_{DAG}}^n - k_{a,3}c_{DAG} \quad \text{(eq. 3.12)}$$

$$\frac{dc_{DGTA}}{dt} = k_{a,4}c_{DAG}^n \quad \text{(eq. 3.13)}$$

Some difficulties arise from including eq. 3.8 and eq. 3.9 in this new model, because of the value for the constant *n*. A typical dimerization reaction would be expected to behave in a second order kinetics [118] and reasonable values for *n* should include or lie between 0 and 2. For *n* = 2, eq. 3.12 is transformed into a nonlinear differential equation, commonly known as the Riccati equation [119]. Leaving aside some mathematical complications that arise from a model with *n* = 2, it should be noted that the dimerization in the present model is a side reaction, with an experimental rate much lower than the formation of TAG. By using *n* = 1, one considers that the production of DGTA requires a variation of a first order dependence on DAG concentration, as happens to the other reactions in the system. However, fits using this approach were not the best.

In conditions of reactant excess, the amount of adsorbed reactants that occupy the surface of a heterogeneous catalyst limits the reaction rate, and may alter profoundly the intrinsic reaction order. It has been observed that a pseudo-zeroth order kinetic fit agrees with such limitations for different cases [120-122]. In the present work, the parallel reaction

for dimerization depends only on the amount of adsorbed DAG. This adsorbed DAG, however, is exposed to an excess of AA, which reacts with DAG at a higher rate than DAG reacts with itself. In other words, it is far more likely for a DAG molecule to find an AA molecule beside it than another DAG or MAG molecule. Therefore, the dimerization and other side reactions should depend much less on the concentration of any given compound, but rather on the available catalyst sites. Assuming *n* = 0, eq. 3.12 and 3.13 then become:

$$\frac{dc_{DAG}}{dt} + k_{a,3}c_{DAG} = k_{a,2}c_{MAG} - k_{a,4} \quad \text{(eq. 3.14)}$$

$$\frac{dc_{DGTA}}{dt} = k_{a,4} \quad \text{(eq. 3.15)}$$

The respective solutions are:

$$c_{DAG} = \frac{k_{a,1}k_{a,2}c_{G,0}}{k_{a,2} - k_{a,1}}\left(\frac{e^{-k_{a,1}t} - e^{-k_{a,3}t}}{k_{a,3} - k_{a,1}} - \frac{e^{-k_{a,2}t} - e^{-k_{a,3}t}}{k_{a,3} - k_{a,2}}\right) - \frac{k_{a,4}c_{G,0}}{k_{a,3}}(1 - e^{-k_{a,3}t}) \quad \text{(eq. 3.16)}$$

$$c_{DGTA} = k_{a,4}t \quad \text{(eq. 3.17)}$$

The molar balance can again be used to calculate the concentration of TAG and the yield:

$$c_{TAG} = c_{G,0} - (c_G + c_{MAG} + c_{DAG} + 2c_{DGTA}) \quad \text{(eq. 3.18)}$$

3.1.3.2 Results and discussion

Nonlinear regression was done using the maximum likelihood methodology through an algorithm specifically written for that purpose with the software Scilab and was also cross-checked with Polymath 6.1 (student version), for least squares nonlinear regression. For deeper understanding of underlying mathematics used on the maximum likelihood method and its applications in kinetic models, the reader is referred to seminal previous applications of this method regarding kinetic fits [123- 127], as well as other problems [128, 129]. Figure 3.10 shows the formation of DAG and TAG over A15 and A70 in the liquid phase, and the respective fits for models A and B, and Table 3.4 shows the values of the apparent kinetic constants obtained from the nonlinear regression in a 95% confidence interval. The difference between the fitted models and the experimental results is subtle.

Table 3.4. Values for the apparent reaction rate constants for A15 and A70.

k_k*	Unit	A15		A70	
		Model A	Model B	Model A	Model B
k_1	min^{-1}	155.37	91.07	332.51	96.95
k_2	min^{-1}	87.29	143.21	166.06	138.45
k_3	min^{-1}	12.71	12.50	14.55	15.54
k_4	min^{-1}	-	0.18	-	0.19

*Experimental conditions: acetic acid: glycerol = 6:1, T = 105 °C; Entrainer: toluene, t = 24 h.

Very little is changed at the beginning of the reaction, but there is an increasing gap towards the end of the reaction, since model A was developed considering no side reactions, and model B agree better with the actual experimental results, as seen in Figure 3.9. A limitation of the experiments impedes the assessment of the models for other temperature, since the reaction is conducted with toluene as an entrainer. This means the reaction temperature is stabilized at 105 °C, around the boiling temperature of toluene (110 °C).

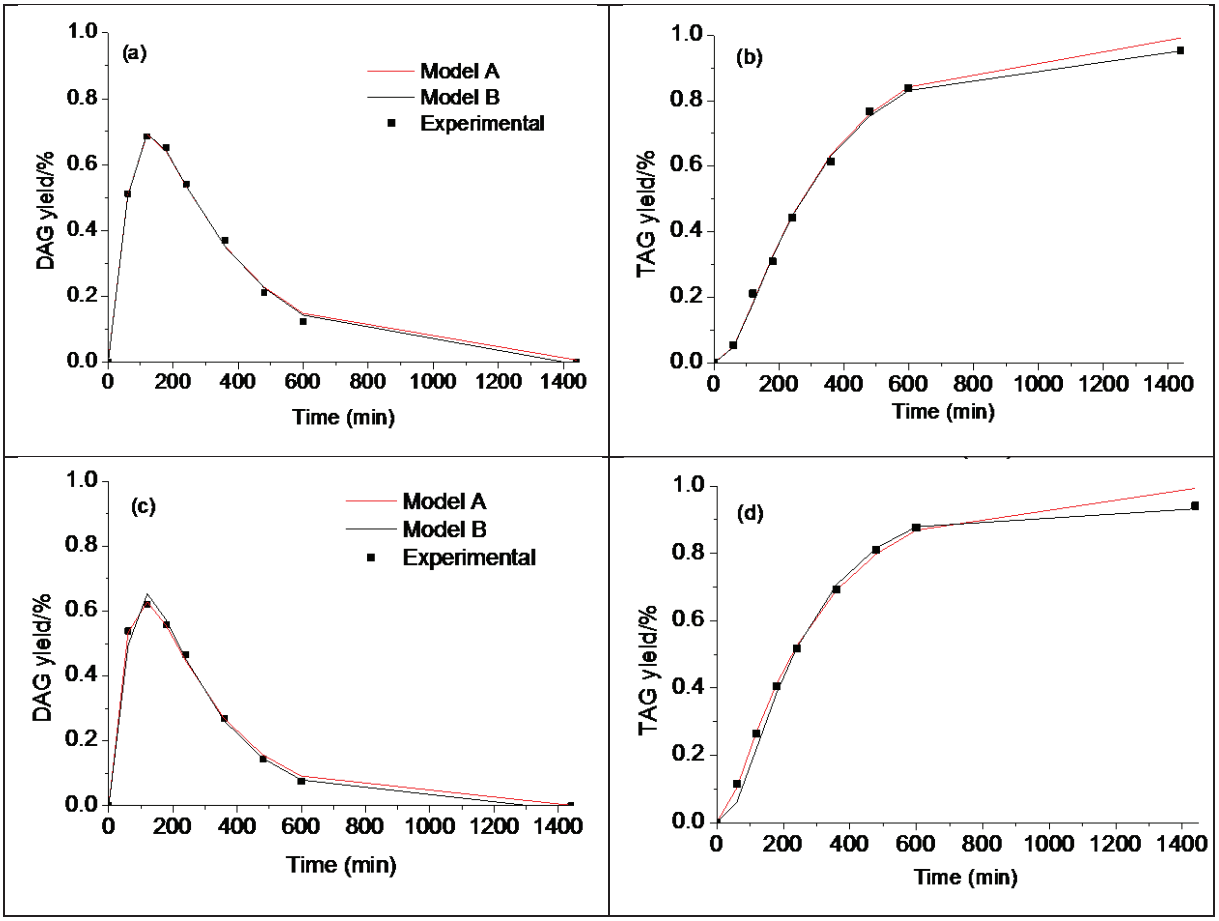

Figure 3.10. Experimental data for DAG and TAG production with A15 ((a) and (b)) and A70 ((c) and (d)) and fits for models A and B (Reaction conditions: as shown in Figure 3.4).

3.1.4 Summary and conclusions

Acetylation of glycerol was performed on ion exchange resins in the presence of toluene as an entrainer in slurry phase using a batch reactor. The use of entrainer with continuous removal of water exhibited much higher conversion of glycerol and selectivity to TAG than the conventional batch operation. Moreover, toluene keeps the reaction temperature below the thermal stability limit of the catalyst. In addition, it prevents the undesired effect of water on the catalysts such as swelling and equilibrium limitation. It was observed that of formation TAG is the most difficult step in all three consecutive reactions; however, with the use of toluene, a nearly quantitative yield of TAG was obtained. Both the catalysts, A15 and A70,

exhibited excellent performances with selectivity to triacetin reaching more than 95% at complete conversion of glycerol. High activity and selectivity of the catalyst can be explained on the basis of strong Brønsted acid sites. A70 showed better catalytic performance in reusability tests compared to A15, though its total number of acid sites and specific surface area were lower. The chlorine content of A70 obviously increases its thermal stability and the strength of acid sites and thus A70 outperformed A15. The formation of the by-product diglycerol tetraacetate (DGTA) was observed first time, most probably formed by dimerization of DAG. Formation of this by-product was only observed at low water concentration and high glycerol conversion, which can be explained first by the reaction rates of esterification and etherification (kinetic control) and the chemical equilibrium (thermodynamic control). In addition, the kinetic investigation showed that formation of DGTA follows zeroth order reaction depending on the adsorption of DAG on the catalyst surface. Kinetic modeling for both catalysts also showed that apparent kinetic rate constant obtained from non-linear regression for DGTA formation matches very well. Deactivation of Amberlysts was observed in reusability tests, probably due to loss of sulfonic acid groups and/or deposition of polymer products (esters or oligomers) on the surface of catalysts, but these effects do not contribute to the homogeneous reaction. This study explains the benefits of a water-free and acid catalyzed process with an excess of acetic acid in glycerol acetylation. The process uses thermodynamic and kinetic effects in an optimum way to produce triacetin in much higher yields as compared to literature data.

3.2 Batch operation – Heteropolyacids

This section present catalytic performance of heteropolyacids (HPA) supported on metal oxides in batch mode under water-free process conditions with respect to catalyst composition and nature of acid sites. Silica, alumina and silica-alumina supported silicotungstic (STA), tungstophosphoric (TPA) and phosphomolybdic acid (PMA) catalysts were synthesized, characterized and evaluated in glycerol acetylation. The results were compared with reference experiments either without catalyst (blank tests) or homogeneously catalyzed (bulk HPAs) under same reaction conditions and correlated with physiochemical properties of the catalysts. In addition, stability and reusability of the best performing catalyst have been investigated.

3.2.1 Characterization of solid catalysts

3.2.1.1 Textural properties of catalysts

Textural properties (BET surface area, pore volume and average pore diameter) for HPA immobilized on three different supports with 20 wt% loading and for bare supports are given in Table 3.5. Compared to the bare support, the specific BET surface area and pore volume

of supported catalysts decreased by 6% to 35% and 9% to 48%, respectively. This is mainly due to blockage of pores caused by HPA component. The effect of a decrease in surface area was stronger on SiO_2-Al_2O_3 compared to SiO_2 and Al_2O_3. The pore diameters range from 7.8-12.0 nm which is typical for mesopores. Interestingly, average pore diameters were not affected, only a marginal decrease after impregnation compared to bare support.

Table 3.5. Textural properties of supports and catalysts

Catalyst	A_{BET} (m^2/g)	Deviation* (%)	Pore volume (cm^3/g)	Deviation** (%)	Average pore diameter (nm)
SiO_2	244	-	0.84	-	12
STA/SiO_2	206	-15.6	0.66	-21.4	11.9
TPA/SiO_2	206	-15.6	0.62	-26.2	11.7
PMA/SiO_2	229	-6.1	0.76	-9.5	11.9
Al_2O_3	303	-	1.32	-	11.4
STA/Al_2O_3	228	-24.7	0.68	-48.4	12.1
TPA/Al_2O_3	267	-11.9	0.84	-36.3	11.8
PMA/Al_2O_3	228	-24.7	0.79	-40.1	11.8
SiO_2-Al_2O_3	520	-	1.00	-	8.4
STA/SiO_2-Al_2O_3	350	-32.7	0.73	-27.0	8.4
TPA/SiO_2-Al_2O_3	341	-34.4	0.67	-33	7.4
PMA/SiO_2-Al_2O_3	377	-27.5	0.81	-19	7.8

*Deviation relative to support A_{BET}.

**Deviation relative to support pore volume.

3.2.1.2 Raman spectroscopy

Raman spectroscopy is well known technique for better understanding of the exact nature of Keggin structure of HPAs impregnated on the surface of support. The Raman spectra were recorded for all supported HPAs, pure bulk STA, TPA and PMA and additionally MoO_3 to study the effect of the interaction of HPA with support (see Figure 3.11). Pure bulk PMA exhibited highly intense Raman bands at 995 and 983 cm^{-1}, which can be assigned to the stretching vibration of terminal Mo=O units, and additional a less intense band at 883 cm^{-1} of bending vibration of Mo-O-Mo units [130].The highly intense band at 995 cm^{-1} and a shoulder at 983 cm^{-1} are characteristic of $[PW_{12}O_{40}]^{3-}$ phosphomolybdic anions (PMA). The spectrum of PMA/SiO_2 exhibits bands at 996 cm^{-1} (low intensity), 903 cm^{-1} (very low intensity), 849 cm^{-1} (moderate intensity), 820 cm^{-1} (high intensity, main band), 776 cm^{-1} (moderate intensity) and 667 cm^{-1} (low intensity). Comparing the spectrum of PMA/SiO_2 with the pure bulk MoO_3 spectrum, the bands at 995, 820 and 667 cm^{-1} resemble with each other and must be ascribed to orthorhombic α-MoO_3 species formed by decomposition of PMA due to calcination at elevated temperature.

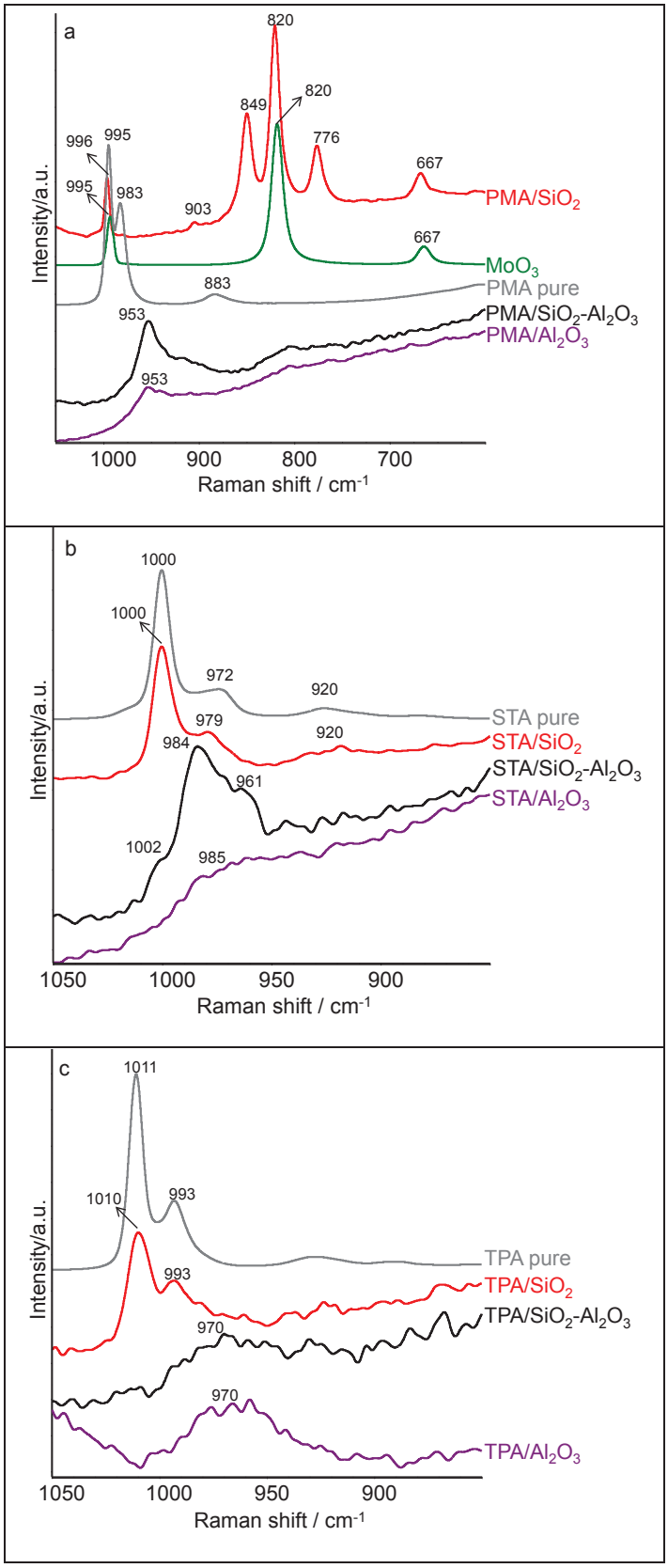

Figure 3.11. Raman spectra of a) PMA/SiO_2, PMA/SiO_2-Al_2O_3 and PMA/Al_2O_3 and reference materials (bulk HPA and MoO_3), b) STA/SiO_2, STA/SiO_2-Al_2O_3 and STA/Al_2O_3 and c) TPA/SiO_2, TPA/SiO_2-Al_2O_3 and TPA/Al_2O_3.

The additional bands represented by PMA/SiO_2 sample at 903, 849, and 776 cm^{-1} can be assigned to β-MoO_3 [131, 132]. The spectra of PMA/Al_2O_3 and PMA/SiO_2-Al_2O_3 represent a broadband at 984 cm^{-1}, most probably due to the high dispersion of PMA on the surface of support. However, strong interaction of PMA with Al_2O_3 can produce also partially degraded, highly dispersed species which could cause the 984 cm^{-1} band (see Figure 3.11 a).

The Raman spectrum of bulk STA exhibits an intense band at 1000 cm^{-1}, a shoulder at 972 cm^{-1} (stretching vibration of W=O) and a weak band at 920 cm^{-1} for the bending vibration of W-O-W, which are the characteristic bands for the Keggin structure (Figure 3.11 b). It was observed that the Raman bands of STA/SiO_2 at 1000 cm^{-1} and 979 cm^{-1} resemble with pure bulk STA, indicating the preservation of the Keggin structure $[SiW_{12}O_{40}]^{4-}$ on the surface of SiO_2. The spectrum of STA/SiO_2-Al_2O_3 exhibited a broadband at 984 cm^{-1} with additional shoulders at 1002 and 961 cm^{-1}. This bright band might appear due to the strong interaction of STA with the acidic hydroxyl group of Al_2O_3 to form partially deteriorated lacunary species $[SiW_{11}O_{39}]^{8-}$ [133, 134]. On the other side, STA/Al_2O_3 showed weakly intense broad bands, most probably due to the high dispersion of partially deteriorated lacunary species $[SiW_{11}O_{39}]^{8-}$. Similar to STA, the Raman spectrum of bulk TPA exhibits intense bands at 1011 and 993 cm^{-1} for stretching vibrations of W=O and a band at 928 cm^{-1} for bending vibration of W–O–W (Figure 3.11 c). Comparing the spectrum of TPA/SiO_2 with the bulk STA, the preservation of bands at 1010, 993 and 925 cm^{-1} can be observed, indicating that the primary structure of TPA ($[PW_{12}O_{40}]^{3-}$) is retained on the surface of SiO_2. In contrast to STA/SiO_2, the spectrum of TPA/SiO_2-Al_2O_3 exhibited a broadband at 970 cm^{-1} indicating the formation of either lacunary species $[PW_{11}O_{39}]^{-7}$ or high dispersion of Keggin units [135].

The Raman spectrum of TPA/Al_2O_3 showed similar feature as TPA/SiO_2-Al_2O_3, represented by a broad band at 970 cm^{-1}, most possibly due to the interaction of TPA with Al_2O_3 support. The presented Raman study revealed that SiO_2 seems to be the better support to stabilize Keggin structures compared to Al_2O_3 and SiO_2-Al_2O_3. Regarding the effect of nature of the support on HPA stability, a ranking in the order SiO_2 > SiO_2-Al_2O_3 > Al_2O_3 can be established.

3.2.1.3 X-ray diffraction (XRD)

The XRD patterns of all supported HPA and for comparison bare supports are shown in Figure 3.12. The bare SiO_2 exhibited a broad reflection at 24°, also observed in supported samples, being the characteristic reflection for amorphous silica (PDF 00-029-0085). The STA/SiO_2 pattern exhibited weak and broad (halo) reflections at 8°, 22° and 27°, indicating a very high dispersion of Keggin units ($[SiW_{11}O_{39}]^{7-}$) over the surface of SiO_2. Similarly, the pattern of TPA/SiO_2 exhibited signals at 10°, 27° and 35° that can be ascribed to $H_3PW_{12}O_{40}\cdot 6H_2O$ (PDF 00-050-0304).

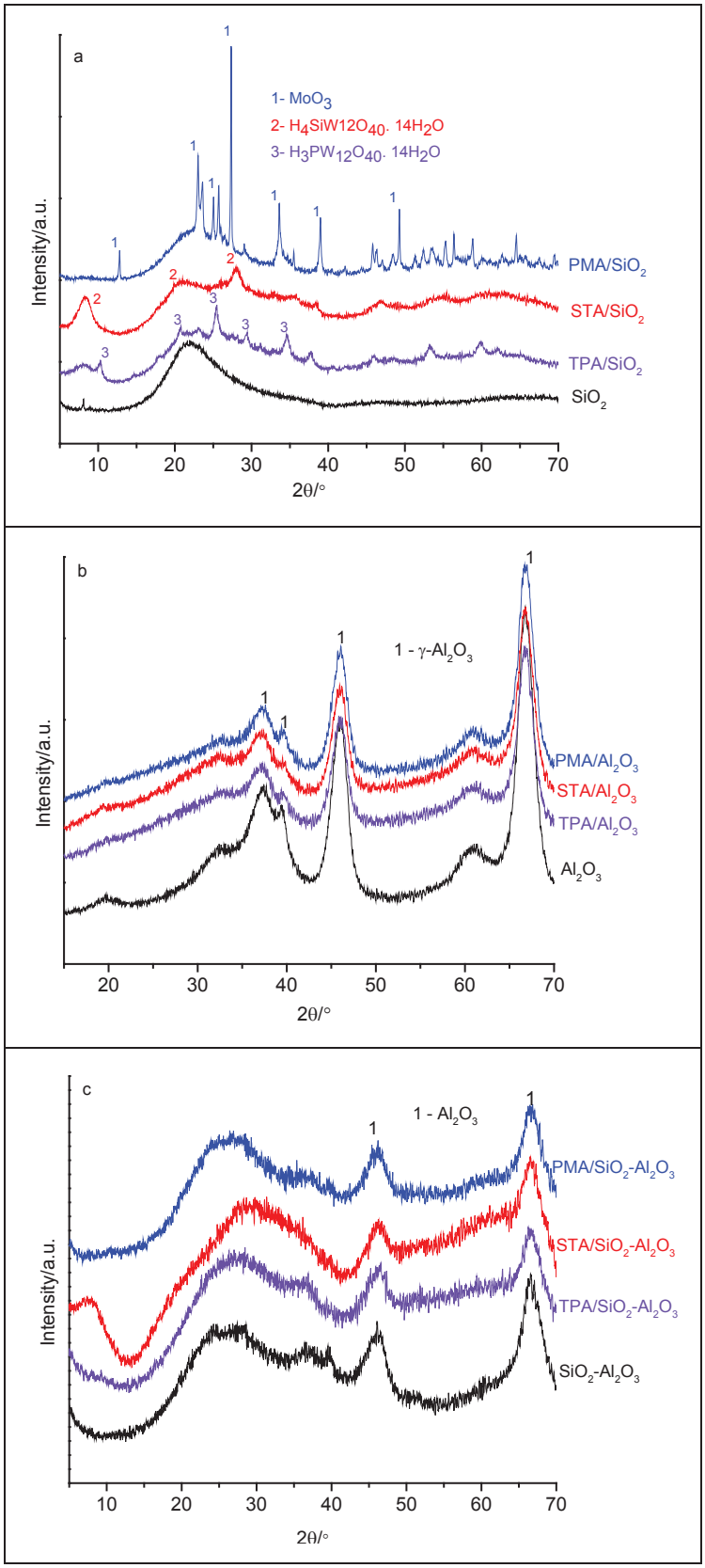

Figure 3.12. X-ray diffractograms of a) SiO_2, TPA/SiO_2, STA/SiO_2 and PMA/SiO_2, b) SiO_2-Al_2O_3, TPA/SiO_2-Al_2O_3, STA/SiO_2-Al_2O_3 and PMA/SiO_2-Al_2O_3 and c) Al_2O_3, TPA/Al_2O_3, STA/Al_2O_3 and PMA/Al_2O_3.

The intensity of the crystalline reflections is rather low, most probably due high dispersion of Keggin units. In contrast to first two samples, PMA/SiO_2 exhibited sharp crystalline reflections overlaying the broad characteristic reflection of amorphous SiO_2. The related pattern showed reflections at 13°, 23°, 25° and 27° that can be assigned to molybdite phase (PDF 00-089-7112). The MoO_3 species were formed by decomposition of heteropolyanions at elevated temperature. Here the results are in excellent agreement with Raman spectroscopic study representing the formation of MoO_3 species (see Figure 3.12 a).

The patterns of γ-alumina supported HPAs represent large humps at 37°, 39°, 43° and 66° which can be assigned to Al_2O_3 (PDF 00-004-0858) together with some minor reflections, which all stem from the support (Figure 3.12 b). None of the reflections can be ascribed to the expected Keggin structures. The same feature was observed for the SiO_2-Al_2O_3 supported samples, exhibiting a broad reflection at 34° for amorphous SiO_2 (PDF 00-078-2315) and 43° and 66° for amorphous Al_2O_3 (PDF 00-004-0858). The support is almost amorphous, similar to Al_2O_3, and none of the reflections for HPAs were found (Figure 3.12 c).

3.2.1.4 Pyridine Fourier transform infrared spectroscopy (Py-FTIR)

The FTIR spectra of adsorbed pyridine were used to study the nature of acid sites on all prepared catalysts. The acidic properties of bare supports, i.e. SiO_2, Al_2O_3 and SiO_2-Al_2O_3, and supported STA, TPA and PMA were determined by recording adsorbed pyridine FTIR spectra at 150 °C, as shown in Figure 3.13. Generally, adsorption of pyridine at Lewis acid sites forms a coordinative bond (L-Py, LS) and the IR bands for L-Py appear in the range of 1445-1460 cm^{-1} and 1610-1620 cm^{-1}, whereas adsorption at Brønsted acid sites forms pyridinium ion (PyH^+, BS) which show bands in the range of 1540-1548 cm^{-1} and 1635-1640 cm^{-1} [136, 137]. The typical IR bands at 1445-1460 cm^{-1} and 1540-1548 cm^{-1} for Lewis acid sites (LS, L-Py) and Brønsted acid sites (BS, PyH^+) were used to calculate the acid site concentration from the band intensities and the absorption coefficients given in [103].On the other side, hydrogen bonded pyridine (hb-Py) bands appear in the range of 1440-1445 cm^{-1} and 1590-1600 cm^{-1} and physically adsorbed pyridine (ph-Py) can show bands at 1440 and 1580 cm^{-1}. Thus, it is difficult to differentiate Lewis-bonded and hydrogen-bonded pyridine (hb-Py) bands when adsorption performed at room temperature. Nonetheless, these pyridine adsorbed species differs in their thermal stability as: ph-Py < hb-Py < L-Py, PyH^+. Based on this principle, it is important to investigate Lewis-bonded pyridine FTIR spectra at high temperature (≥150 °C). The band intensities and the acid site concentrations (BS and LS) calculated from absorption coefficients are shown in Table 3.6. The bare SiO_2 support does not contribute to surface acidity. As expected, STA/SiO_2 and TPA/SiO_2 exhibited higher BS concentration compared to LS; this is mainly due to preservation of the Keggin structure on the support. On the other side, PMA/SiO_2 exhibited higher LS concentration than BS.

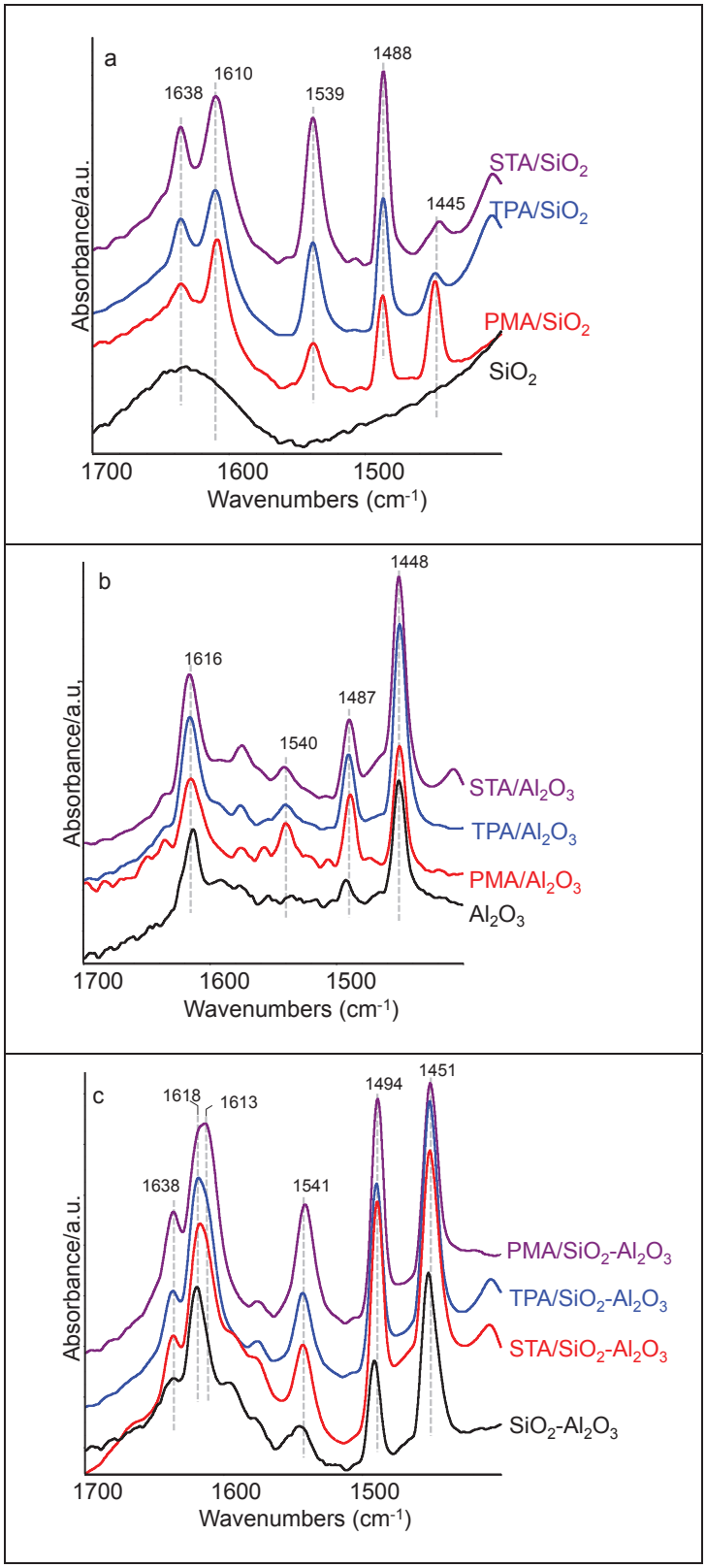

Figure 3.13. FTIR spectra of adsorbed pyridine on a) SiO_2, TPA/S11, STA/S11 and PMA/S11, b) Al_2O_3, TPA/S11, STA/S11 and PMA/S11 and c) SiO_2-Al_2O_3, TPA/SiO_2-Al_2O_3, STA/SiO_2-Al_2O_3, and PMA/SiO_2-Al_2O_3 at 150 °C.

The high LS concentration in PMA/SiO_2 is contributed by MoO_3 species formed by decomposition of Keggin structure during calcination. However, it is clear that the Brønsted acidities of the catalysts with this support correlate well with the results obtained from Raman and XRD studies and the stabilization of the HPAs in the order STA > TPA > PMA (see Figure 3.13 a).

In contrast to the pure SiO_2 support, the bare Al_2O_3 support contributed high LS concentration whereas BS was not observed. The samples STA/Al_2O_3 and TPA/Al_2O_3 exhibited less Brønsted acidity than PMA/Al_2O_3 as they may lose more BS by stronger interaction with the support. On the other hand, PMA/Al_2O_3 showed lower LS concentration compared to STA/Al_2O_3 and TPA/Al_2O_3 catalysts. PMA/Al_2O_3 may form MoO_3 species which contribute more to the BS by interacting with Al_2O_3 compared to MoO_3 species formed in PMA/SiO_2. However, the formation of MoO_3 species in PMA/Al_2O_3 is not clear (Figure 3.13 b). Interestingly, use of bare silica-alumina resulted in high LS but moderate BS concentration. The SiO_2-Al_2O_3 supported HPAs exhibited a reverse trend in the BS concentration compared to SiO_2 supported samples: STA < TPA < PMA. At the same time, LS concentration remained nearly the same. This indicates that not all of the HPAs seem to decompose with simultaneous formation of new LS as observed for the silica supported samples. A possible explanation for the observed trend in Brønsted acidity might be that this SiO_2-Al_2O_3 support offers plenty of reactive sites and a significant amount of BS from HPA might interact with those via dehydration or condensation during calcination. It is also known that LS can be transformed into BS in the presence of moisture at elevated temperatures [138] (Table 3.6 and Figure 3.13 c).

Table 3.6. Acid properties of supports and supported heteropolyacids at 150 °C.

Catalyst	Intensity PyH^+ (1545 cm^{-1})	Brønsted acidity (μmol/g)	Intensity L-Py (1445 cm^{-1})	Lewis acidity (μmol/g)
SiO_2	0.00	0.00	0.00	0.00
STA/SiO_2	3.65	274.48	0.43	24.34
TPA/SiO_2	2.06	154.9	0.55	31.13
PMA/SiO_2	1.09	81.97	1.87	105.84
Al_2O_3	0.00	0.00	3.03	171.49
STA/Al_2O_3	0.54	40.61	4.96	280.74
TPA/Al_2O_3	0.51	38.35	5.26	297.72
PMA/Al_2O_3	0.87	65.42	2.98	168.69
SiO_2-Al_2O_3	1.09	81.96	4.19	237.15
STA/SiO_2-Al_2O_3	1.94	145.89	4.92	278.47
TPA/SiO_2-Al_2O_3	2.00	150.4	5.12	289.79
PMA/SiO_2-Al_2O_3	2.96	222.57	4.09	231.49

3.2.2 Catalytic performance of supported HPA

In the previous section, ion exchange resins were studied in glycerol acetylation to TAG. The high yield of TAG was attributed to the high Brønsted acidity of resins and removal of water. Karl Fischer titration confirmed that very low amount of water was present in the reaction mixture (concentration < 0.05%). This had a significant effect on the conversion of glycerol and yield of TAG. Blank reaction without catalyst was carried out under typical reaction conditions showing 52% glycerol conversion and 85% and 15% selectivities to MAG and DAG, respectively (Table. 3.7 and Figure 3.2 in section 3.1.3.2). Glycerol acetylation over supported STA, TPA and PMA, bare supports and bulk STA, TPA and PMA under identical reaction conditions was studied (Figure 3.14). Based on the nature of catalysts and the catalytic activity measured after 4 hours, the catalysts can be classified into two groups.

Table 3.7. Glycerol conversion and acetins formation in blank test run*

Time (h)	Glycerol conversion (%)	Selectivity to MAG (%)	Selectivity to DAG (%)	Selectivity to TAG (%)
1	28	99	1	0
2	31	92	8	0
3	44	88	12	0
4	52	85	15	0

*(glycerol = 10 g, acetic acid = 39.16 g, molar ratio acetic acid: glycerol = 6, toluene = 60 g, T = 105 °C, t = 4 h)

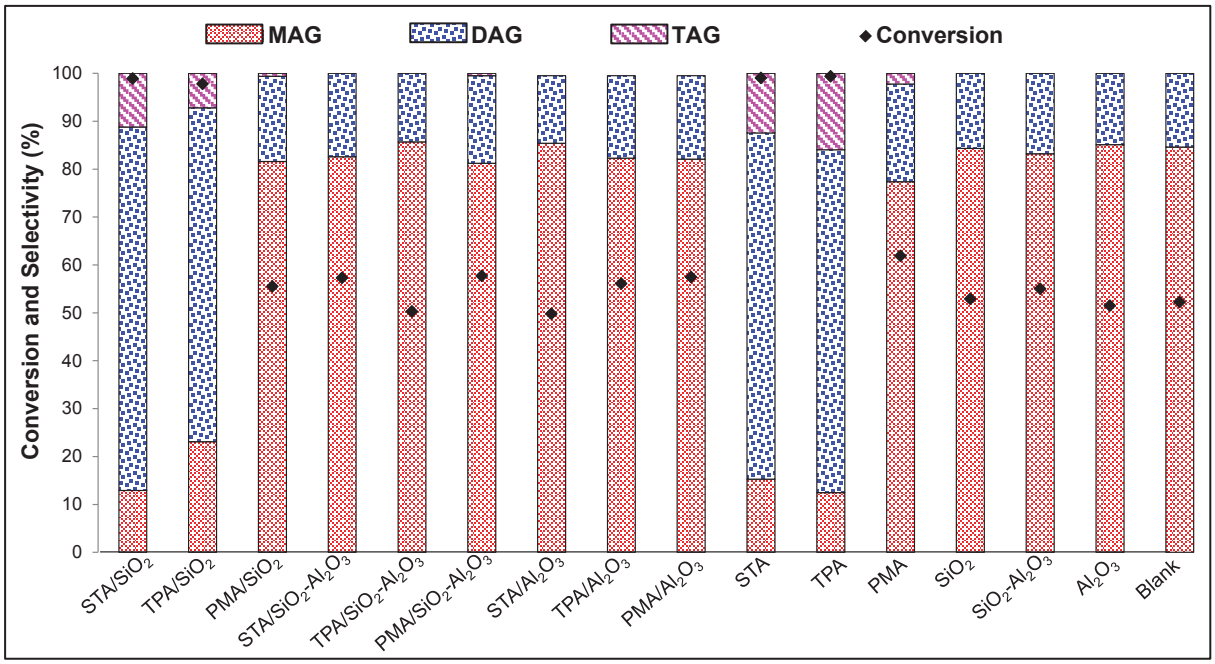

Figure 3.14. Glycerol acetylation with supported HPA catalysts, pure HPA and bulk supports using toluene as an entrainer (glycerol = 10 g, acetic acid = 39.16 g, molar ratio acetic acid: glycerol = 6:1, toluene = 60 g, T = 105 °C, t = 4 h; catalyst mass = 0.5 g (supported) or 0.1 g (bulk HPA)).

Among all the supported catalysts, STA/SiO_2 and TPA/SiO_2 exhibited excellent catalytic performances with almost complete glycerol conversion with a maximum selectivity of 70 and 75% to DAG and 11% and 7% selectivity to TAG, respectively. Interestingly, the results obtained with the bulk STA and TPA analogues showed almost same results although their specific BET surface area is much lower, with almost complete glycerol conversion after 4 h and selectivity to TAG of 12% and 16%, respectively. In contrast, all other HPAs either supported on SiO_2, SiO_2-Al_2O_3 and Al_2O_3 or used as bulk catalysts exhibited much less activity than the SiO_2 supported or non-supported tungsten-containing HPAs. Moreover, PMA as active component showed much less activity compared to STA and TPA. In the related test with PMA, the glycerol conversion never exceeded 65% and the product selectivities (MAG: 80-85%, DAG: 12-18%, TAG: < 3%) were comparable to the reaction without catalyst or with bare supports SiO_2, SiO_2-Al_2O_3 or Al_2O_3 (see Figure 3.14). It is well known that solid HPA possess high Brønsted acidity and their acid strength as well as stability decrease in the order TPA > STA > PMA, which might explain the high activity of tungsten-containing bulk HPA [139]. Surprisingly, STA/SiO_2 catalyst performed slightly better than TPA/SiO_2 even though TPA has higher acid strength; this might be explained on the basis of the high hydrolytic stability of STA, i.e. resistance to water [89, 139, 140]. Moreover, STA has four protons for donation whereas TPA has three protons. The poor performance of PMA/SiO_2 catalyst might be due to thermal decomposition of PMA to MoO_3 which has the lower Brønsted acid strength and does not to catalyze glycerol acetylation [141]. A similar activity ranking was observed by Atia et al. in dehydration of glycerol catalyzed by SiO_2 supported HPA [142].

The high catalytic activity of STA/SiO_2 and TPA/SiO_2 is attributed to the high Brønsted acidity with simultaneous stabilization of Keggin structure on the surface of SiO_2 as observed in XRD and Raman spectroscopic investigation. Pyridine-FTIR analysis revealed that SiO_2-Al_2O_3 supported HPAs exhibited high Brønsted acidity as well as Lewis acidity, Al_2O_3 supported HPAs showed high Lewis acidity and SiO_2 supported HPAs (except PMA/SiO_2) showed high Brønsted acidity. It can be clearly stated that the catalyst is active and selective only if the Keggin structure is stabilized on the surface of the support and possesses a high amount of Brønsted sites but low amount of Lewis sites. Surprisingly, the high specific BET surface areas of SiO_2 supported STA and TPA have no significant effect on the catalytic activity and selectivity compared to bulk HPA analogues.

3.2.3 Reaction progress monitoring

Among all the supported HPA and bare supports, STA/SiO_2 and TPA/SiO_2 exhibited highest catalytic activity. Thus, the catalytic activity of these solids was monitored for 24 hours to study the change in product distribution (towards TAG) under identical reaction conditions as described in Figure 3.15. As expected, with an increase in reaction time TAG

selectivity increased with the decrease in selectivity of MAG and DAG. From Figure 3.15 can be seen clearly that product formation follows the classical behaviour of a consecutive reaction. After 2 h, the glycerol conversion was more than 95% for both catalysts. As the reaction proceeded the selectivity to DAG reached maxima of 75% over STA/SiO_2 after 4 h and of 71% over TPA/SiO_2 after 6 h. After 24 h, selectivity for TAG increased to 71% with STA/SiO_2 and 67% with TPA/SiO_2. Again, the by-product diglycerol tetraacetate (DGTA) was formed during the reaction after 4 h (in case of STA/SiO_2) and 6 h (in case of TPA/SiO_2). This was already mentioned in the studies with Amberlyst catalysts in section 3.1.

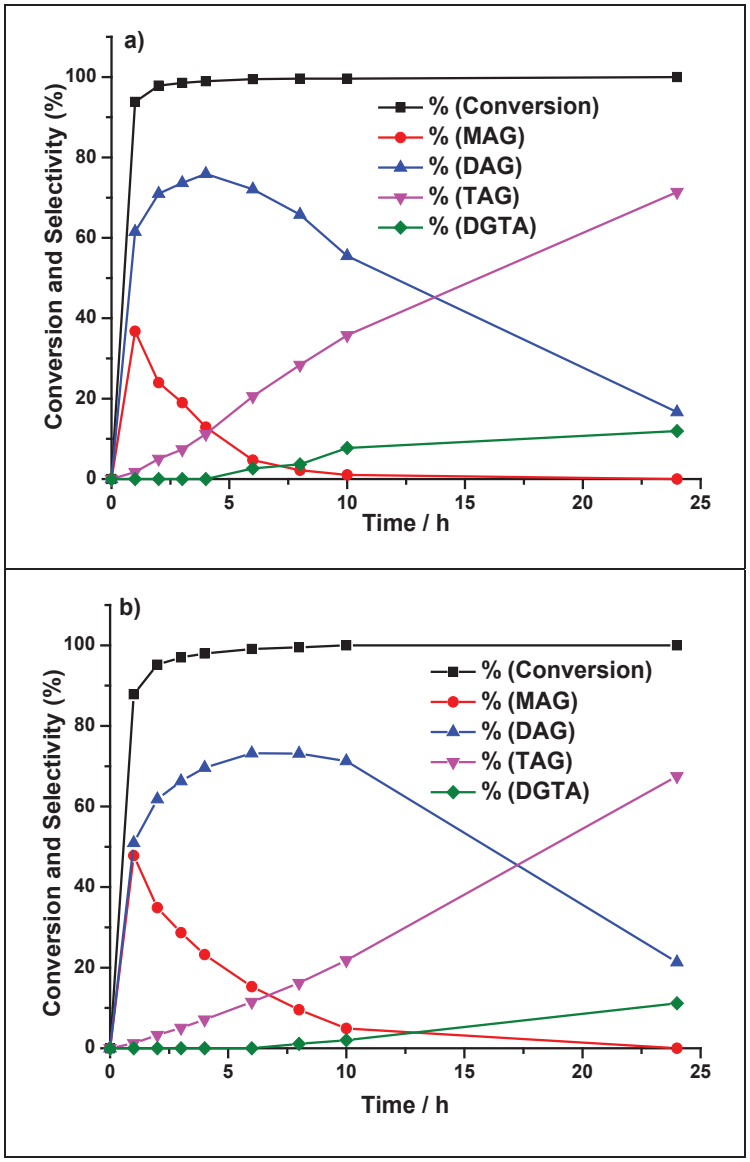

Figure 3.15. Glycerol conversion and selectivities for products over a) STA/SiO_2 and b) TPA/SiO_2 during 24 h reaction (glycerol = 10 g, acetic acid = 39.16 g, molar ratio acetic acid: glycerol = 6, toluene = 60 g, catalyst = 0.5 g, T = 105 °C).

3.2.4 Catalyst reusability and homogeneous catalysis test

With the aim to investigate the stability of STA/SiO_2 and TPA/SiO_2, these catalysts were reused under usual reaction conditions. In a typical procedure, after 10 h reaction time, the catalyst was filtered off, washed with toluene in order to clean the catalyst's surface, dried at 110 °C overnight and reused. Conversion and selectivity in the first run with both the catalysts are very similar to the data obtained in long-term tests (see Figure 3.15. and 3.16.), which proved that the results were reproducible. In the reusability tests, a marginal decrease in the conversion of glycerol was observed for both STA/SiO_2 (100% to 97%) and TPA/SiO_2 (100% to 94%).

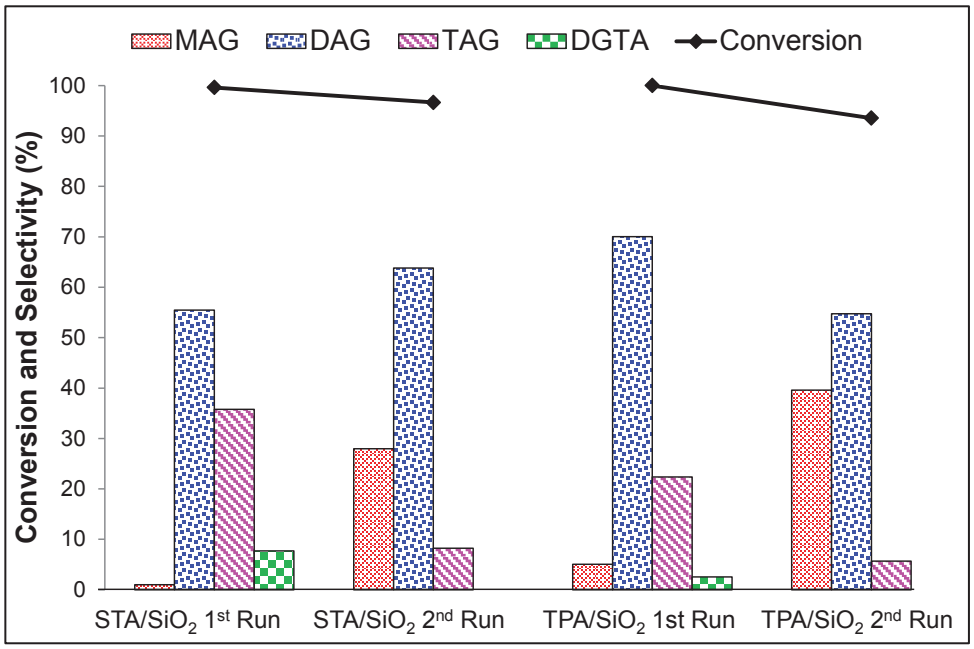

Figure 3.16. Results of reusability test on glycerol acetylation in the presence of toluene as an entrainer over STA/SiO_2 and TPA/SiO_2 (glycerol = 10 g, acetic acid = 39.16 g, molar ratio acetic acid: glycerol = 6, toluene = 60 g, catalyst = 0.5 g, T = 105 °C, t = 10 h).

However, the selectivity of TAG decreased drastically with STA/SiO_2 (35.8% to 8%) and TPA/SiO_2 (22.4% to 5.7%), indicating a lower number of consecutive reaction steps (turnover number). Thus, the selectivity toward TAG serves as a measure for the catalyst activity rather than the initial glycerol conversion. This decline is most probably due to leaching of active components from the surface of SiO_2. Hence, both the spent catalysts received after the second run was analyzed by ICP and the results compared with the fresh catalysts are shown in Table 3.8. The results proved that both catalysts suffer from leaching of active component tungsten into the reaction mixture under operating conditions. The tungsten content of the catalysts decreased from 14.71% to 8.17% (STA/SiO_2) and from 14.70% to 10.42% (TPA/SiO_2). Moreover, the presence of tungsten species in the reaction mixture was confirmed by XRF analysis.

Table 3.8. ICP-OES analysis of the fresh and spent catalysts STA/S11 and TPA/S11.

Catalysts		Element load, wt%	
		W	P
STA/S11[#]	Fresh	14.71	-
	Spent	8.17	-
TPA/S11	Fresh	14.44	0.2
	Spent	10.42	0.13

[#]Due to the silica support used, the amount of leached Si from STA was not estimated.

Leaching of the active species from the support deactivated the catalysts. However, it is important to know whether the leached species can act as a homogeneous catalyst in glycerol acetylation. Therefore, a separate stop experiment was carried out with STA/SiO_2 under identical conditions as shown in Figure 3.17. The catalyst was filtered off from the reaction mixture after 4 h and at this point the selectivities to MAG, DAG and TAG were 12.9%, 75.7% and 11.4%, respectively; at the almost complete conversion of glycerol. The activity of filtrate was tested by adding new reactant solution (19.56 g of acetic acid and 5 g of glycerol) and running reaction for another 4 h under the same reaction conditions.

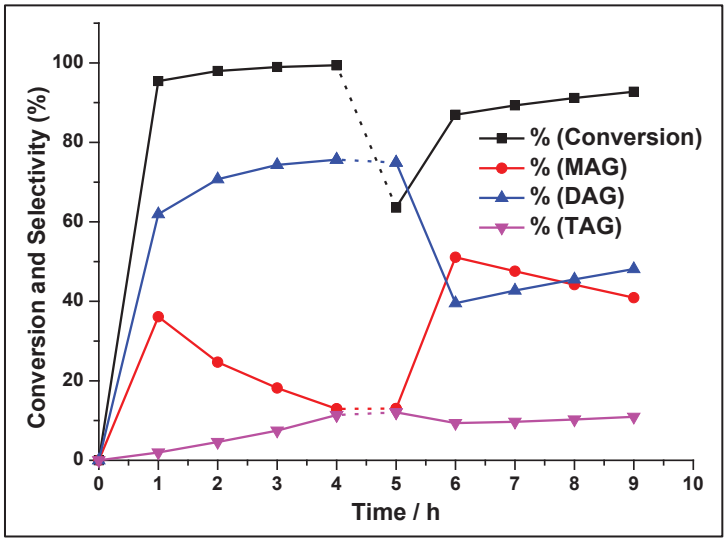

Figure 3.17. Glycerol conversion and product selectivities with 0.5 g of STA/SiO_2 in stop-experiment (reaction conditions same as described in Figure 3.16; the catalyst was removed after 4 h and the run was continued for further 4 h without catalyst). The dotted lines represent the time period for catalyst removal and the addition of fresh feed (glycerol = 5 g, acetic acid = 19.56 g).

After 4 h, slight decreases in the conversion of glycerol and DAG selectivity were observed. On the other side, selectivity to MAG increased whereas TAG selectivity remained nearly constant. Resulting conversion and selectivity curves were similar to those of the blank test as shown in Figure 3.2 (section 3.1.3.2) and Table 3.7. Thus, it seems that the leached active component does not contribute to homogeneous catalysis. This means that

the supported HPA catalysts in glycerol acetylation at given conditions exclusively works heterogeneously. It still has to be clarified whether the catalyst deactivation is due to simple loss of active species or if other effects like deposition of high-molecular oligomers (possibly formed in a similar way as DGTA) play a role.

3.2.5 Summary and conclusions

The impregnation of various HPAs on common materials led only to few supported catalysts with an excellent activity that were able to produce triacetin in high yield (71%) within an acceptable period of time (24 h). These catalysts are tungsten containing heteropolyacids supported on silica. The high activity of the catalysts is accredited to the Brønsted acid properties, which in further seems to be linked to the preservation of Keggin structure on the surface of support. This is possible if neutral support like silica is used, which has neither Brønsted acid sites nor Lewis acid sites. The interaction of neutral support with the active component is minimum, which promotes the agglomeration of HPA crystals. On the other side, if the supports possess intrinsic acidic properties (either Brønsted or Lewis acidity), it seems to be ruinous for stabilization of Keggin structure of HPAs. This is typical for the alumina or silica-alumina supports in this study. In such case, the active hydroxyl group from alumina may react with acidic sites of HPA during calcination at elevated temperature. Typical reactions might be condensation or dehydration, which could remove part of the constitutional water from the Keggin structure. Hence, the original structure is distorted or completely destroyed to produce respective oxides which are highly dispersed over the surface of support and hard to detect by XRD or Raman spectroscopy. Otherwise, with a large number of Lewis acid sites under water-free conditions, the formation of necessary Brønsted acid sites will be impossible. All these effects explain the observed catalyst performances quite well. On the other hand, it is yet not understood why the BET surface area enlargement does not show any effect on global reaction rates.

HPA catalysts also suffered from deactivation most likely due to the partial leaching of the active component from the surface of supports into the reaction mixture. The highly polar and hydrophilic glycerol and acetic acid are most likely responsible for leaching and deactivation. Surprisingly, such leached species do not act as homogeneous catalysts in glycerol acetylation. This might be due to the use of the entrainer toluene to establish water-free conditions, which suppresses the formation of Brønsted acids away from the solid supported catalysts. The use of an entrainer is definitely beneficial for the overall process as the chemical equilibrium of the esterification is shifted toward the target product triacetin. Yet it is not fully understood how the absence of water affects the structure and performance of SiO_2 supported heteropolyacids while other polar compounds like glycerol and acetic acid are present.

4 Gas phase glycerol acetylation

In the previous chapter, liquid phase glycerol acetylation over ion exchange resins and supported heteropolyacid catalysts using toluene as an entrainer has been evaluated. From the results, it can be concluded that strong Brønsted sites (without Lewis acid sites) are necessary for high activity and selectivity to TAG. However, the catalysts get deactivated due to the leaching of active species into a liquid bulk phase. On the other side, it would be attractive to transform liquid phase batch process to continuous flow process. Continuous flow process has several advantages over batch process such as no leaching of the active components from catalyst surface, no catalysts separation and downtime, no need of solvent, safety and process reliability as reaction parameters are more easily controlled, low energy costs, financial benefits and minimization of wastes.

This chapter is again divided into two sub-sections based catalysts systems: first sub-section shows the catalytic performances using supported heteropolyacids (HPAs) and mixed metal oxide catalysts. In addition, the influence of reaction conditions such as acetic acid/glycerol molar ratio and WHSV on conversion, selectivity and catalyst stability (long-term test) has been studied. In the second sub-section, the role of nature of SiO_2 support on glycerol acetylation was investigated. In both sections fresh and spent catalysts were characterized by N_2 physisorption, XRD, NH_3-TPD, py-IR, Raman, ATR-IR, UV-vis and XP spectroscopy, TEM, and ICP-OES techniques.

4.1 Continuous operation – Supported HPAs and mixed metal oxides

In the present sub-section, selected supported heteropolyacids catalysts from liquid phase experiments were tested in gas phase glycerol acetylation. Due to the low thermal stability of A70 and A15 catalysts were not used. For comparison, another series of low acidic SiO_2-MO_x (mixed metal oxide) were prepared, characterized and tested in gas phase glycerol acetylation.

4.1.1 Catalytic performance of supported HPA

The catalysts with STA supported on SiO_2 and γ-Al_2O_3 were prepared by impregnation method and γ-Al_2O_3 as a support was prepared by sol-gel method. These solids were characterized with various techniques as reported in the previous chapter (section 3.2.1). The catalytic tests of STA/SiO_2, STA/Al_2O_3 and Al_2O_3 were measured in continuous flow operation at selected reaction condition (225-325 °C, acetic acid: glycerol = molar ratio 6:1, catalyst weight 0.6 g and WHSV = 2.73 h^{-1}) with N_2 as diluent gas and methane as internal standard at ambient pressure (see Figure 4.1). Almost complete conversion of glycerol was observed for STA supported catalysts in the given temperature range (225-325 °C), whereas γ-Al_2O_3 showed maximum glycerol conversion of 98% at 275 °C (due to higher temperature compared to batch runs). However, the selectivities to desired acetins were rather low; MAG was obtained in high selectivity compared to DAG and TAG with the named catalysts. Bare γ-Al_2O_3 showed 68%, 27% and 1% selectivities to MAG, DAG and TAG, respectively, at 225 °C and 75% glycerol conversion. The maximum selectivity to TAG was nearly 16% showed by STA/Al_2O_3 at complete conversion of glycerol at 250 °C. On the other side, high selectivity to acrolein was achieved with the all three catalysts by dehydration of glycerol. Such high activity catalysts is linked with high acidity properties (independent of either Brønsted or Lewis acidity) and selectivity to acrolein seems to be linked with Lewis acid sites. As, STA/Al_2O_3 and γ-Al_2O_3 being Lewis acid materials (Table 3.6) they exhibited excellent selectivity to acrolein (94% and 89%, respectively) at 325 °C at the almost complete conversion of glycerol. Whereas for STA/SiO_2 being a Brønsted acidic catalyst showed 67% selectivity to acrolein at lower temperature 225 °C and with the increase in temperature selectivity dropped to 53.6% at 325 °C. The selectivity to acrolein decreased in the order STA/Al_2O_3 > γ-Al_2O_3 > STA/SiO_2. Theoretically, glycerol dehydration is Brønsted acid catalyzed reaction, but still high conversion of glycerol and selectivity to acrolein was achieved with Lewis acidic materials. This is most probably linked to the transformation of Lewis acid sites by water into Brønsted sites at high temperature; moreover, partially destroyed Keggin structure of STA on the surface of Al_2O_3 might be regenerated to form Brønsted acid sites. In addition, presence of acetic acid in the reaction mixture may activate catalyst by removing carbon deposits from the catalyst surface. On the other side, strong

Brønsted acid sites of STA/SiO_2 might decompose the formed acrolein at high temperature to produce polymers which ultimately deactivate catalysts by heavy coke formation.
However, the selected acidic supported heteropolyacid catalysts (STA/SiO_2, STA/Al_2O_3) and γ-Al_2O_3 were more active towards dehydration than esterification of glycerol to produce TAG (target product). Hence, another series of low acidic material prepared by sol-gel method were tested in gas phase glycerol acetylation which might offer different catalytic behaviour.

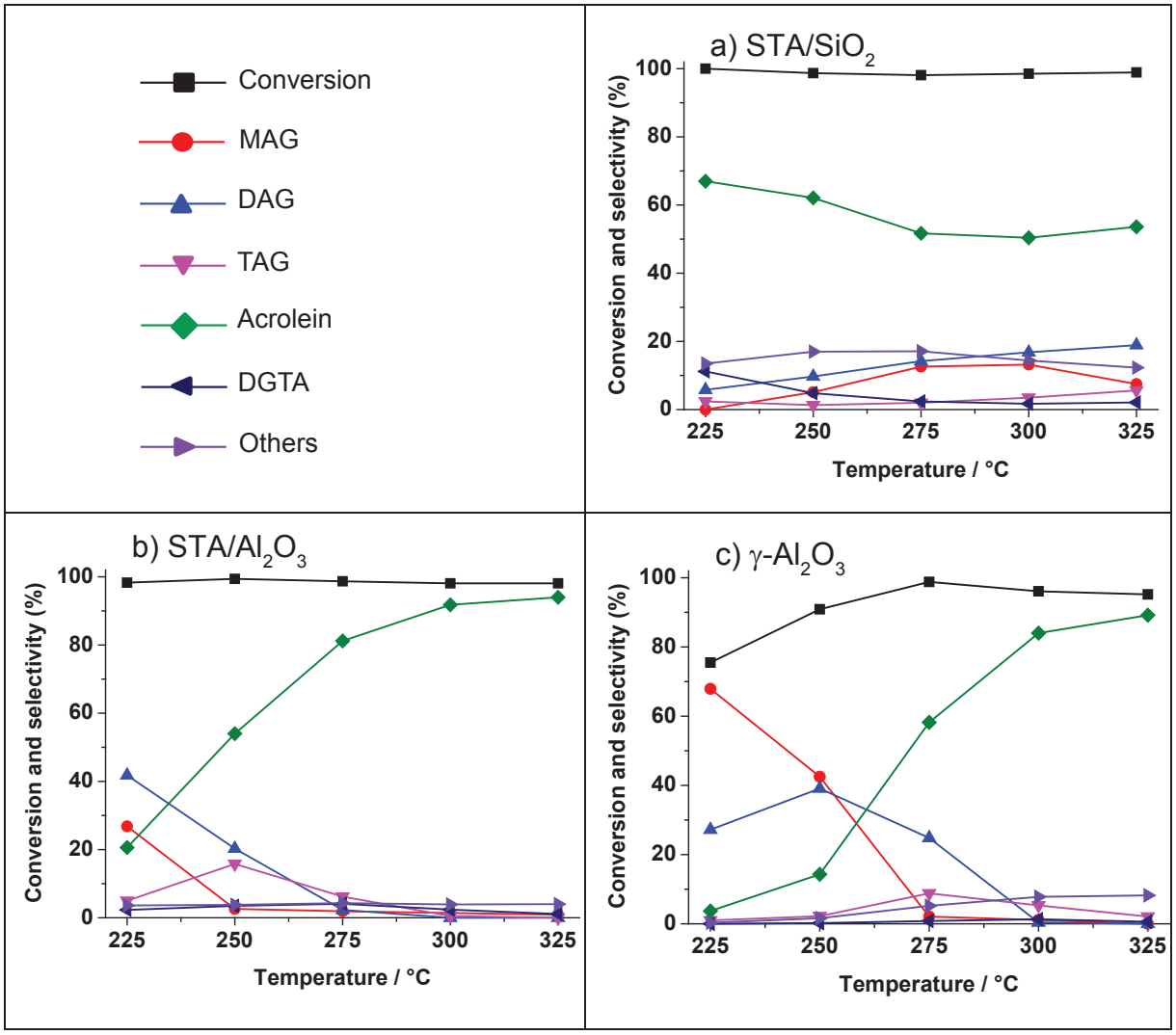

Figure 4.1. Acetylation of glycerol with a) STA/SiO_2, b) STA/γ-Al_2O_3 and c) γ-Al_2O_3. Reaction conditions: Acetic acid: glycerol molar ratio = 6/1 and catalysts amount = 0.6 g, flow rate = 0.025 ml/min, N_2 = 29.7 ml/min, WHSV = 2.73 h^{-1}.

4.1.2 Catalytic performances of SiO_2-based catalysts

4.1.2.1 Influence of temperature

The tests with bare SiO_2 (neutral support), bare TiO_2 and SiM30 solids (M = TiO_2, MgO, ZrO_2, SrO and Sc_2O_3) were evaluated in continuous flow reactor at the selected reaction conditions (acetic acid: glycerol molar ratio = 6: 1, 225-325 °C, N_2 = 29.7 ml/min, WHSV = 2.73 h^{-1}, methane = 1 ml/min as an internal standard). The glycerol conversion and product selectivities over SiO_2-MO_x at different temperatures are shown in Figure 4.2. The conversion of glycerol with bare SiO_2 support increased with the increase in temperature and reached 58% at 325 °C (Figure 4.2 a). Similar behavior was observed with bare TiO_2 where almost complete conversion of glycerol was observed at 325 °C (see Figure 4.2 b). The conversion of glycerol over SiO_2-MO_x catalysts (mixed metal oxide) was complete at 300 °C only (Figure 4.2). Such high conversion might be due to the presence of an acetic acid which can act as a homogeneous catalyst at high temperature and/or the thermal decomposition of glycerol.

The selectivity for MAG and DAG over bare SiO_2 remained nearly constant at 85% and 15%, respectively, throughout all the temperature set points (see Figure 4.2 a). On the other hand, bare TiO_2 at a lower temperature (225 °C) showed 90% selectivity to MAG with 30% glycerol conversion and with the increase in temperature selectivity to acrolein increased to 52% at the cost of MAG at 325 °C (see Figure 4.2 b). However, formation of the desired TAG over bare SiO_2 support and bulk TiO_2 catalysts was not observed. At 300 °C, SiZr30 catalyst showed 60% selectivity to acrolein whereas selectivities to MAG, DAG, and TAG were 17.4%, 10% and 1.2%, respectively, at 93.1% conversion of glycerol (see Figure 4.2 c). With further increase in temperature (325 °C), the selectivity to acrolein as well as the conversion of glycerol decreases. This is most probably due to the formation of coke/polymer from acrolein on the surface of catalysts which blocks the surface acid sites. Similarly, SiSc30 also showed 54% selectivity to acrolein at 325 °C with complete conversion of glycerol. In addition, SiSc30 also favours the formation of several unknown by-products which might be oligomers of glycerol and polymers of acrolein (see Figure 4.2 d). At low temperature (225 °C), SiSr30 showed 75.3% glycerol conversion with 83.3% selectivity to MAG and 15.6% selectivity to DAG. With increasing temperature to 325 °C, selectivity to DAG increased to 63.7% at the cost of MAG (29.6%) with complete conversion of glycerol (see Figure 4.2 e). SiMg30 catalyst showed high selectivity to acrolein (28%), however, it also showed considerable selectivity to desired TAG (16.8%) at 325 °C with complete conversion of glycerol (see Figure 4.2 f). Interestingly, SiTi30 catalyst showed maximum selectivity of 39.3% to TAG and 38%, 8%, and 10.6% selectivity to DAG, MAG and acrolein, respectively, at complete conversion of glycerol at 300 °C (see Figure 4.2 g). However, at 325 °C with SiTi30 catalyst, the selectivity of acrolein increased to 30% at the cost of DAG and TAG.

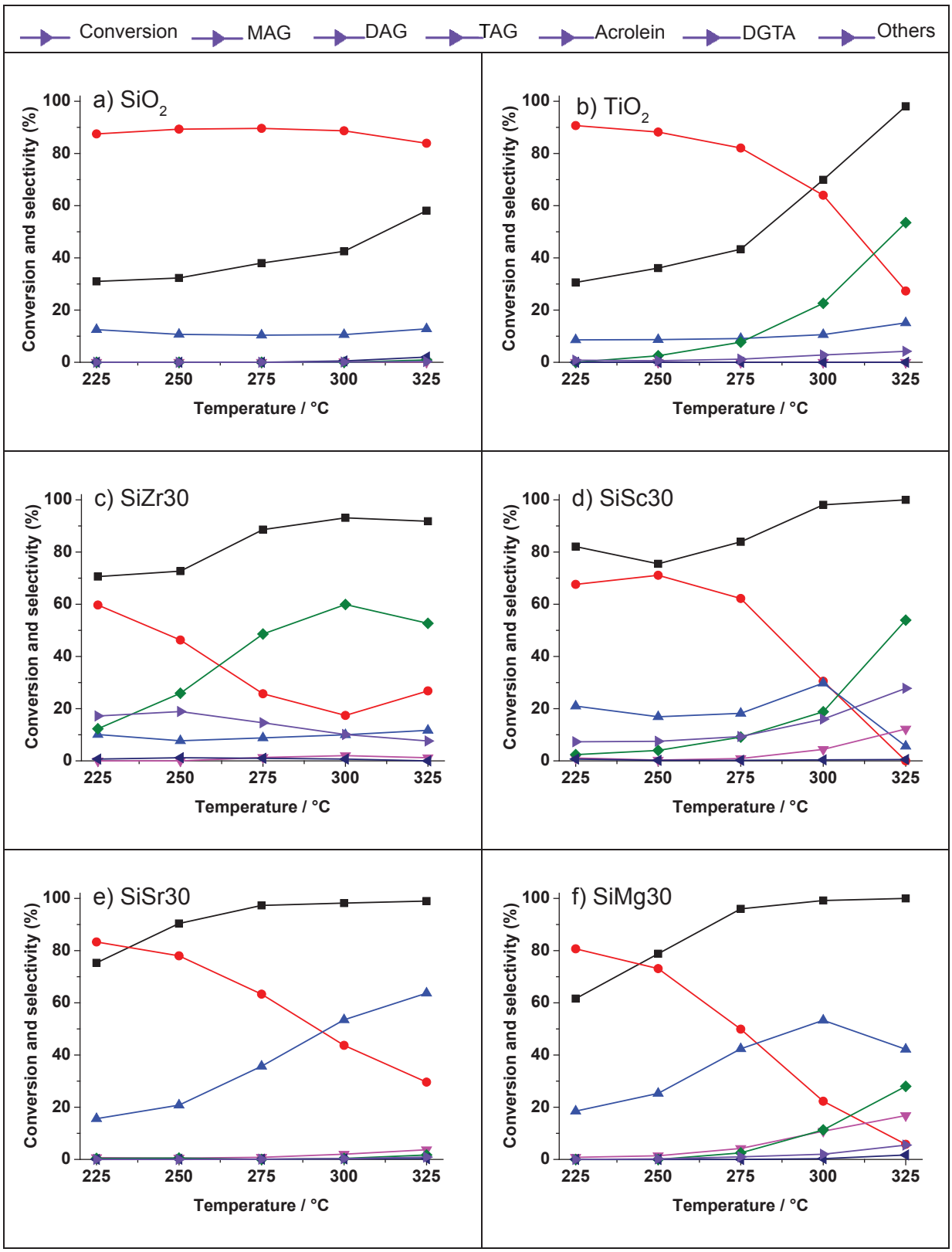
Conversion
MAG
DAG
TAG
Acrolein
DGTA
Others
a) SiO2
b) TiO2
c) SiZr30
d) SiSc30
e) SiSr30
f) SiMg30
Conversion and selectivity (%)
Temperature / °C
0
20
40
60
80
100
225
250
275
300
325

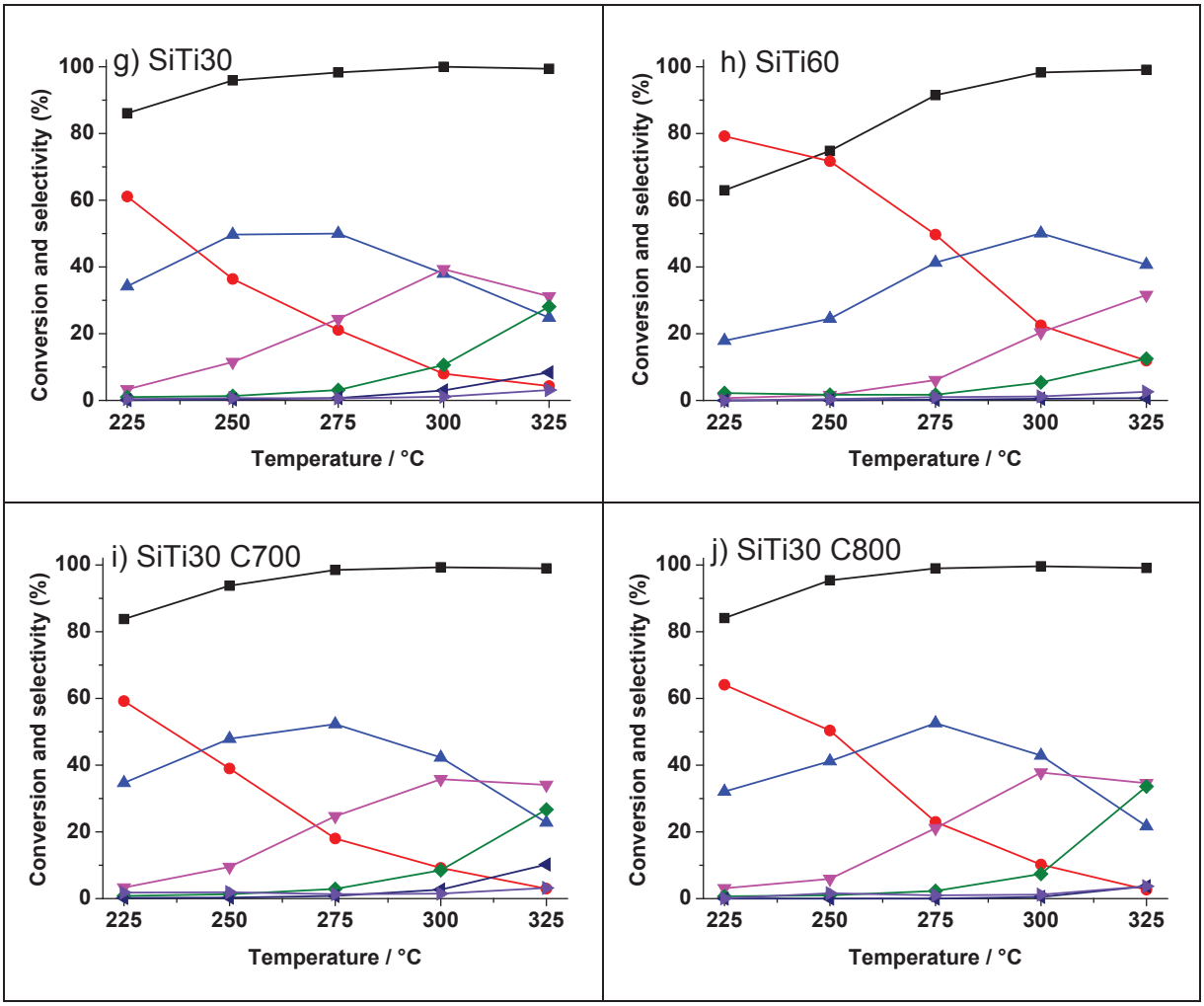

Figure 4.2. Influence of temperature on the glycerol conversion and product selectivities of SiO_2, TiO_2 SiM30 and SiTi60 catalysts. Reaction conditions: Acetic acid: glycerol molar ratio = 6: 1 and catalysts amount = 0.6 g, flow rate = 0.025 ml/min, N_2 = 29.7 ml/min, WHSV = 2.73 h^{-1}.

On the other side, low titania containing catalyst SiTi60 also showed high selectivity of 32% to TAG and 42%, 10% and 11% selectivity to DAG, MAG and acrolein, respectively (see Figure 4.2 h) at higher temperature (325 °C). In addition, the formation of diglycerol tetraacetate (DGTA) was detected on SiTi30 catalyst which was previously observed in liquid phase system at water free condition. Among all tested catalysts, SiTi30 showed excellent catalytic performance with complete glycerol conversion and selectivity to the desired TAG was 39.3%. It can be clearly seen that high activity and selectivity to TAG were achieved below 300 °C. Above 300 °C, reaction favours dehydration of glycerol over esterification (acetylation). Separate samples of the SiTi30 solid prepared by sol-gel method were further calcined at 700 °C and 800 °C to check the thermal stability of the catalysts in comparison to parent sample calcined at 500 °C. The glycerol conversion was not affected by calcination temperature compared to parent sample. On the other side, slight variation in TAG selectivity was observed; however, the difference is rather small as shown in Figure 4.2 i and j. Overall

the average C-balance was found to be 90-95% with remaining 5-10% might be due to the formation of higher oligomers or polymers which are not detected by GC. Randomly made TOC analyses of carbon content in liquid product samples and fresh feed showed good agreement (nearly 99%).

4.1.2.2 Long-term stability test of SiTi30 catalyst

From the above illustrated catalytic experiments, SiTi30 was found to be active and selective towards the desired TAG. All other catalysts were either less active or selective towards acrolein. Hence, a long-term stability test was performed with SiTi30 at 300 °C over 200 h without interruption to investigate deactivation. The conversion of glycerol remained nearly 100% throughout the experiment, whereas the selectivity of TAG started to decrease slightly after 100 h. The initial selectivity was 30% and decreased to 23% within 216 h as shown in Figure 4.3. At the same time, an increase in DAG and MAG selectivities was observed. The deactivation of the catalyst might be due to the organic deposit that reduces the availability of the active sites; on the other side, nature of the active sites which control catalytic conversion remain unaffected. In order to regain the original selectivity of TAG, regeneration of SiTi30 catalyst was performed. Initially, nitrogen was replaced by 3% oxygen and the temperature was increased to 400 °C for 24 h. In regeneration test under identical reaction condition, the conversion was maintained at 100%, but the selectivity of TAG dropped to 20% in 15 h time-on-stream.

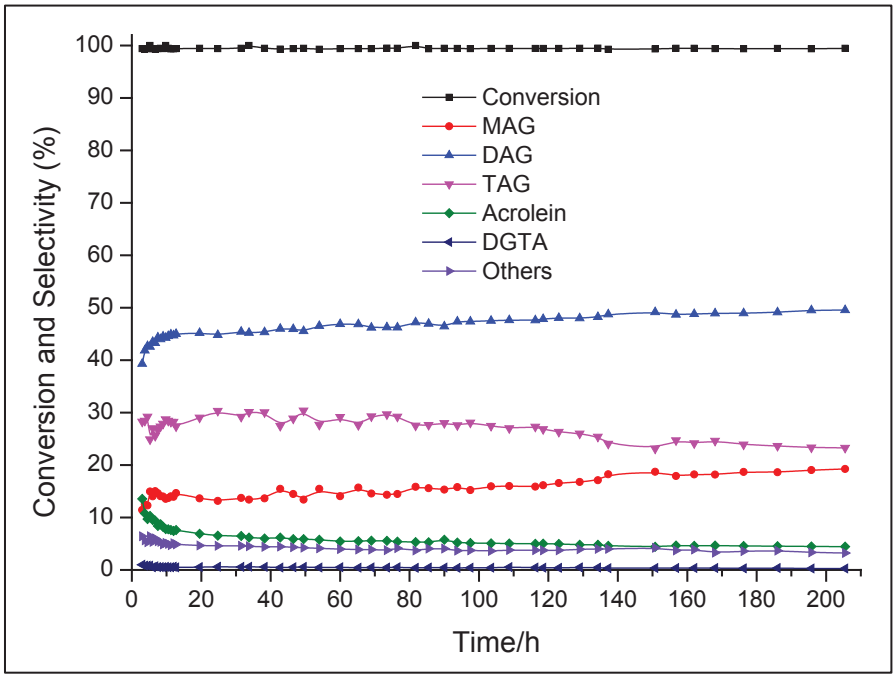

Figure 4.3. Long-term stability test with SiTi30 catalyst at 300 °C. Reaction conditions: Acetic acid: glycerol molar ratio = 6: 1, catalyst amount = 0.6 g, flow rate = 0.025 ml/min, N_2 = 29.7 ml/min, WHSV = 2.73 h^{-1}.

It seems that the temperature might not enough to burn-off carbon deposits. Thus, 3% of oxygen was replaced by air at 500 °C for 24 h, but in second regeneration test, the selectivity to TAG dropped to 12% in 9 h time-on-stream at complete glycerol conversion. Later, the spent catalyst was recovered and calcined in a muffle at 600 °C but after resuming the acetylation (third regeneration test), the conversion and selectivity of TAG dropped to 95% and 7% in 9 h time-on-stream, respectively. The spent catalyst was again calcined at 600 °C for 5 h (henceforth denoted as SiTi30-reg) and characterized by N_2 physisorption, Pyridine-IR, TEM, XPS and UV-vis to compare the structure and morphology with fresh catalyst.

4.1.2.3 Influence of acetic acid to glycerol molar ratio and WHSV with SiTi30

SiTi30 was found to be the most effective catalyst among all prepared catalysts in terms of catalytic performance. Hence, further reaction parameter was evaluated more in detail by varying WHSV (residence time) and acetic acid to glycerol molar ratio at 300 °C. The conversion of glycerol was almost complete throughout all the runs. When the WHSV was gradually varied from 1.82 h^{-1} to 5.45 h^{-1} (catalyst weight = 0.3-0.9 g) at constant acetic acid to glycerol molar ratio (6:1), a significant effect on TAG and acrolein selectivity was observed. At 5.45 h^{-1} WHSV, TAG and acrolein selectivities were 18.3% and 3.6% which increased to 39.3% and 10.6% at 2.73 h^{-1} WHSV and 300 °C. Further variation in WHSV to 1.82 h^{-1} didn't show a significant difference in TAG selectivity (nearly 40%), however, acrolein selectivity increased to 14% (Table 4.1).

Table 4.1. Influence of acetic acid to glycerol molar ratio and WHSV with SiTi30 on glycerol conversion and product selectivities.

Catalyst amount (g)	AA: G	WHSV (h^{-1})	X** (%)	MAG (%)	DAG (%)	TAG (%)	Acrolein (%)	DGTA* (%)	Others (%)
0.3	6	5.45	98.2	23.8	52.8	18.3	3.6	0.4	1.1
0.6	6	2.73	100	8	38	39.3	10.6	3	1.1
0.9	6	1.82	99.9	7	34.7	40.6	14.1	1.2	2.4
0.6	4	2.16	98.6	21.3	45.6	19.5	7	3.8	2.8
0.6	9	3.85	99.8	3.3	30.7	54.9	8.1	0.9	2.1

Acetic acid: glycerol (AA/G) molar ratio = 4:1-9:1, and catalysts amount = 0.3 g-0.9 g, flow rate = 0.020-0.035 ml/min, N_2 = 29.7-31.4 ml/min, T = 300 °C, WHSV = 1.89-5.45 h^{-1}.
*DGTA: diglycerol tetraacetate, **X: Conversion of glycerol

Similarly, variation of acetic acid to glycerol molar ratio from 4: 1 to 9: 1 (WHSV = 2.16-3.85 h^{-1}) with constant catalyst weight (0.6 g) was evaluated. The selectivity to TAG was affected remarkably by increasing the molar ratio. At lower acetic acid to glycerol molar ratio of 4:1, the selectivities to TAG and acrolein were 19.5% and 7%, respectively. Whereas at

high acetic acid to glycerol molar ratio of 9:1, the TAG selectivity increased to 54.9% and acrolein selectivity decreased to 8.1% (Table 4.1). Increasing the acetic acid amount in the feed has remarkable effect on TAG selectivity, i.e. it favours the acetylation (esterification) over dehydration most probably by activating active species and/or by reducing carbon deposition. In addition, it also shifts the chemical equilibrium towards TAG. These observed results are better than the results in liquid phase without water removal.

4.1.3 Characterization of catalysts

4.1.3.1 ICP-OES analysis and textural properties

The content of metal in the MO_x species (MO_x = TiO_2, MgO, ZrO_2, SrO and Sc_2O_3) was determined by ICP analysis and results are shown in Table 4.2. The SiTi60, SiMg30 and SiSr30 catalysts showed significantly less metal in MO_x (in the range of 25% to 50%) compared to the nominal metal content. On the other side, deviations for MO_x species in SiTi30, SiZr30 and SiSc30 were less than 13%. BET surface areas, pore volumes and pore diameters for sol-gel synthesized SiO_2-MO_x catalysts are also shown in Table 4.2. The bare SiO_2 support prepared by sol-gel method exhibited BET surface area of 395 m^2/g compared to SiO_2. SiZr30 and SiSc30 showed the higher surface areas of 572 and 451 m^2/g, respectively, compared to SiO_2. Whereas, SiMg30 and SiSr30 showed lower surface areas of 375 and 275 m^2/g, respectively the surface area of SiTi30 and SiTi60 were close to bare SiO_2 support with 404 and 399 m^2/g, respectively. Pore volumes for prepared catalysts were in the range of 0.75-0.92 cm^3/g, except SiZr30, which showed low pore volume (0.60 cm^3/g). The pore diameter data revealed that the prepared catalysts are mesoporous in nature.

Table 4.2. ICP-OES analysis and textural properties of the prepared catalysts.

Catalysts	Nominal metal content (wt%)	Metal content by ICP-OES (wt%)	Deviation (%)	A_{BET} (m^2/g)	Pore Volume (cm^3/g)	Pore diameter (nm)
SiO_2	-	-	-	395	0.92	9.8
SiMg30	1.30	0.86	33	375	0.85	9.1
SiZr30	4.74	4.30	9	572	0.60	3.7
SiSc30	2.40	2.08	13	451	0.75	6.3
SiSr30	4.60	2.24	51	275	0.86	11.3
SiTi30	2.55	2.21	13	404	0.81	8.7
SiTi60	1.30	0.97	25	399	0.88	9.0
SiTi30 C700	-	-	-	365	0.78	8.5
SiTi30 C800	-	-	-	338	0.71	7-8.9
TiO_2	-	-	-	29	0.18	8-10
SiTi30-reg	-	-	-	272	0.54	8-9

* SiTi30 sample calcined at 600°C after long-term and regeneration test

After calcination of SiTi30 at a higher temperature (700 and 800 °C), a drop in surface area was observed without affecting pore volume and pore diameter. TiO_2 solid prepared from ammonium titanyl oxalate showed relatively low surface area of 29 m^2/g. It seems that high activity and selectivity, somehow can also be related to the mesoporosity (pore diameter) of the catalysts. The catalyst SiZr30 and SiSc30 have relatively small pores (4-6 nm) which favour dehydration to form acrolein whereas other catalysts (more than 8 nm) favour acetylation to produced acetins (compare Figure 4.2). The surface area and pore volume of SiTi30-reg catalyst decreased to 272 m^2/g and 0.54 cm^3/g, respectively, whereas the pore diameters remained 8-9 nm nearly same as fresh SiTi30 catalyst. Thus, the deactivation of the catalyst is most probably due to the changes in structural arrangements.

4.1.3.2 X-ray diffraction (XRD)

The XRD patterns of bare SiO_2 and SiO_2-MO_x catalysts are shown in Figure 4.4 a. These materials were amorphous in nature and the only broad reflection at 24° was observed for amorphous SiO_2. Since no peaks related to MO_x species were detected, one can say that MO_x species are highly distributed in the SiO_2 matrix.

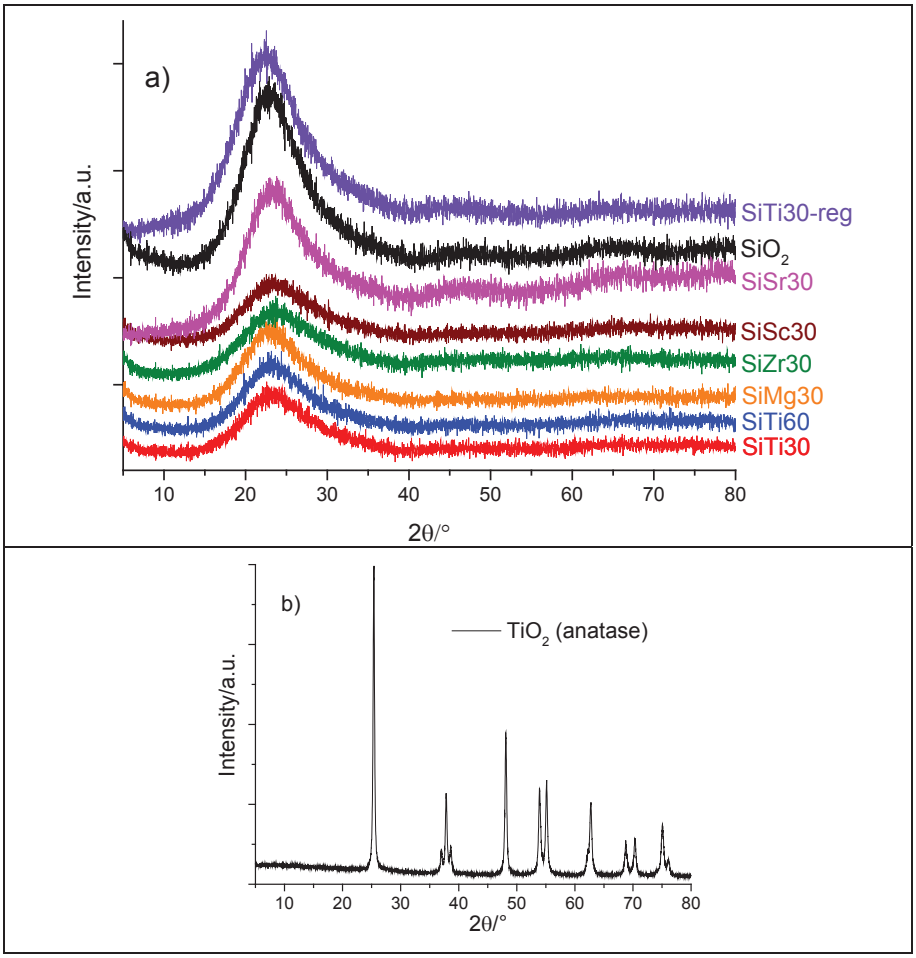

Figure 4.4. X-ray diffractograms of fresh a) SiTi30, SiTi60, SiMg30, SiZr30, SiSc30, SiSr30, SiO_2 and SiTi30-reg catalysts and b) TiO_2.

The only differences in the represented patterns are the intensities of the reflections. Similar behaviour was observed on SiTi30-reg catalyst. In addition, XRD of bare TiO_2 showed its crystalline nature with sharp reflections at 26°, 38°, 48°, 54°, 56°, 63°, and 75° which can be assigned to the anatase phase (PDF 01-084-1286 and see Figure 4.4 b).

4.1.3.3 Pyridine Fourier transform infrared spectroscopy (Py-FTIR)

FTIR spectra of adsorbed pyridine of bare SiO_2 and SiO_2-MO_x were routinely recorded at 250 °C to investigate the nature of acid sites on the surface of catalysts as shown in Figure 4.5 and related band intensities are listed in Table 4.3. Generally, pyridine is coordinatively adsorbed at Lewis acid sites (L-Py, LS) showing bands at 1445-1460 cm^{-1} and 1610-1620 cm^{-1}, while Brønsted acid sites (PyH^+, BS) are characterized by bands at 1540-1548 cm^{-1} and 1635-1640 cm^{-1} [136].

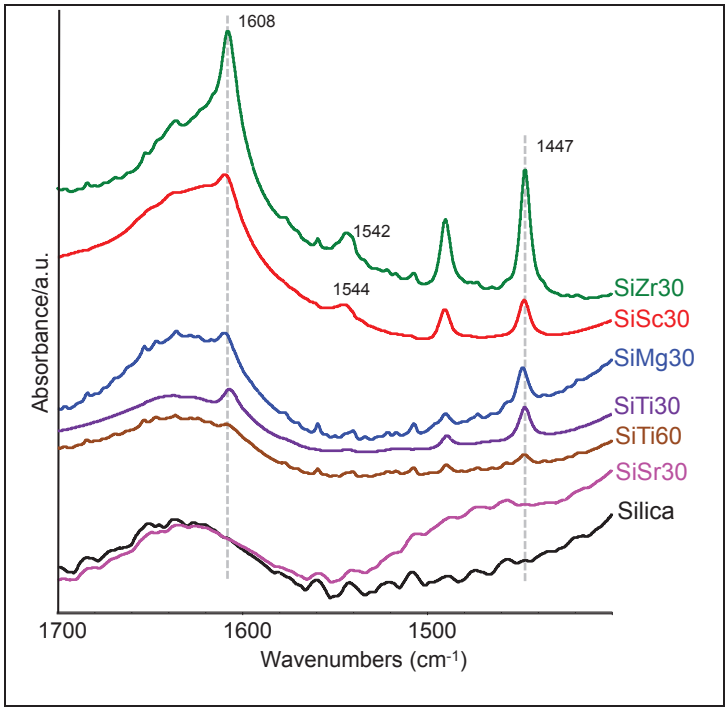

Figure 4.5. FTIR spectra of adsorbed pyridine of SiZr30, SiSc30, SiMg30, SiSr30, SiTi30, SiTi60 and silica catalysts at 250 °C

The bands around 1600 cm^{-1} represent the Lewis acid sites and can be considered as the measure of Lewis acid strength on the surface of catalysts. The bands at around 1595 cm^{-1} and 1605 cm^{-1} can be assigned to the weak-medium Lewis acid site as well as strong-medium Lewis acid sites, respectively [136]. It is important to note that the band at around 1447 cm^{-1} was considered to calculate the number of Lewis acidic (L-Py) sites. The sol-gel prepared SiO_2 obviously doesn't contribute to the surface acidity.

Table 4.3. Pyridine band intensity for Lewis acid sites at 250 °C of SiM30 catalysts.

Catalysts	Band intensity at 250 °C (L-Py)
SiTi30	0.46
SiTi30-reg	0.39
SiTi60	0.13
SiMg30	0.42
SiZr30	1.64
SiSc30	0.45
SiSr30	0.06
SiO_2	0

Among all prepared catalysts, SiZr30 exhibited highest Lewis acidic bands at 1447 and 1600 cm^{-1} with the band intensity of 1.64 at 250 °C and SiSc30 showed weak Lewis acidic band with the band intensity of 0.45. SiZr30 and SiSc30 catalysts also showed small and weak bands at 1542 cm^{-1} and 1544 cm^{-1}, respectively, which can be attributed to the Brønsted acid site. However, concentration of these acid sites was found to be negligible. These large numbers of Lewis acidic sites and few Brønsted acidic sites might be responsible for high activity and selectivity to acrolein (60% and 54%). Similarly, SiMg30 also showed the Lewis acidic bands at 1447 cm^{-1}, with the band intensity of 0.42 being nearly the same as SiSc30. The selectivity to acrolein with SiMg30 catalyst was found to be rather low (28%), however, it showed considerable selectivity to the desired TAG (17%). SiSr30 didn't show any bands for acidic sites and TAG selectivity was also found to be the poorest among all catalysts (except for neutral SiO_2 and TiO_2). However, it may possess some basic sites which might be a determining factor for high conversion towards acetylation. Interestingly, the Lewis acid band intensity of SiTi30 catalyst was nearly same as SiMg30 and SiSc30 catalysts at 1447 cm^{-1} (see Table 4.3). But SiTi30 catalyst exceptionally exhibited highest catalytic activity and selectivity to the desired TAG as 39.3% at 300 °C. Moreover, SiTi60 catalysts showed very low band intensity (0.13) at 1445 cm^{-1} due to lower titanium content compared to SiTi30 (Figure 4.6 and Table 4.3), and still showing high selectivity to TAG (32% at 325 °C). In order to understand more in detail, FTIR spectra of pyridine adsorbed on fresh SiTi30, spent SiTi30 from regular experiment (Figure 4.2 g) and SiTi30-reg catalysts were recorded and studied in the temperature range from 150 °C to 400 °C (See Figure 4.6 and Table 4.3). The obtained results were compared with each other in terms of band intensities calculated at 250 °C. The band intensity at 1447 and 1595 cm^{-1} of the fresh SiTi30 sample was essentially lowered with the increase in temperature, suggesting that the bands arises from physically adsorbed pyridine or hydrogen bonded pyridine. On the spent SiTi30 sample, only the broad bands for the adsorbed esters were observed at around 1750 and 1440 cm^{-1} and they were stable up to 300 °C; whereas on the SiTi30-reg catalyst low pyridine adsorption was observed.

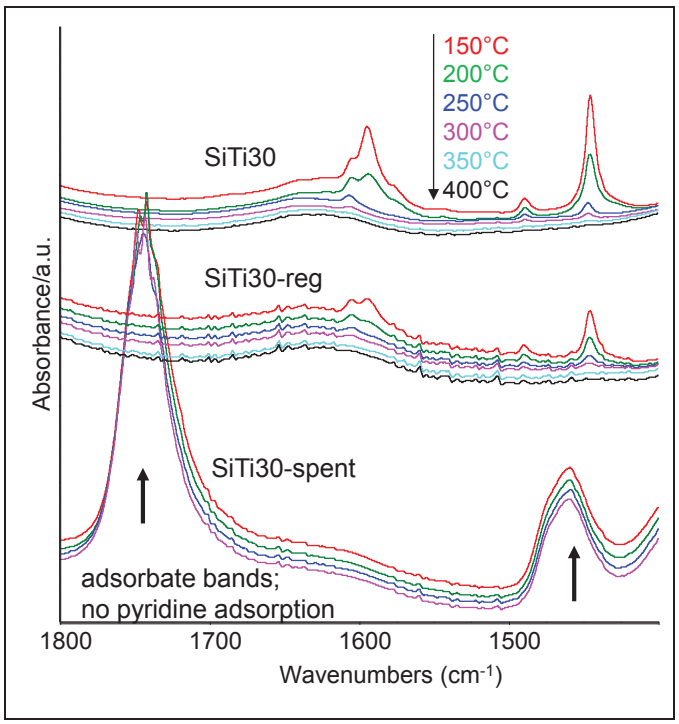

Figure 4.6. FTIR spectra of pyridine adsorbed on SiTi30 fresh, SiTi30 spent (regular experiment Figure 4.2 g) and SiTi30-reg catalysts.

The band intensity of SiTi30-reg catalyst at 1447 cm^{-1} obtained at 250 °C (0.39) is very similar to the fresh catalyst (0.45). On the other side, a significant change in surface area and pore volume of SiTi30-reg was observed (section 4.1.3.1). From these results it seems that not only acidity, but some other factor plays a significant role in glycerol acetylation under applied experimental conditions. If acidity would be only the significant factor, then SiMg30 and SiSc30 should show similar activity and selectivity to TAG as SiTi30 catalyst. Thus, in addition to acidity, some other factor should dominate the catalytic activity and selectivity. It is well-known that Ti may be incorporated into the tetrahedral framework of SiO_2 by substitution of lattice Si atoms to form Si–O–Ti bonds [143] which might be a dominating factor in gas phase glycerol acetylation. To determine structure activity-relationship and to confirm the formation of Si–O–Ti bonds, fresh SiTi30 and SiTi30-reg catalysts were further intensively characterized using sophisticated techniques.

4.1.3.4 Temperature programmed desorption (TPD) of NH_3

In order to investigate the strength and total number of acid sites of fresh SiTi30 sample and other two calcined at 700 and 800 °C, NH_3-TPD profiles were recorded as shown in Table 4.4 and Figure 4.7. Complete ammonia desorption for all three catalysts was observed at 180 °C, indicating presence of weak acid sites. The total acidity of fresh SiTi30 increased from 102.6 to 108.9 µmol/g with the increase in calcination temperature from 500 °C to 700 °C.

Table 4.4. Total acidity of selected catalysts.

Catalysts	Total acidity (μmol/g)
SiTi30	102.6
SiTi30 C700	108.9
SiTi30 C800	84

However, SiTi30 catalyst calcined at 800 °C showed less acidity (84 μmol/g), which might be due to changes in the structural arrangement of Ti species within SiO_2 matrix occurred during thermal treatment. Although there is slight variation in total acidity as well as surface area (see section 4.1.3.1), it has no significant effect on catalytic activity and selectivity towards acetins.

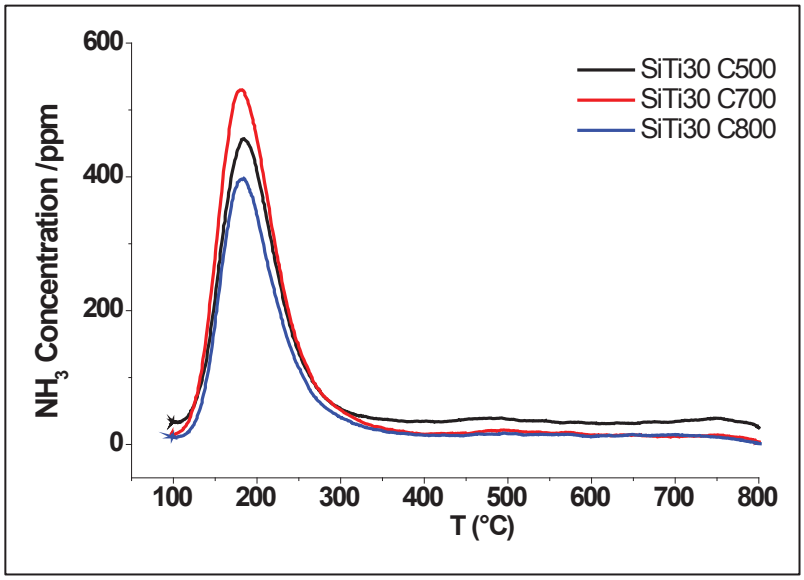

Figure 4.7. Ammonia TPD profile for SiTi30 C500 (parent sample), SiTi30-C700 and SiTi30-C800.

4.1.3.5 UV-visible and ATR-IR spectroscopy

In order to understand the nature and coordination of Ti^{4+} ions in the silica, UV-vis spectra of SiTi30, SiTi30-C700, SiTi30-C800 and SiTi30-reg catalysts were recorded (see Figure 4.8). The spectroscopic data associated with SiTi30 and other higher calcined catalysts were compared with the reference and well-published titanium silicate (TS-1 zeolite) catalyst. In TS-1 catalyst system, Ti-species are well occupied tetrahedrally within the framework of silica in the form Si-O-Ti bonds. This comparison of characterization data could show some insight on understanding the behaviour of Ti when added to a silica matrix. In general, isolated Ti^{4+} in TS-1 exhibits LMCT (ligand to metal charge transfer) bands in the range of 200-220 nm which can be ascribed to the tetrahedral environment whereas Ti in anatase shows LMCT band at 333 nm which can be assigned to the octahedral environment [144, 145]. Comparative study was performed by On et al. on TS-1 and SiO_2-TiO_2 mixed

oxide, where tetrahedral Ti in TS-1 exhibited three LMCT transitional bands at 199, 226 and 248 nm, whereas tetrahedral Ti in TiO_2-SiO_2 showed LMCT bands at 250 nm [146]. This is most probably due to the difference in Si-O-Ti bond angles of 163° and 159° in TS-1 and TiO_2-SiO_2, respectively. The higher bond angle may result in higher π-electron donation which ultimately contributes to higher LMCT transition energy [147]. Another factor is Ti-O bond length, which is different in TS-1 and SiO_2-TiO_2 mixed oxide and can affect the resulting LMCT band wavelength [148]. Hadi Nur et al. reported that LMCT for Ti in tetrahedral environment appears in the range of 230-280 nm and Ti in octahedral at 260-330 nm [149].

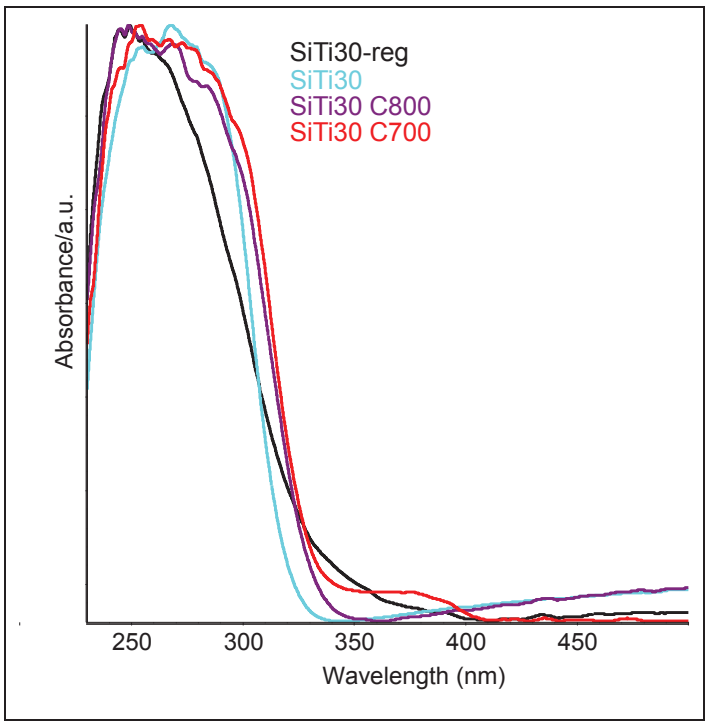

Figure 4.8. UV-vis spectra for SiTi30, SiTi30-C700, SiTi30-C800 and SiTi30-reg catalysts.

The sample SiTi30 exhibits LMCT transition bands at around 245 nm indicating that most of Ti-species are present in tetrahedral state. Increasing the calcination temperature, the LMCT transition band shifts to higher wavenumber referred to as blue shifts (250 nm and 260 nm), might be due to change in tetrahedrally coordinated Ti-species into polymeric penta-, hexa- or octa-coordinated Ti-species [150]. In the UV-vis analysis of SiTi30-reg sample, the LMCT transition band shifted to lower wavelength (247 nm) compared to fresh catalyst (260 nm) and tailing of the band was also reduced. Nevertheless, from these results it seems that most of the Ti-species are incorporated in tetrahedral framework within the SiO_2 matrix in the fresh as well as SiTi30-reg catalysts.

Infrared spectra of the above mentioned catalysts were also recorded as shown in Figure 4.9. All the catalysts exhibited strong bands around 1060 and 800 cm^{-1} which can be assigned to the stretching and bending vibration of Si-O-Si, respectively. According to

literature reports, the vibrational band for Si-O-Ti bond appears in the range of 965–945 cm^{-1} [143, 151-154]. Thus, a band at around 955 cm^{-1} showed by SiTi30 can be ascribed to the Si-O-Ti stretching vibration. With an increase in calcination temperature, the band slightly shifted to the lower wavenumber (947 cm^{-1}), which again suggest that it could be due to changes in the structural arrangement of Ti species. The FTIR spectra of SiTi30-reg catalyst showed similar bands as the fresh catalyst. More importantly, the intensity of the band at 960 cm^{-1} which obviously represents Si-O-Ti bond which was very similar in the SiTi30-reg catalyst compared to fresh SiTi30 catalyst.

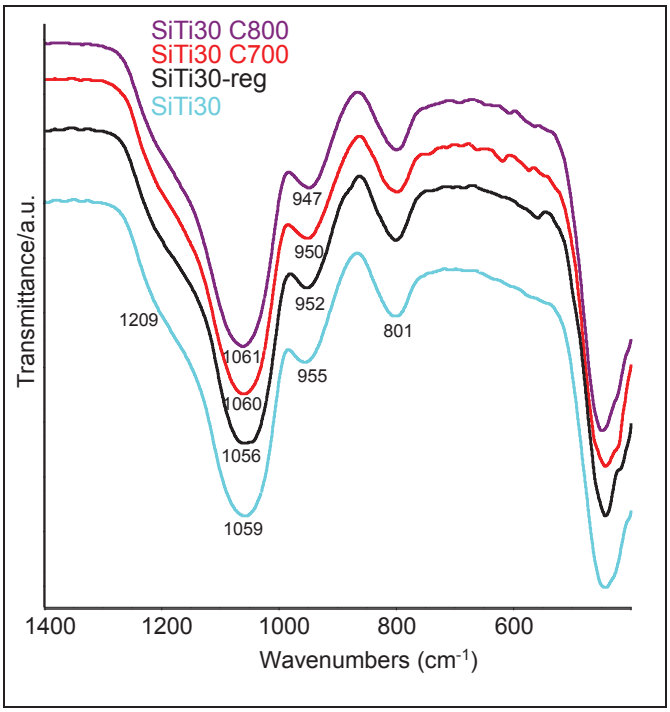

Figure 4.9. ATR-IR spectra for SiTi30, SiTi30-C700, SiTi30-C800 and SiTi30-reg catalysts.

Based on the UV-vis, ATR-IR and catalytic activity results, it is clear that the TiO_2 as a particle on the surface should not be thought as active species. The incorporation of Ti into the SiO_2 matrix to form the Si-O-Ti bond seems to be most likely related to the high activity and selectivity to acetins. However, SiTi30-reg catalyst (deactivated) also showed the vibrational band at 960 cm^{-1} for Si-O-Ti bond, which is somehow surprising. Thus, in order to confirm the presence of Si-O-Ti bonds and to understand the structure-activity relationship and deactivation of catalysts in detail, fresh SiTi30 and SiTi30-reg samples were further investigated with TEM-EDX and XPS techniques.

4.1.3.6 Transmission electron microscopy (TEM)

TEM analysis was studied in order to get more information on morphology and distribution of TiO_2 within the SiO_2 matrix (Figure 4.10). From the TEM image of SiTi30, it can be clearly seen that the TiO_2 species are homogeneously dispersed into silica matrix. However, on

magnifying image at the edge (as shown by arrow at 10 and 5 nm scale), some indications for small heavy TiO_2 particles were observed (Appendices Figure A3 'a' and 'b'). EDX analysis showed that Si: Ti atomic ratios were constant (97.73: 2.27 and 97.18: 2.82) throughout the sample. The TEM-EDX analysis further revealed that the particle size distribution of TiO_2 in SiO_2 is much narrow which indicates that most of the added TiO_2 species are distributed into bulk.

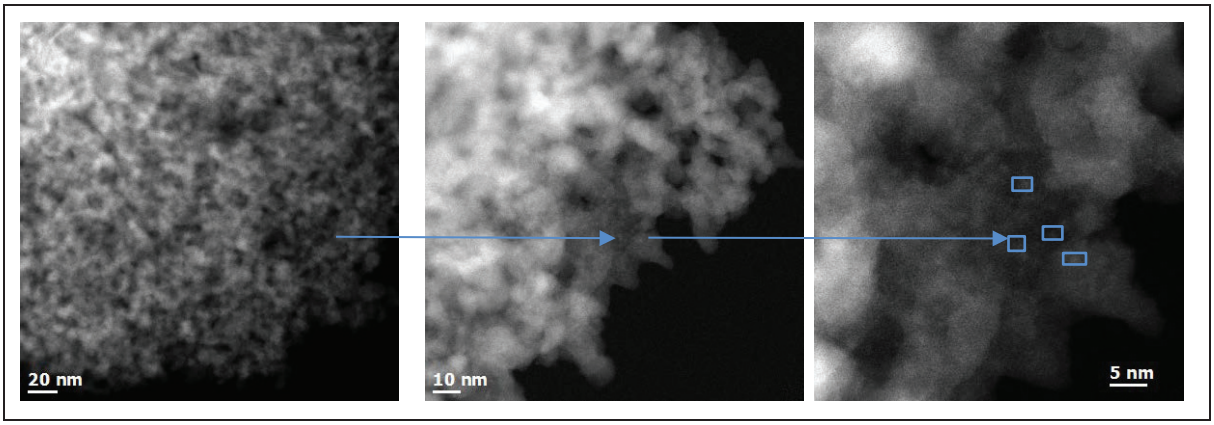

Figure 4.10. STEM-HDAAF images of fresh SiTi30 at 20, 10 and 5 nm magnification.

Similarly, SiTi30-reg catalyst was analyzed by TEM (see Figure 4.11) and compared with the fresh SiTi30 catalyst. The image of regenerated catalyst showed non-homogeneous elemental distribution. This is most probably due to the migration of TiO_2 species from bulk on to the surface of silica. In addition, one very large TiO_2 particle was observed (Appendices Figure A4 b).

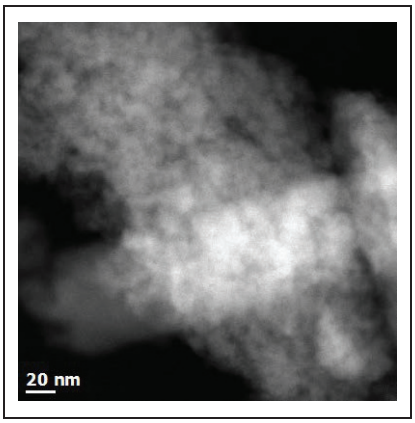

Figure 4.11. STEM-HDAAF images of SiTi30-reg catalyst.

The TEM-EDX analysis of the SiTi30-reg sample showed that the size distribution of TiO_2 was less narrow compared to fresh catalyst. Moreover, Si: Ti atomic ratio (97.97: 1.03 and 85.23: 14.77) was also found to be different (see Figure A4 'a' and 'b' in appendices). From this result, one can say that SiTi30 is active and selective as long as Ti is incorporated in the bulk in the form of Si-O-Ti. However, on regeneration enrichment of Ti on the surface from bulk is observed, which might be the most probable reason for deactivation.

4.1.3.7 X-ray photoelectron spectroscopy (XPS)

To clarify the elemental composition in the near surface region of SiTi30 of fresh and SiTi30-reg catalysts, XPS was measured and results are represented in Table 4.5. The surface Ti content (calculated based on atom-%) of SiTi30 was only 39% compared to bulk concentration. This indicates that less Ti-species are present on the surface of the catalyst i.e. most of the added Ti is embedded in the tetrahedral sites of SiO_2 matrix. On the other hand, a fraction of surface Ti species of SiTi30-reg catalyst increased to 71%, which indicates that Ti species have migrated from bulk to surface.

Table 4.5. Comparison of the near surface region and bulk composition of fresh SiTi30 and SiTi30-reg catalysts.

Catalysts	Near surface	Bulk
	Ti/(Si+Ti) from XPS	Ti/(Si+Ti) from ICP
SiTi30	0.011	0.028
SiTi30-reg	0.020	0.028

To confirm the existence of Si-O-Ti bonds in the structure of SiTi30, the binding energies (BE) value of Ti and O were measured as shown in Table 4.6. According to the literature in TiO_2-SiO_2 composites, Ti $2p_{3/2}$ exhibiting BE value at 458.4 eV can be assign to TiO_2 whereas O 1*s* exhibiting BE values at 530 eV, 531.5 eV and 533.1 eV can be assign to Ti-O-Ti, Ti-O-Si and Si-O-Si bonds, respectively [155]. SiTi30 fresh sample showed BE value of Ti $2p_{3/2}$ at 459.79 eV (highly intense) and 465.93 eV (low intensity). Similarly, O 1*s* showed BE at 532.3 eV (high intensity) which matches best with reported value for Si-O-Ti bonds formation. From these results, it is confirmed that the most of the Ti present in the framework of SiO_2 in the form of Si-O-Ti bond. On the other side, the BE of the Ti $2p_{3/2}$ level in SiTi30-reg shifted from 459.79 eV (fresh SiTi30) to 460.7 eV. The BE values of the O 1*s* level were 533.17 eV and 530.05 eV, which can be assigned to the Si-O-Si and Ti-O-Ti bonds. The BE value for Si-O-Ti bond was not observed which is most likely due to the enrichment of Ti species on the surface to form TiO_2 particles. Based on the XPS results, one can say that the TiO_2 as particles on surface should not be thought as active species. This results also confirms that the incorporation and existence of Ti into the SiO_2 matrix to form the Si-O-Ti bonds and should be the responsible factor for high activity and selectivity to acetins.

Table 4.6. Binding energy values for Ti 2p3/2 and O 1s of SiTi30 and SiTi30-reg catalysts.

Catalysts	Binding energy values (eV)	
	$Ti2p_{3/2}$	O1s
SiTi30	459.79	527.7
	465.94	532.3
SiTi30-reg	460.71	530.05
	466.44	533.17

4.1.3.8 Thermal gravimetric analysis (TGA) and elemental (C, H and O) analysis

The deposition of carbonaceous deposits on the surface of spent SiTi30 catalyst from a regular experiment (section 4.1.3.1, Figure 4.2 g) was measured by TGA and C, H, N analyses. The thermal analysis of spent catalyst SiTi30 revealed 34% of weight loss (Figure 4.12). The DTA curve of spent SiTi30 catalyst exhibited two exothermic peaks at 350 °C and 500 °C, which clearly indicate two different types of carbon deposits. The large intensity peak at 350 °C indicates that low-stability deposit formation is more pronounced. The intensity of the second peak at 500 °C is much less but represents indeed thermally stable carbon deposits. From the DTA curve, it can be concluded that the regeneration temperature should be at least 500 °C for the complete removal of carbon deposits. The same sample was also analyzed by CHN elemental analyzer, in order to determine the carbon content on the surface of the catalyst. Nearly 14.1 wt% carbon and 1.9 wt% hydrogen were observed on the catalyst surface indicating that formation of carbon deposits is mainly from oxygenates (esters).

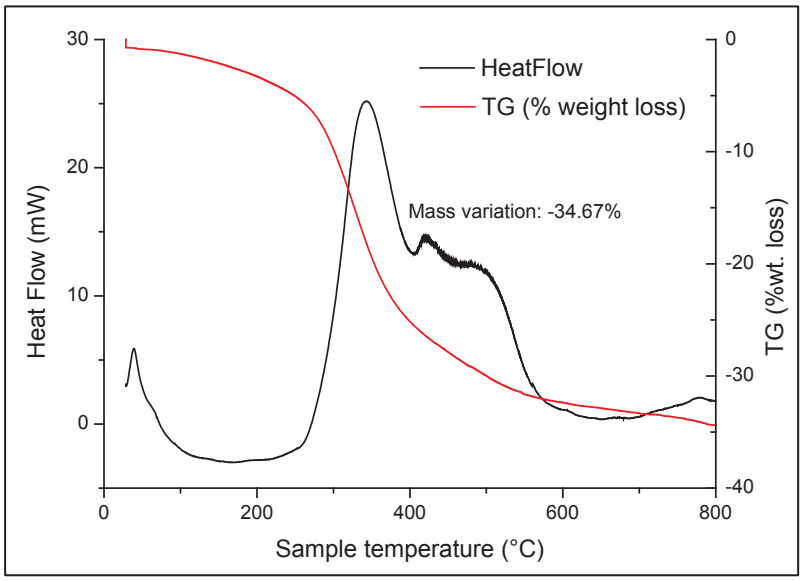

Figure 4.12. TGA and DTA profiles for SiTi30 catalyst.

4.1.4 Summary and conclusions

Acetylation of glycerol was studied over solid acidic catalysts in the gas phase for the first time. Initially, bare support γ-Al_2O_3 and silicotungstic acid (STA) supported on SiO_2 and Al_2O_3 were used as a catalyst (selected from liquid phase studies) in gas phase glycerol acetylation in the temperature range of 225 – 325 °C. The catalytic results revealed a high conversion of glycerol, however, low selectivity towards desired triacetin (TAG) was achieved and instead a very high selectivity to acrolein was obtained. The maximum selectivity for acrolein was more than 90% over STA/Al_2O_3 and γ-Al_2O_3 at 325 °C and 67% over STA/SiO_2 at 225 °C, always at

complete conversion of glycerol. On the other side, maximum selectivity to TAG was 16% over STA/Al_2O_3 at complete conversion of glycerol at 250 °C. The high selectivity to acrolein is attributed to the high acidity of catalysts (either Lewis or Brønsted acidic sites). Also the presence of acetic acid the reaction mixture may activate the catalysts by removing carbon deposits adsorbed on the catalysts surface and increase the yield of acrolein. Anyway, the acrolein yield achieved over STA/Al_2O_3 is comparable to the state of art. The catalysts stability in long-term test is not evaluated

Thus, another series of weakly acidic mixed metal oxide (SiO_2-MO_x) catalysts were prepared by sol-gel method, characterized and evaluated in gas phase glycerol acetylation. Among the prepared catalysts, titanium containing SiO_2 (SiTi30 and SiTi60) catalysts were active and selective towards desired triacetin (39%), whereas SiSr30 and SiMg30 were active but less selective toward TAG (3% and 16%) at complete glycerol conversion. Using high acetic acid to glycerol molar ratio (6/1), SiTi30 showed the highest selectivity of 55% to desired TAG. In addition, strong temperature-selectivity dependence was observed, especially with TAG and acrolein. Interestingly, diglycerol tetraacetate (DGTA) is formed as previously observed in batch operation at water-free conditions. On the other side, SiZr30 and SiSc30 catalyst gave high selectivity to undesired acrolein as 60% and 54%, respectively, with complete conversion of glycerol. The influence of reaction conditions such as acetic acid to glycerol molar ratio and WHSV over SiTi30 showed a positive effect on TAG selectivity with 40% and 55%, respectively. Long-term stability test was performed and this catalyst is stable up to 200 h with a marginal decrease in TAG selectivity. However, upon regeneration at elevated temperature the selectivity to TAG dropped due to changes in the dispersion of the Ti species.

The prepared catalysts were mesoporous in nature and specific BET surface area was in the range of 275-570 m^2/g. Increasing calcination temperature of SiTi30 catalyst decreased surface area most probably due to the changes in the structure. Prepared catalysts were X-ray amorphous which indicated that the MO_x species were highly dispersed in the SiO_2 matrix. Pyridine FTIR spectroscopic analysis all of the prepared catalysts showed Lewis acid sites without any Brønsted acid sites. ATR-IR, Raman and UV-vis spectroscopic analyses proved the formation of Si–O–Ti bonds and that most of Ti-species were present in the tetrahedral geometry. XPS analysis of SiTi30 revealed that the content of Ti on the surface of the catalyst is very low compared to bulk; however, it was also confirmed measured from binding energy (XPS) that most of the Ti is incorporated in the silica matrix in the form of Si–O–Ti bonds. TEM-EDX analysis also showed that Ti was uniformly distributed in the silica matrix. The high selectivity to acrolein is attributed to the strong acidic sites present on the surface of the catalysts. On the other side, high selectivity to TAG is related to the formation of Si–O–Ti bonds.

4.2 Continuous operation – Effect of nature of SiO_2 support

This section presents a refined investigation of catalytic performance of SiO_2 supported titania with respect to the nature of silica support. In particular, mesoporous silica-based materials SBA-15 and MCM-41 were chosen. The obtained catalytic results were correlated with the results from several characterization techniques such as N_2 physisorption, XRD, XPS, Py-FTIR and TEM. A series of TiO_2 containing SiO_2 catalysts with a molar ratio of SiO_2/TiO_2 = 30/1 with different types of SiO_2 support (SiO_2-gel, SBA-15 and MCM-41) were prepared and tested in glycerol acetylation at 225-325 °C.

4.2.1 Catalytic performance

4.2.1.1 Influence of temperature

The glycerol conversion and product selectivities measured with Ti-SiO_2, Ti-SBA-15 and Ti-MCM-41 in continuous flow operation at selected reaction conditions (225-325 °C, acetic acid: glycerol molar ratio = 6:1, 0.6 g catalyst loading and WHSV = 2.73 h^{-1}) with N_2 as diluent and methane as internal standard at ambient pressure are shown in Figure 4.13. The conversion of glycerol was 84% and 88% with Ti-SiO_2 and Ti-SBA-15, respectively, at 225 °C and reached almost 100% at 275 °C (Figure 4.13 ‘a’ and ‘b’). On the other side, glycerol conversion was almost complete with Ti-MCM-41 at any given temperature (Figure 4.13 c).

For all the catalysts the TAG selectivity runs through a maximum in the temperature 225-325 °C. The highest selectivity for TAG of 47.5% was achieved with Ti-MCM-41 at 275 °C whereas Ti-SiO_2 and Ti-SBA-15 showed maximum selectivity to TAG of 42% and 44% at 300 °C with a complete conversion of glycerol. Ti-MCM-41 performed slightly better than Ti-SiO_2 and Ti-SBA-15, which can be explained on the basis of catalysts preparation methods. The Ti-MCM-41 catalyst was prepared by a sol-gel method which might lead to a high distribution of Ti species in SiO_2 support compared to Ti-SiO_2 and Ti-SBA-15 catalysts prepared by impregnation method.

With further increase in reaction temperature to 325 °C, selectivity for acrolein increased remarkably, mainly at the expense of TAG. Ti-SBA-15 and Ti-MCM-41 exhibited 82% and 79.5% selectivity to acrolein, whereas Ti-SiO_2 showed 60% selectivity at 325 °C. It seems that glycerol above 300 °C starts to dehydrate to produce acrolein as the major product. In addition, acetic acid might play a role by activating catalyst surface (removing adsorbed coke) to achieve such a high selectivity of acrolein. Similar behaviour was also observed in the previous section where at a high temperature (> 300 °C) glycerol favours dehydration over esterification (acetylation).

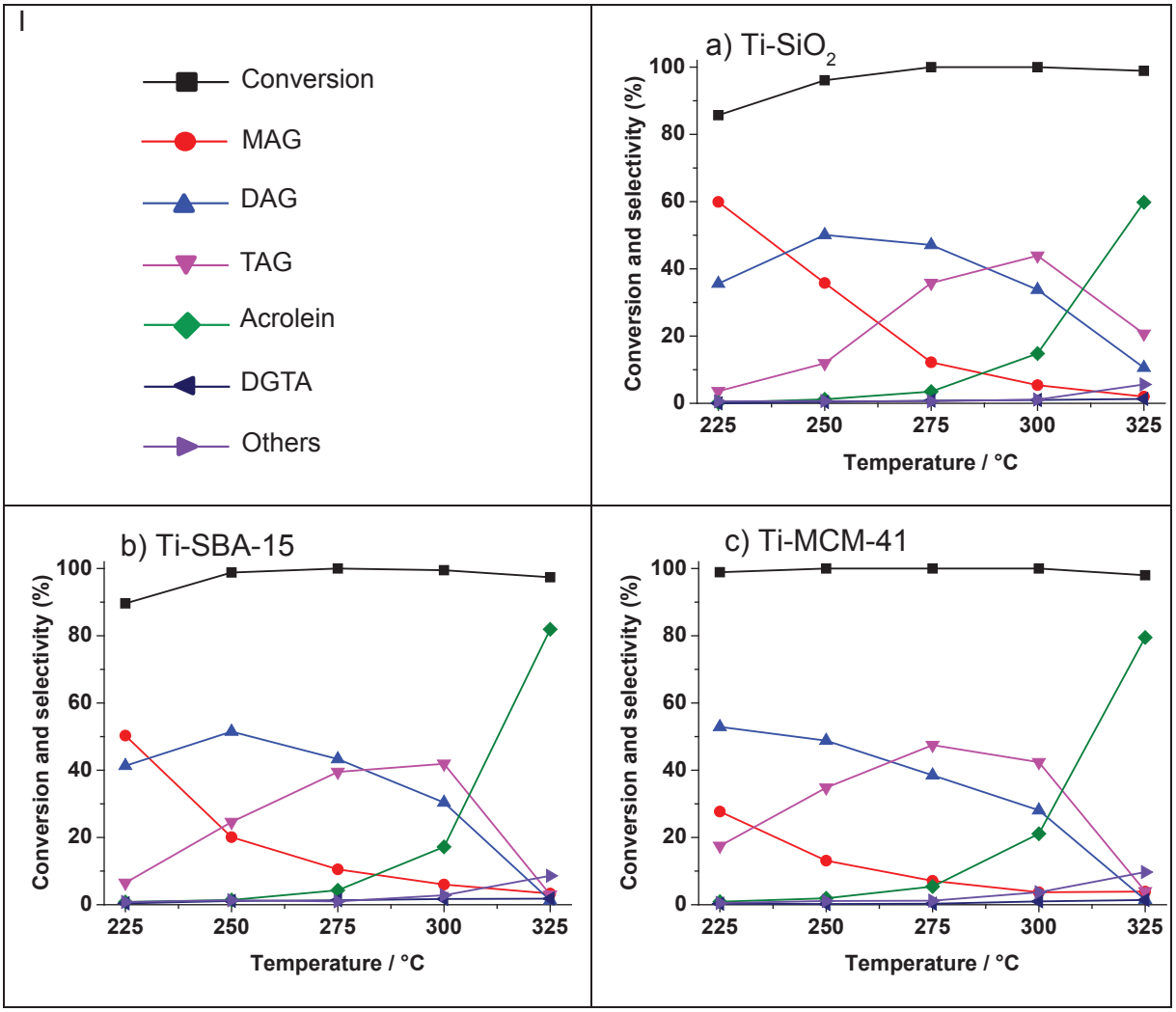

Figure 4.13. Influence of temperature on glycerol conversion and product selectivities for Ti-SiO_2, Ti-SBA-15 and Ti-MCM-41. Reaction conditions: acetic acid: glycerol molar ratio = 6/1, catalysts amount = 0.6 g, flow rate = 0.025 ml/min, N_2 = 29.7 ml/min, WHSV = 2.73 h^{-1}.

4.2.1.2 Influence of WHSV

In order to study the effect of WHSV on catalyst activity and selectivity, tests were performed with Ti-MCM-41, Ti-SBA-15 and Ti-SiO_2 using 0.3 g, 0.6 g and 0.9 g catalysts weight, i.e., varying WHSV from 5.45 h^{-1} to 1.82 h^{-1} under identical reaction conditions (Figure 4.14). For 0.6 g experiment (WHSV = 2.73 h^{-1}) refer to previous section 4.2.1.1 (Figure 4.13). Varying WHSV in the range of 5.45-1.82 h^{-1}, conversion of glycerol increases and also change in product distribution was clearly seen. However, at low WHSV = 1.82 h^{-1} (i.e. high catalyst weight = 0.9 g) and high temperature (325 °C), a slight decrease in conversion of glycerol (98%) was observed. Along with the variation of WHSV in the given range in particular at low temperature (≤ 300), the TAG selectivity consistently increased and reached 43.9%, 45.7% and 47.8% with Ti-SiO_2, Ti-SBA-15 and Ti-MCM-41, respectively.

Table 4.7. Influence of WHSV (h^{-1}) on TAG (%) selectivity at 275 and 300 °C.

Catalysts	275 °C			300 °C		
	WHSV (h^{-1})			WHSV (h^{-1})		
	5.45	2.73	1.82	5.45	2.73	1.82
Ti-SiO_2	10.1	35.8	40.0	26.1	43.9	38.1
Ti-SBA-15	24.4	39.5	45.7	37.2	41.2	29.7
Ti-MCM-41	30.8	47.5	47.8	45.0	42.4	36.7

The selectivity of TAG on these catalysts seems to pass through a maximum by further variation of WHSV at 275 °C and 300 °C (see Table 4.7). This is a most likely due to the parallel reaction running simultaneously such as glycerol dehydration and/or polymerization. At high temperature i.e. from 300 °C, a dramatic increase in selectivity toward acrolein was observed. At 325 °C with Ti-SiO_2, selectivity for acrolein increases from 60% to 77%, when WHSV varied from 2.73 h^{-1} to 1.82 h^{-1}. On the other side, at 325 °C, Ti-SBA-15 and Ti-MCM-41 showed nearly the same acrolein selectivity (≈ 80%) at 2.73 h^{-1}. Further varying WHSV to 1.82 h^{-1} showed a slight change in acrolein selectivity (84% and 81%, respectively). In general, dehydration of glycerol to acrolein is performed at high temperature (> 300 °C) [156] and the use of strong acidic catalysts such as supported HPAs can lower reaction temperature (≤ 300) as previously observed (see section 4.1.1). However, the present catalyst systems possess weak acid sites that are not able to catalyze dehydration of glycerol to acrolein at low temperature.

This is reasonable as, acetylation of glycerol is an endothermic, non-spontaneous and thermodynamically resistant reaction ($\Delta G_{Gly \rightarrow TAG}$ = 92.53 kJ/mol) [82], whereas dehydration of glycerol is endothermic but spontaneous and thermodynamically favoured reaction ($\Delta G°$= – 12.12 kJ/mol) [157]. This might be a possible explanation for the rise in acrolein selectivity in particular at higher temperatures. Moreover, due to high activation energy for dehydration of glycerol, a high reaction temperature is needed. On the other side, activation energy for acetylation of glycerol attained at lower temperature compared to dehydration of glycerol (as observed in liquid phase system). The activation energy for glycerol acetylation in liquid phase system was not measured due to the use of toluene as an entrainer which stabilized reaction temperature at 105 °C and the detailed kinetic and thermodynamic investigation in gas phase system is planned to be studied in future.

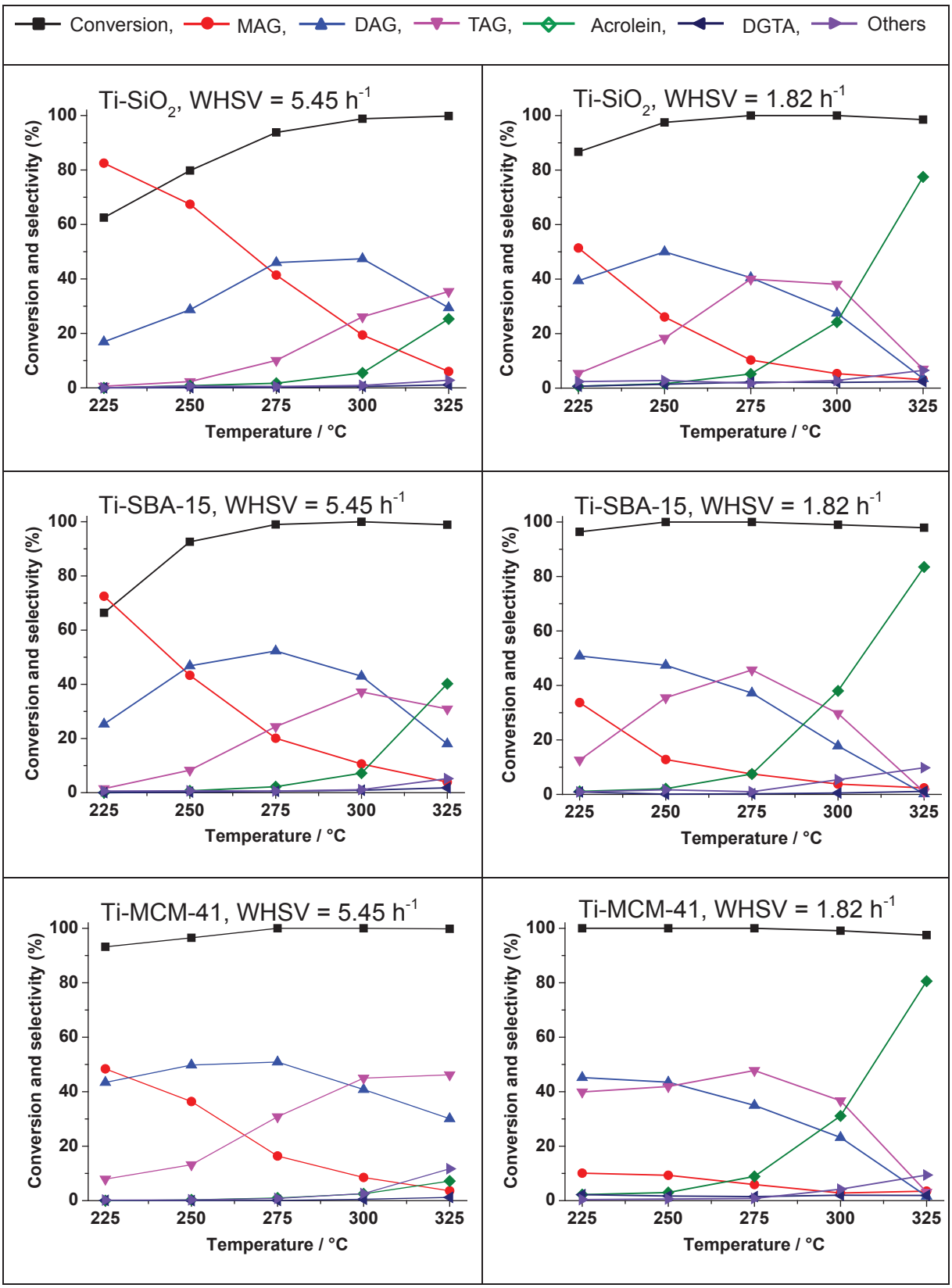

Figure 4.14. Influence of catalyst weight of Ti-MCM-41, Ti-SBA-15 and Ti-SiO_2 on glycerol conversion and product selectivities. Acetic acid: glycerol molar ratio = 6:1, catalysts amount = 0.3 -0.9 g, flow rate = 0.025 ml/min, N_2 = 29.7 ml/min, WHSV = 1.82-5.45 h^{-1}.

4.2.1.3 Long-term stability test of Ti-MCM-41

The Ti-MCM-41 catalyst was found to be active and selective and thus, it was selected for long-term stability test. The catalyst was tested at 275 °C over 100 h without interruption in order to study deactivation under identical condition. A conversion of glycerol was found to be completed throughout the experiment (Figure 4.15. a). Selectivity to TAG was more than 40% in the first hour, but decreased significantly with time to 20% within 24 h and then remained then almost stable for next 75 h with slight decreased in TAG selectivity.

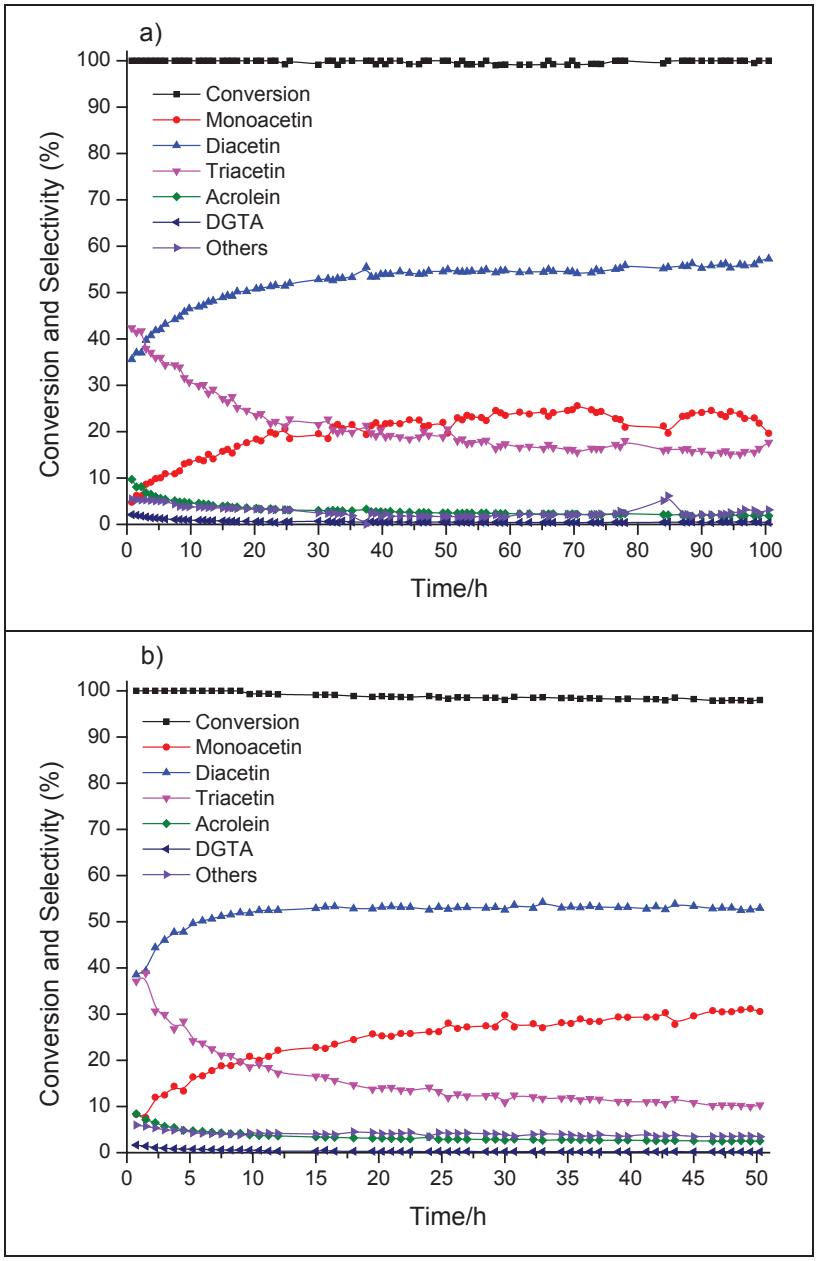

Figure 4.15. a) Long-term stability test with Ti-MCM-41 catalyst and b) regeneration test. Reaction condition: acetic acid: glycerol molar ratio = 6/1, catalysts amount = 0.6 g, flow rate = 0.025 ml/min, N_2 = 29.7 ml/min, WHSV = 2.73 h^{-1}.

The deactivation is most probably due the strong adsorption of the carbonaceous material. On the other side, low selectivity to acrolein was observed. Hence, one can say that the carbonaceous deposits formed on the surface of the catalyst are most likely from esters. The catalyst was regenerated by calcination (500 °C, 5 h) in the presence of air in a muffle furnace in order to burn-off carbon deposits. Then the catalyst test (regeneration test) was repeated under an identical condition in order to compare its performance with the fresh one. In the first 1 hour of reaction time, regenerated catalyst showed nearly 40% selectivity to TAG but later it continuously decreased to 13% within 25 h which remained nearly constant for next 25 hours (see Figure 4.15 b). After 50 h, the selectivity to TAG was 10% at complete conversion of glycerol. Based on these results, one can say that the catalyst had reached some kind of equilibrium state, as it showed same selectivity pattern when fresh catalyst is used. This catalyst was recovered and again calcined at 500 °C for 5 h in air (denoted as Ti-MCM-41-reg). To gain more knowledge of the structure-activity relationship, a thorough characterization of both fresh and regenerated catalysts is needed. Hence, Ti-SiO_2, Ti-SBA-15, Ti-MCM-41 and Ti-MCM-41-reg were further characterized by sophisticated techniques.

4.2.2 Characterization of catalysts

4.2.2.1 Textural properties and ICP analysis

The BET surface area, pore volumes and pore diameters of prepared catalysts are presented in Table 4.8. The surface areas of the Ti-SBA-15 and Ti-SiO_2 catalysts are significantly less compared to Ti-MCM-41. The impregnation of TiO_2 over the SBA-15 and SiO_2 partially blocks the pores resulting in a decrease in its surface area. However, there was no significant change in the pore diameter as well as pore volume. This indicates that the impregnated TiO_2 species are located inside the mesopores of SBA-15 and SiO_2. On the other side, Ti-MCM-41 catalyst was prepared by sol-gel method and exhibited high specific surface area and low pore diameter compared to Ti-SBA-15 and Ti-SiO_2. There was no impregnation step that might plug pores.

Table 4.8. Textural properties and results from ICP-OES analysis of the prepared catalysts.

Catalysts	A_{BET} (m^2/g)	Pore Volume (cm^3/g)	Pore diameter (nm)	Nominal metal content (Ti wt%)	ICP-OES (Ti wt%)
SiO_2	395	0.92	9.8	-	-
Ti-SiO_2	341	0.84	10.1	2.55	2.37
SBA-15	608	0.66	4.5	-	-
Ti-SBA-15	518	0.58	4	2.55	2.47
Ti-MCM-41	989	0.94	2.5 -3.5	2.55	2.22
Ti-MCM-41*	828	0.62	2.5-4	-	-
Ti-MCM-41-reg	733	0.55	2-4	-	-

*calcined at 500 °C for 5h after long-term test

In addition, Ti-MCM-41 also showed some large pore size (40-50 nm) but the amount of these pores was considerably low. The high surface area of Ti-MCM-41 is most probably due maximum incorporation of TiO_2 species into the MCM-41 framework compared to SiO_2 and SBA-15. Thus, this can be one of the reasons to show high catalytic activity and selectivity to TAG. On calcination of Ti-MCM-41 catalyst after long-term test at 500 °C for 5 h in air, a significant decrease in surface area (989 to 828 m²/g) as well as pore volume (0.94 to 0.62 cm^3/g) was observed (denoted as Ti-MCM-41*, see Table 4.8). However, the decrease in surface area of Ti-MCM-41* (828 to 733 m²/g) as well as pore volume (0.62 to 0.55 cm^3/g) was less as on calcination of Ti-MCM-41 (500 °C for 5 h in air) catalyst after regeneration test (denoted as Ti-MCM-41-reg, see Table 4.8). This is most probably due to structural changes which occurred during regeneration of the catalyst. On the other hand, pore diameter of the Ti-MCM-41-reg catalyst was found to be comparable with the fresh catalyst. ICP-OES analysis showed that the composition of the prepared catalysts is comparable with the nominal metal content (see Table 4.8).

4.2.2.2 X-ray diffraction (XRD)

The XRD patterns of the Ti-SiO_2, Ti-MCM-41 and Ti-SBA-15 samples are depicted in Figure 4.16. All the catalysts exhibited only a broad reflection at 24°, which is a characteristic reflection for amorphous silica. Moreover, reflections for the expected TiO_2 were not observed. From these results it can be concluded that TiO_2 species are highly distributed in the SiO_2, SBA-15 and MCM-41 matrices. Similar phenomenon was also observed with the Ti-MCM-41-reg catalyst.

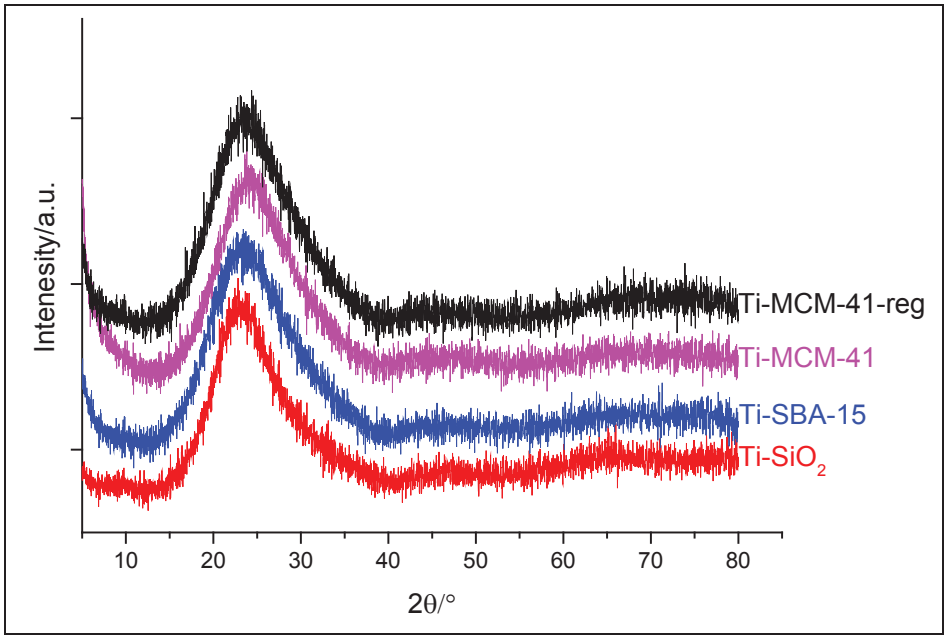

Figure 4.16. XRD patterns of Ti-SiO_2, Ti-SBA-15, Ti-MCM-41 and Ti-MCM-41-reg catalysts.

4.2.2.3 Pyridine Fourier transform infrared spectroscopy (Py-FTIR)

The FTIR spectra of adsorbed pyridine of Ti-SiO_2, Ti-SBA-15, Ti-MCM-41 and Ti-MCM-41-reg were recorded at 250 °C in order to investigate the nature of acid sites. All the catalysts exhibited only Lewis acidic sites, thus the band at around 1600 cm^{-1} can be used as a measure of Lewis acid strength [138] and the band at 1445 cm^{-1} was considered to calculate band intensities of Lewis acid sites as shown in Figure 4.17 and Table 4.9.

Ti-MCM-41 catalyst exhibited more Lewis acid sites compared to the other catalysts, most probably due to the very high dispersion of TiO_2 species in the matrix of MCM-41. The catalysts Ti-SBA15 and Ti-SiO_2 also owe Lewis acid sites; however, the band intensity is nearly half of that of Ti-MCM-41. The difference in acidity and dispersion of Ti on the support is related to preparation method. Ti-MCM-41 was prepared by a sol-gel method which leads to a high dispersion compared to Ti-SiO_2 and Ti-SBA-15 which were prepared by impregnation method. On the other side, there was no significant adsorption of pyridine on the Ti-MCM-41-reg catalyst (see Figure 4.17). Moreover, band intensity at 1445 cm^{-1} for Ti-MCM-41-reg catalyst measured at 250 °C was also negligible. This is most probably due to the structural rearrangements or partial destruction of the MCM-41 matrix. Based on these results one can say that the high catalytic activity of Ti-MCM-41 is most likely due to high Lewis acidity. However, if Lewis acidity alone was responsible for the better catalytic activity, then the Ti-MCM-41-reg should not show comparable catalytic activity as the fresh catalyst.

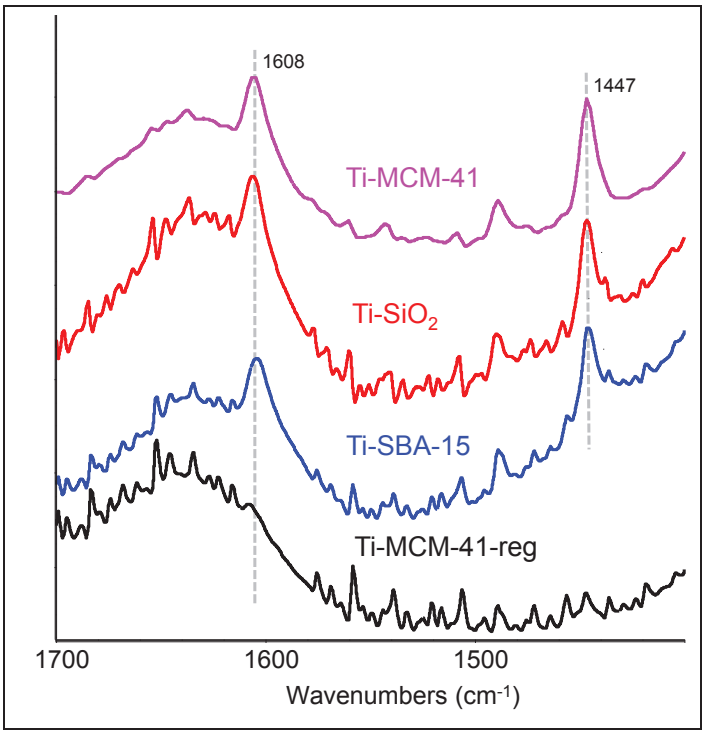

Figure 4.17. FTIR spectra of adsorbed pyridine on Ti-SiO_2, Ti-SBA-15, Ti-MCM-41 and Ti-MCM-41-reg catalysts at 250 °C.

On the same side, Ti-SBA15 and Ti-SiO_2 should show poor activity or less selectivity to TAG as they possess nearly half of Lewis acid site band intensity in comparison to Ti-MCM-41. A similar phenomenon was also observed with SiTi30 catalyst in previous section 4.1.3.3. Hence, in addition to acidity, some other factor should be responsible for the high catalytic activity. As discussed in previous section 4.1, Ti can incorporate into the SiO_2, SBA-15 or MCM-41 matrix to form Si-O-Ti bonds. Hence, the formation of Si-O-Ti bonds might be a most probable responsible factor to achieve high activity and selectivity to TAG. To confirm this, the prepared catalysts together with Ti-MCM-41-reg were further characterized by NH_3-TPD, UV-vis, ATR-IR, TEM and XPS techniques.

Table 4.9. Band intensity at Lewis acid sites of Ti-SiO_2, Ti-SBA-15, Ti-MCM-41 and Ti-MCM-41-reg catalysts at 250 °C.

Catalysts	Band intensity at 250 °C (L-Py)
Ti-SBA-15	0.53
Ti-SiO_2	0.65
Ti-MCM-41	0.97
Ti-MCM-41-reg	0

4.2.2.4 Temperature-programmed desorption of ammonia (NH_3-TPD)

The strength of the acid sites and their total amount in Ti-SiO_2, Ti-SBA-15 and Ti-MCM-41 were determined by thermal desorption of ammonia (Figure 4.18). Complete ammonia desorption was observed at around 180 °C with all catalysts, indicating the presence of weak acid sites. The Ti-MCM-41 catalyst showed highest amount of NH_3 desorption (151 µmol/g),

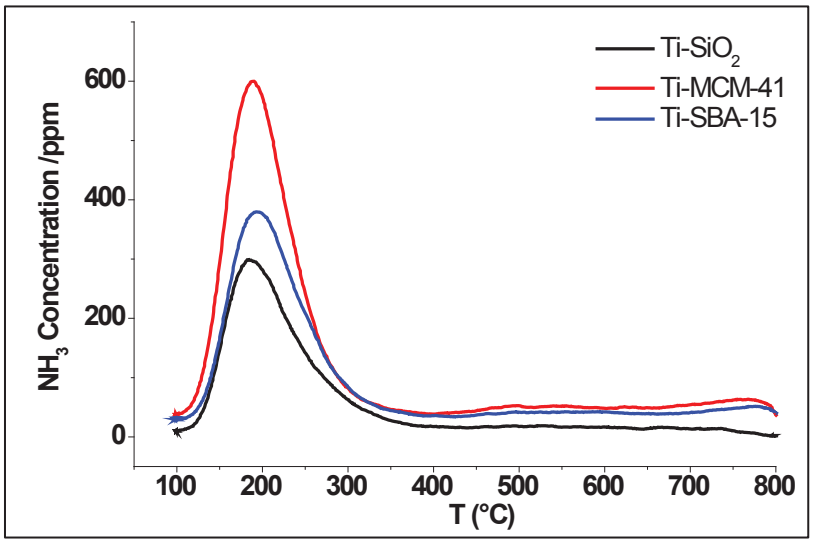

Figure 4.18. Ammonia TPD profiles for Ti-MCM-41, Ti-SBA-15 and Ti-SiO_2.

indicating large amount of Lewis acidic sites as Brønsted sites are not present (Py-FTIR data). Ti-SBA-15 and Ti-SiO_2 exhibited less acidity (120.8 and 112.5 µmol/g, respectively)

compared to Ti-MCM-41. It can be clearly noticed that the Ti-MCM-41 catalyst prepared by sol-gel method leads to a high dispersion of Ti species into MCM-41 support which produces large amount of acidic sites compared to the Ti-SBA-15 and Ti-SiO_2 prepared by impregnation method. The observed NH_3-TPD results are in good agreement with the Pyridine FTIR results.

4.2.2.5 UV-visible and ATR-IR spectroscopy

UV-vis spectra were recorded for Ti-SiO_2, Ti-SBA-15, Ti-MCM-41 and Ti-MCM-41-reg catalysts in order to get insight into the Ti coordination sites (Figure 4.19). According to the literature, tetrahedrally coordinated (Ti^{+4}) in TS-1 catalyst exhibited a band at around 215 nm. However, in the case of mixed oxide TiO_2-SiO_2, it can be extended up to 250 nm [144]. The Ti-MCM-41 catalyst showed a sharp LMCT transition band at 245 nm indicating that most of the Ti^{+4} were in tetrahedral coordination state [158]. On the other side, Ti-SBA-15 and Ti-SiO_2 solids present LMCT transition bands at 250 nm and extended up to 270 nm, indicating the formation of polymeric hexa- or penta-coordinated Ti species besides tetrahedral coordination [144].

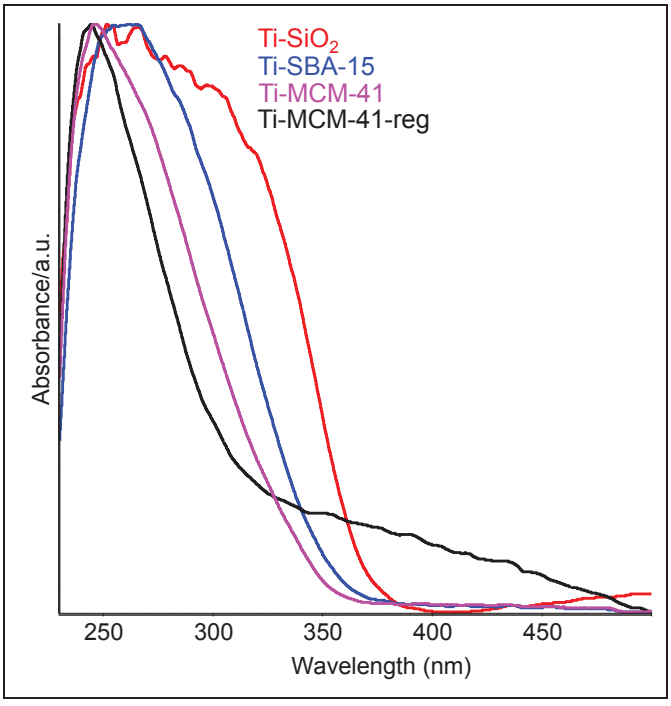

Figure 4.19. UV-vis spectra for Ti-MCM-41, Ti-SiO_2, Ti-SBA-15 and Ti-MCM-41-reg catalysts.

The extension of the band is smaller in case of Ti-SBA-15 compared to Ti-SiO_2, which might be due to the high surface area of SBA-15 which allows high dispersion of Ti species. Similarly, UV-vis spectrum of Ti-MCM-41-reg reveals a band at same wavenumber (245 nm) as the fresh catalyst. However, the tailing of the band for the Ti-MCM-41-reg catalyst is broadening (Figure 4.19), probably due to that changes occurred in the framework of the Ti-MCM-41 catalyst after regeneration.

ATR-IR spectra of Ti-MCM-41, Ti-SBA-15 and Ti-SiO_2 catalysts were recorded in order to get more insight into interatomic and intermolecular interaction as shown in Figure 4.20. In addition, a spectrum of Ti-MCM-41-reg catalyst was also recorded and compared with the fresh Ti-MCM-41 catalyst. The bands around 1055 cm^{-1} and 800 cm^{-1} can be ascribed to stretching and bending vibration of Si-O-Si bonds. The band around 960 cm^{-1} can be assigned either to the Si-OH (hydroxyl group from SBA-15 or MCM-41 support which will not introduce any Brønsted acidic sites to the system) or Si-O-Ti bonds [159- 162]. However, based on previous investigations of SiTi30 catalyst (section 4.1.3), one can say that the band at 960 cm^{-1} can be assigned to the Si-O-Ti bonds.

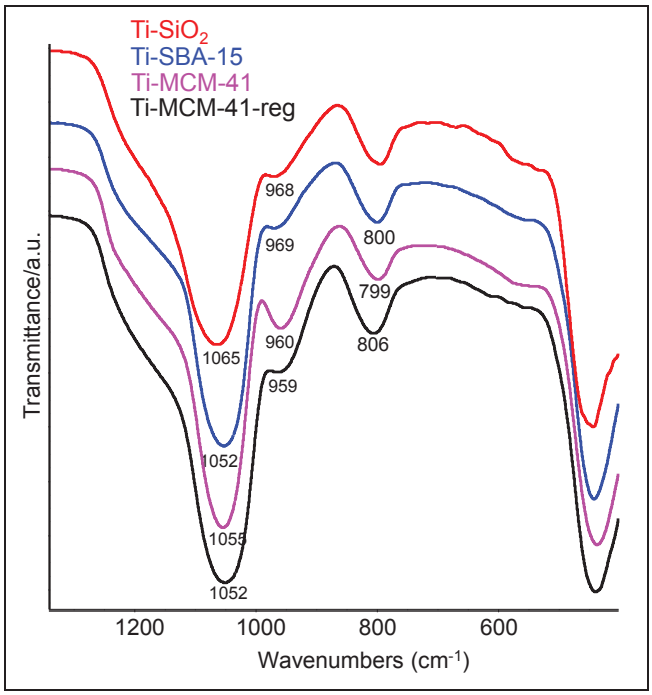

Figure 4.20. ATR-FTIR spectra for Ti-MCM-41, Ti-SiO_2, Ti-SBA-15 and Ti-MCM-41-reg catalysts.

In addition, a slight shift in the bands towards higher wavenumber with low intensity in the case of Ti-SBA-15 and Ti-SiO_2 samples compared to Ti-MCM-41 sample was observed. Such effect might occur due to the strong interaction of Si-OH (silanol group) with Ti species to form Si-OH---Ti species [151]. In addition, the effect of different catalysts preparation method can cause a band to appear at different wavenumbers. The ATR-IR spectrum of Ti-MCM-41-reg is very much similar to the fresh catalyst. However, the intensity of the band mainly at 960 cm^{-1} is slightly reduced compared to the fresh catalyst (Figure 4.20). This is again most probably due to structural alteration occurred during the regeneration of the catalyst. In order to confirm the existence of Si-O-Ti bonds and to better understand the morphology, surface properties and compositions, the catalysts were further analyzed with TEM-EDX and XPS characterization techniques.

4.2.2.6 Transmission electron microscopy (TEM)

In order to get more insight into morphology and the relationship of Ti species with the mesoporous silica support, the Ti-SiO_2, Ti-SBA-15, Ti-MCM-41 and Ti-MCM-41-reg catalysts were analyzed by TEM technique. In general, homogeneous distributions of Ti species in the silica support were observed for the fresh samples. Ti-SiO_2 (Figure 4.21 a) image showed randomly scattered black and white spots which are most likely due to homogeneously distributed TiO_2-SiO_2 composites. In the case of Ti-SBA-15 (Figure 4.21 b), the ordered (hexagonal array) structure of SBA-15 was preserved; however, at some places white spots (see Appendices A7 'a' and 'b') were observed which are due to the partially destroyed SBA-15 forming disordered SiO_2 units on the surface of SBA-15. Similar phenomenon was reported by Jung et al. for Ti containing SBA-15 material [159]. The stabilization of basic MCM-41 structure can be seen in the image of Ti-MCM-41 catalyst (Figure 4.21 c). In addition, formation of several MCM-41 sub-units was also observed. Similar behaviour was also reported by Signoretto et al. [163]. Interestingly, formation of TiO_2 particles was not seen on any of the fresh samples. This is most likely due to either presence of Ti species in the bulk of SiO_2, SBA-15 and MCM-41 and/or formation of ultra-small nanoparticles which are not detected by TEM.

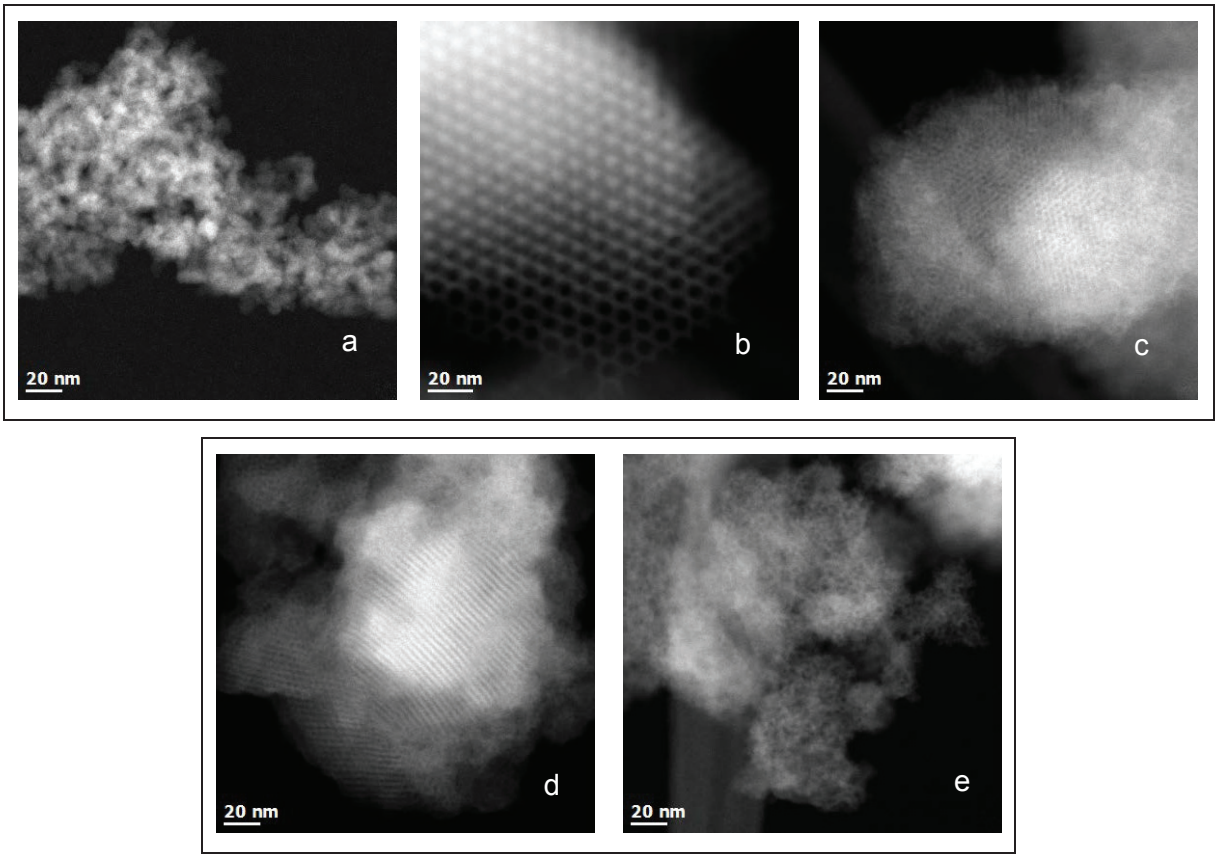

Figure 4.21. STEM-HDAAF images of a) Ti-SiO_2, b) Ti-SBA-15, c) Ti-MCM-41, d) ordered Ti-MCM-41-reg and e) disordered Ti-MCM-41-reg catalysts.

In addition, EDX analyses of samples were made in order to get more information on the composition of solids (Figures A5, A6 and A7 in appendices). The data showed that Si: Ti atomic ratio was consistent over all samples and regions. The Si: Ti atomic ratios were 97.24: 2.76 and 97.81: 2.19 for Ti-SiO_2 catalyst, 99.16: 0.84 and 98.71: 1.29 for Ti-SBA-15 and 99.22: 0.78 and 99.06: 0.94 for Ti-MCM-41. From the TEM-EDX analysis it is evident that the size distribution of TiO_2 in mesoporous silica is much narrower and hence one can conclude that the most of the added Ti species are incorporated into the silica support.

In Ti-MCM-41-reg TEM image, both ordered and partially destroyed (disordered) MCM-41 structure is observed (see Figures 4.21 d and e). The EDX analysis of two spots in ordered and partially destroyed images didn't show a significant difference in Si: Ti atomic ratios (98.79: 1.21 and 98.98: 1.02). This indicates that the size distribution of Ti species in MCM-41 is still narrow and should possess a nearly same distribution of TiO_2 in MCM-41 matrix (Figure A8 in appendices). However, Si: Ti atomic ratios in the Ti-MCM-41-reg sample found to be different compared to fresh Ti-MCM-41 sample indicating changes occurred in the structural arrangement.

4.2.2.7 X-ray photoelectron spectroscopy

In order to get more information on the surface composition and structural arrangements near the surface region of Ti-SiO_2, Ti-SBA-15, Ti-MCM-41 and Ti-MCM-41-reg catalysts, XP spectra were recorded. The surface Ti content was calculated based on atom% data obtained from XPS analysis and compared with data obtained from ICP-OES analysis as shown in Table 4.10. It is obvious that the fraction of Ti species on the surface of the solids is only 25-33% compared to bulk composition. This XPS analysis indicates that there is only small amount of Ti-species in the outer 10 nm surface region which implies that most of the added TiO_2 is incorporated in bulk. However, this was expected for Ti-MCM-41 catalyst, as it was prepared by sol-gel method but Ti-SiO_2 and Ti-SBA-15 catalysts also showed less Ti-species on the surface even though they were prepared by impregnation method. The binding energies of specific elements (Ti and O) were measured as shown in Table 4.11. According to literature reports, Ti 2*p*3/2 signal at BE value of 458.4 eV represents TiO_2, whereas O1*s* signals at BE value of 530, 531.5 and 533.1 eV corresponds to the Ti–O–Ti, Ti–O–Si and Si–O–Si bonds, respectively [155].

Table 4.10. Comparison of the surface and bulk composition of fresh and Ti-MCM-41-reg catalysts.

Catalysts	Ti/(Si+Ti) from XPS	Ti/(Si+Ti) from ICP
Ti-SiO_2	0.010	0.030
Ti-SBA-15	0.008	0.031
Ti-MCM-41	0.009	0.028
Ti-MCM-41-reg	0.008	0.028

The Ti-SiO_2 exhibited Ti2$p_{3/2}$ BE value at 459.46 and 465.31 eV attributes to the TiO_2. Similarly, Ti-SBA-15 also showed Ti2$p_{3/2}$ BE values at 459.49 eV and 465.17 eV for TiO_2. For O1*s*, the BE values were 528.79, 531.74 and 533.77 eV related to Ti–O–Ti, Ti–O–Si and Si–O–Si bonds, respectively. In the case of Ti-MCM-41, Ti2$p_{3/2}$ exhibited BE values at 460.04 and 466.04 eV, whereas O1*s* showed values at 532.47 eV and 533.36 eV which can be ascribed to the Si–O–Ti and Si–O–Si bonds. Similar XPS investigations were reported by Signoretto et. al. for TiO_2-MCM-41 catalyst [163].

Table 4.11. Binding energy values for Ti$p_{3/2}$ and O1*s* for fresh and Ti-MCM-41-reg catalysts.

Catalysts	Binding energy values (eV)	
	Ti2$p_{3/2}$	O1*s*
Ti-SiO_2	459.46	532.78
	465.31	
Ti-SBA-15	459.49	528.79
	465.17	531.74
		533.77
Ti-MCM-41	460.04	530.89
	466.04	532.99
Ti-MCM-41-reg	460.17	532.47
	465.66	533.36

On the other side, surface Ti content of Ti-MCM-41-reg sample decreased compared to a fresh sample. This result suggests that some of the surface Ti species have been migrated into bulk. This might be also due to structural changes or partial destruction of MCM-41 support during regeneration where Si species migrate on to the surface and covers the surface Ti species which are then not able to detect by XPS. This observed behaviour is exactly opposite to that what was observed in the case of SiTi30 sample as described in previous section 4.1.3.7. The BE value of Ti 2$p_{3/2}$ was retained at 460.17 eV and 465.66 eV and can be assigned to the TiO_2 (see Table 4.11). Similarly, BE value for O 1*s* at 532.47 eV was retained in the Ti-MCM-41-reg catalyst. In addition, BE value at 533.36 eV for O 1*s* was observed which represents Si-O-Si; however, this peak was not observed in the fresh sample which clearly indicates that some structural changes took place in MCM-41 support during regeneration. On the other side, BE value of O 1*s* representing Ti-O-Ti completely disappeared in the Ti-MCM-41-reg catalyst. These observed results are in good agreement with TEM-EDX results.

From the XPS results, it can be concluded that less Ti species are present on the surface. This confirms that the most of added Ti-species are embedded in the mesoporous silica structure (SiO_2, SBA-15 and MCM-41) tetrahedrally in the form of Si-O-Ti bonds. Based on these results, it seems reasonable to conclude that the formation of Si-O-Ti bonds within the catalysts and responsible for the increase in activity and selectivity towards acetins.

4.2.2.8 Thermal gravimetric analysis (TGA) and elemental (C, H and O) analyses

In general, at the end of experiments, the catalyst surfaces were covered with carbonaceous material referred as deposits. The thermal gravimetric analysis of Ti-MCM-41 from regular experiment (section 4.2.1.1) was performed and the spent catalysts showed 44% of weight loss (Figure 4.22). The DTA curve showed an exothermic peak at 350 °C and another shoulder at 500 °C. Based on observed temperature peaks, two different types of deposits seem to be adsorbed on the surface. However, the quantity of more stable deposits (500 °C) was relatively low. From the DTA curve, it was observed that deposits were completely desorbed from the surface at around 550 °C. The same sample was also analyzed by C, H, and N elemental analyzer in order to measure the carbon content on the surface of the catalyst. Nearly 22.4 wt% carbon and 2.6 wt% hydrogen were observed on the catalyst surface, indicating that formation of carbon deposits is mainly due to oxygenate (esters) by-product.

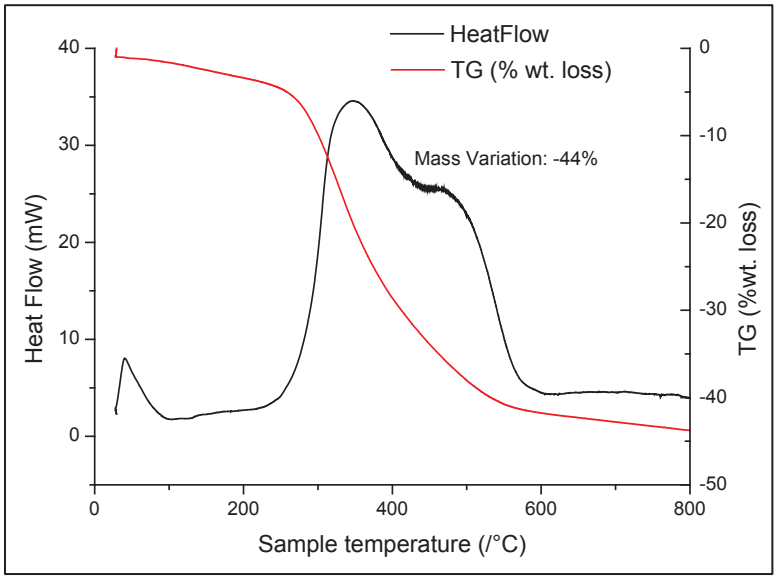

Figure 4.22. TGA and DTA profiles for Ti-MCM-41 spent catalyst.

4.2.3 Summary and conclusions

The nature of the mesoporous silica support (SiO_2, SBA-15 and MCM-41) has shown a significant influence on the distribution of TiO_2 species, acidic properties, morphology and surface composition. The prepared catalysts were X-ray amorphous. The XPS and TEM-EDX analyses showed that TiO_2 is highly dispersed on mesoporous SiO_2, MCM-41 and SBA-15. ATR-IR and UV-vis spectroscopic analyses showed the existence of Si–O–Ti and most of the Ti species were tetrahedrally coordinated in a mesoporous silica matrix. Pyridine FTIR showed that only Lewis acid sites existed in the catalysts, however, Ti-MCM-41 showed higher Lewis acid site concentration compared to the Ti-SiO_2 and Ti-MCM-41. The obtained results from pyridine FTIR analysis strongly correlate with the data from NH_3-TPD.

Ti-MCM-41 catalysts showed higher selectivity towards TAG than Ti-SiO_2 and Ti-SBA-15 catalysts at complete conversion of glycerol. The high activity and selectivity to TAG is mainly due to high dispersion of Ti species into the mesoporous silica. Besides that, the selectivity to TAG strongly depends on the temperature and WHSV. The maximum selectivity to TAG is obtained below 300 °C, whereas a further increase in temperature resulted in increasing selectivity to acrolein. It seems that activation energy of glycerol dehydration is slightly higher than glycerol acetylation. In addition, diglycerol tetraacetate (DGTA) is also formed which was observed in batch runs under water-free conditions. The long-term stability test was performed with Ti-MCM-41 at 275 °C for 100 h. The catalyst deactivated immediately within 2 h and selectivity dropped from 42% to 13% within 50 h and remains consistent up to 100 h. The regeneration of catalyst at 500 °C for 5 h and repeating catalytic test under identical reaction condition showed more or less same selectivity pattern.

5 Overall summary and outlook

5.1 Liquid phase glycerol acetylation

Acetylation of glycerol has been studied in the liquid phase using several solid acid catalysts such as ion exchange resins and supported heteropolyacids. However, the selectivity of desired triacetin (TAG) was always limited as reaction remains in chemical equilibrium in presence of water. Glycerol acetylation in the presence of toluene as an entrainer to remove the water from reaction system shifted the equilibrium toward the desired product TAG. In this, ion exchange resins such as Amberlyst-15 and Amberlyst-70 were excellent catalysts. Both catalysts showed excellent catalytic performance with the selectivity to TAG reaching more than 95% at complete conversion of glycerol. This is attributed to the high amount of Brønsted acid sites and continuous removal of water. The reaction conditions such as feed: catalysts ratio and acetic acid: glycerol molar ratio had a strong effect on the TAG selectivity. Both catalysts showed deactivation in recyclability tests, most likely due to loss of sulfur or carbonaceous material deposition on the surface of the catalyst. However, Amberlyst-70 showed slightly better performance than Amberlyst-15 due to its higher thermal stability and acid strength.

In addition, heteropolyacids (STA, TPA and PMA) supported on different metal oxides like SiO_2, SiO_2-Al_2O_3 and γ-Al_2O_3 were prepared, characterized and employed in liquid phase glycerol acetylation under identical reaction conditions. The catalytic results revealed that the stabilization of Keggin structure is crucial for the preservation of Brønsted acid sites which is indeed necessary for the high activity and selectivity to TAG. SiO_2 was found to be the best support for the stabilization of Keggin structure as it is neutral (neither Brønsted nor Lewis acidic sites). STA/SiO_2 and TPA/SiO_2 showed more than 67% selectivity to TAG at complete conversion of glycerol. On the other side, supports like SiO_2-Al_2O_3 and γ-Al_2O_3 are not suitable for effective stabilization of Keggin HPAs. Their acidic hydroxyl groups strongly interact with the Keggin structure at an elevated temperature and destroy it partially or completely to generate respective metal oxides. The catalysts suffer from deactivation most likely due to leaching of active components from catalysts surface. However, homogeneous catalysis test with the leached species and fresh feed showed that they do not contribute to the activity in glycerol acetylation. Interestingly, the formation of a new by-product diglycerol tetraacetate (DGTA) was observed during the course of reaction. It seems that DGTA is a consecutive product of DAG because the formation of DGTA is significant as soon as DAG is present in high concentration. Toluene is able to form an azeotropic mixture with water in the ratio of 80:20 at 84 °C and hence it also helps to keep the reaction temperature below the thermal stability limit of the Amberlyst catalysts.

5.2 Gas phase glycerol acetylation

Acetylation of glycerol in gas phase was performed for the first time with selected supported strongly acidic heteropolyacids catalysts (STA/SiO_2, STA/Al_2O_3 and γ-Al_2O_3) and weakly acidic mixed metal oxide catalysts (SiO_2-MO_x, MO_x = TiO_2, MgO, ZrO_2, SrO and Sc_2O_3) prepared by impregnation and sol-gel method, respectively. Surprisingly, supported heteropolyacid catalysts showed a high selectivity to acrolein (>85%) at complete conversion of glycerol. This is most likely due to strong acidic sites present on the surface of the catalysts. Moreover, presence of acetic acid in reaction media seems to play an important role resulting high selectivity to acrolein. This has not been investigated further.

Among the weakly acidic catalysts, SiO_2-TiO_2 (SiTi30 and SiTi60) composites showed the highest activity and selectivity toward TAG, whereas other samples showed either low activity or undesired high selectivity to acrolein. Characterization of SiTi30 composite revealed that most of the added Ti species are highly distributed in bulk via Si–O–Ti bonds. The distribution of Ti and Si–O–Ti bonds are most likely to be responsible for high activity and selectivity. The long-term test at the optimum reaction conditions (300 °C, acetic acid to glycerol molar ratio 6/1, flow rate 0.025 ml/min) showed that SiTi30 activity is stable with 100% conversion, but selectivity to TAG drops within 200 h from 32% to 23%; however, upon on regeneration at 600 °C in air, conversion and selectivity to TAG could not be restored. It seems that the catalysts structure is destroyed partially during regeneration and hence, the loss in selectivity to TAG was observed.

In general, distribution of Ti species and textural properties of the catalyst play a great role to achieve high activity. Hence, other silica supports such as SiO_2 (prepared by sol-gel method), SBA-15 and MCM-41 were selected in order to study the effect of support. Ti-SiO_2 and Ti-SBA-15 were prepared by incipient wetness impregnation, whereas Ti-MCM-41 catalyst was prepared by sol-gel method. Most of the added Ti species were highly distributed in mesoporous silica in the form of Si–O–Ti bonds. The Ti-MCM-41 catalyst exhibited higher and exclusively Lewis acidity compared to Ti-SiO_2 and Ti-SBA-15 catalysts. These catalysts exhibited high conversion and selectivity toward the desired TAG. As expected, Ti-MCM-41 catalyst exhibited slightly higher selectivity towards TAG compared to Ti-SiO_2 and Ti-SBA-15 as the Ti-MCM-41 was prepared by sol-gel method, which leads to higher dispersion of Ti species, which in further a generate higher amount of Lewis acid sites. Interestingly, at 325 °C, a very high selectivity to acrolein (~80%) was observed over these catalysts. Ti-MCM-41 sample was tested in a long-term test at 275 °C and exhibited high activity with the reduction in TAG selectivity from 42% to 13% within 100 h. Regenerating the catalyst at 500 °C in the presence of air resulted in an almost similar performance in a repeated run. Surprisingly, diglycerol tetraacetate (DGTA) was formed in the gas phase which was observed previously in liquid phase operation.

These results demonstrate the basic feasibility of acetylation in the gas phase and provide the basis for a continuous and solvent-free process as a previously described, alternative to esterification in the liquid phase. The reaction can be performed under comparatively mild reaction conditions (ambient pressure, ≤300 ° C). The conversions and selectivities measured easily reach the level of homogeneously catalyzed esterification (without water removal) near the chemical equilibrium. The catalyst productivity (based on the mass of TAG and catalyst per time) in the liquid phase with Amberlyst-70 (section 3.1.2.3) for a single batch was about 1.9 $g_{TAG}/(g_{cat} \times h)$ and the entire TAG was about 45 g_{TAG}/g_{cat} (24 h). Thereafter, the catalyst could be used, although again, however, with decreasing activity, and triacetin selectivity. In a continuous gas phase reaction, the best ever catalyst SiTi30 (section 4.1.2.2) showed more than 30% initial TAG selectivity which further declines slowly over the period of 200 h. Considering average yield TAG of 20%, the space-time-yield was 0.25 $g_{TAG}/(g_{cat} \times h)$ and the entire TAG was about 50.5 g_{TAG}/g_{cat} (200 h) under applied reaction condition. Thus, the gas phase acetylation offers the potential for a substantial improvement in terms of specific catalyst performance compared to the heterogeneously catalyzed liquid phase reaction.

5.3 Outlook

The results from liquid phase experiments have provided new opportunities for future development of catalysts with higher stability and performance. The use of entrainers (for instance cyclohexane, benzene) which have lower boiling points might increase the lifetime of catalyst. To make the oxidic catalysts more stable, a proper balance has to be found between the described intra- and intercrystallite interactions to preserve the HPAs structure and simultaneously to strengthen the bonding to the support to avoid leaching.

The results of gas phase experiments might open new perspectives for future development of the process and to find new catalysts. Some deeper investigations are necessary to understand the role of TiO_2 in SiO_2-TiO_2 composites which has changed the catalytic performance drastically. Further in-situ analyses are needed in order to elucidate the catalytically active sites, to identify reaction mechanism and to derive structure-reactivity relationships. Moreover, a kinetic model would provide valuable information on efficiency and for further scale-up. Another concept of reaction engineering to develop membrane based reactor can be used to remove the water formed in the reaction which will increase the yield of desired product TAG. In addition, the beneficial effect of acetic acid in acrolein formation can be studied in detail, which might be a new approach.

6 References

[1] L. Caspeta, N.A.A. Buijs, J. Nielsen, Energy Environ. Sci. 6 (2013) 1077-1082.

[2] http://www.ifpenergiesnouvelles.com/Publications/Available-studies/Panorama-technical-reports/Panorama-2012.

[3] World Enegry Outlook 2014, International Energy Agency (IEA).

[4] http://www.ifpenergiesnouvelles.com/Publications/Available-studies/Panorama-technical-reports/Panorama-2015.

[5] D. M. Alonso, J. Q. Bond, J. A. Dumesic, Green Chem. 12 (2010) 1493-1513.

[6] M. J. Climent, A. Corma, S. Iborra. Green Chem. 16 (2014) 516-547.

[7] N. Narkhede, S. Singh, A. Patel, Grean Chem. 17 (2015) 89-107.

[8] A. F. Lee, J. A. Bennett, J. C. Manayil, K. Wilson, Chem. Soc. Rev. 43 (2014) 7887-7916.

[9] BP, BP Energy Outlook 2030, 2011.

[10] OECD/Food and Agriculture Organization of the United Nations (2014), OECD-FAO Agricultural Outlook 2014, OECD Publishing. http://dx.doi.org/10.1787/agr_outlook-2014-en.

[11] H. W. Tan, A. R. Abdul Aziz, M. K. Arora, Renewable Sustainable Energy Rev. 27 (2013) 118-127.

[12] https://en.wikipedia.org/wiki/Oleochemical.

[13] M. R. Nanda, Z. Yuan, W. Qin, M. A. Poirier, X. Chunbao, Austin Chem. Eng. 1 (2014) 1004.

[14] M. Ayoub, A. Z. Abdullah, Renewable and Sustainable Energy Rev. 16 (2012) 2671-2686.

[15] C. H. Zhou, J. N. Beltramini, Y. X. Fan, G. Q. Lu, Chem. Soc. Rev. 37 (2008) 527-549.

[16] http://www.solvay.com/en/media/press_releases/20120611-epicerol-china.html

[17] S. Bagheri, N. M. Julkapli, W. A. Yehye, Renewable and Sustainable Energy Rev. 41 (2015) 113-127.

[18] B. Katryniok, H. Kimura, E. Skrzynska, J. S. Girardon, P. Fongarland, M. Capron, R. Ducoulombier, N. Mimura, S. Paul, F. Dumeignil, Green Chem.13 (2011) 1960-1979.

[19] B. Katryniok, S. Paul, F. Dumeignil, ACS Catal. 13 (2013) 1819-1834.

[20] A. Martin, U. Armbruster, H. Atia, Eur. J. Lipid Sci. Technol. 114 (2012) 10-23.

[21] P. N. Caley and R. C. Everett, US Pat., 3 350 871, 1967 (DuPont).

[22] D. Zimmerman and R. B. Isaacson, US Pat., 3 814 725, 1974, (Celanese Corp).

[23] I. Gandarias, J. Requies, P. L. Arias, U. Armbruster, A. Martin, J. Catal. 290 (2012) 79-89.

[24] A. Martin, U. Armbruster, I. Gandarias, P. L. Arias, Eur. J. Lipid Sci. Technol. 115 (2013) 9-27.

[25] N. H. Tran, G. S. Kamili Kannangara, Chem. Soc. Rev. 42 (2013) 9454-9479.

[26] M. B. Guemez, J. Requiez, I Agirre, P. L. Arias, V. L. Barrio, J. F. Cambra, Chem. Eng. J. 228 (2013) 300-360.

[27] P. Ferreira, I.M. Fonseca, A.M. Ramos, J. Vital , J.E. Castanheiro, Appl. Catal., B 98 (2010) 94-99.

[28] P. Sudarsanam, B. Mallesham, A. N. Prasad, P. S. Reddy, B. M. Reddy, Fuel Process. Technol. 106 (2013) 539–545.

[29] B. Mallesham, P. Sudarsanam, G. Raju, B. M. Reddy, Green Chem. 15 (2013) 478-489.

[30] C. J. A. Mota, C. X. A. da Silva, N. Rosenbach, Jr., J. Costa, F. da Silva, Energy Fuels 24 (2010) 2733-2736.

[31] K. Klepacova, D. Mravec, A. Kaszonyi, M. Bajus, Appl. Catal., A 328 (2007) 1-13.

[32] F. Frusteri, L. Frusteri, C. Cannilla, G. Bonura, Bioresour. Technol. 118 (2012) 350-358.

[33] B. Ikizer, N. Oktar, T. Dogu, Fuel Process. Technol. 138 (2015) 570-577.

[34] Z. Yuan, S. Xia, Ping. Chen, Z. Hou, X. Zheng, Energy Fuels 25 (2011) 3186-3191.

[35] M. D. Gonzalez, P. Salagre, E. Taboada, J. Llorca, E. Molins, Y Cesteros, Appl. Catal., B 136-137 (2013) 287-293.

[36] M. A. Jaworski, S. R. Vegac, G. J. Siri, M. L. Casellaa, A. R. Salvador, A. S. López, Appl. Catal., A 505 (2015) 36-43.

[37] J. Zhou, Y. Wang, X. Guo, J. Mao, S. Zhang, Green Chem. 16 (2014) 4669-4679.

[38] Z. Gholami, A. Z. Abdullah, K. T. Lee, Renewable and Sustainable Energy Rev. 39 (2014) 327-341.

[39] J.-M. Clacens, Y. Pouilloux, J. Barrault, Appl. Catal., A 227 (2002) 181-190.

[40] A. Martin, M. Richter, Eur. J. Lipid Sci. Technol. 113 (2011) 100-117.

[41] M. A. Medeiros, M. H. Araujo, R. Augusti, L.C. A. de Oliveira, R. M. Lago, J. Braz. Chem. Soc. 20 (2009) 1667-1673.

[42] J. I. Eshuis, J. A. Laan, R. P. Potman, US patent 5,635,588 (1997).

[43] K. Cottin, J.-M. Clacens, Y. Pouilloux, J. Barrault, OCL. Oléagineux, corps gras, lipides 5 (1998) 407-412.

[44] M. Richter, Y. K. Krisnandi, R. Eckelt, A. Martin, Catal. Commun. 9 (2008) 2112-2116.

[45] M. Calatayud, A. M. Ruppert, B. M. Weckhuysen, Chem. Eur. J. 15 (2009) 10864-10870.

[46] Y. K. Krisnandi, R. Eckelt, M. Schneider, A. Martin, M. Richter, ChemSusChem 1 (2008) 835-844.

[47] M. Popova, Á. Szegedi, A. Ristić, N. No. Tušar, Catal. Sci. Technol. 4 (2014) 3993-4000.

[48] A. Patel, S. Singh, Fuel 118 (2014) 358-364.

[49] http://www.foodchemadditives.com/applications-uses/2023

[50] http://techcenter.lanxess.com/fcc/emea/de/products/datasheet/Triacetin_e.pdf?docId=182496&gid=3166&pid=777

[51] N. Rahmat, A, Z. Abdullah, A. R. Mohamed, Renewable and Sustainable Energy Rev. 14 (2010) 987-1000.

[52] P. S. Reddy, P. Sudarsanam, G. Raju, B. M. Reddy, Catal. Commun.11 (2010) 1224-1228.

[53] S. B. Troncea, S. Wuttke, E. Kemnitz, S. M. Coman, V. I. Parvulescu, Appl. Catal., B 107 (2011) 260-267

[54] J. A. Melero, R. van Grieken, G. Morales, M. Paniagua, Energy Fuels 21 (2007) 1782-1791.

[55] M. L. Testa, V. L. Parola, L. F. Liotta, A. M. Venezia, J. Mol. Catal. A: Chem. 367 (2013) 69-76.

[56] I. Kim, J. Kim, D. Lee, Appl. Catal., B 148–149 (2014) 295-303.

[57] J. A. Sánchez, D. L. Hernández, J. A. Moreno, F. Mondragón, J. J. Fernández, Appl. Catal., A 405 (2011) 55– 60.

[58] M.S. Khayoon, B.H. Hameed, Bioresour. Technol. 102 (2011) 9229-9235.

[59] Inbae Kim, Jaesung Kim, Doohwan Lee, Appl. Catal., A 482 (2014) 31-37.

[60] C. de la Calle, J. M. Fraile, E. García-Bordejé, E. Pires, L. Roldán, Catal. Sci. Technol. 5 (2015) 2897-2903.

[61] P. S. Reddy, P. Sudarsanam, G. Raju, B. M. Reddy, J. Ind. Eng. Chem. 18 (2012) 648–654.

[62] B. Mallesham, P. Sudarsanam, B. M. Reddy, Ind. Eng. Chem. Res. 53 (2014) 18775-18785.

[63] I. Dosuna-Rodríguez, E.M. Gaigneaux, Catal. Today 195 (2012) 14-21.

[64] L. Zhou, T. Nguyen, A. A. Adesina, Fuel Process. Technol. 104 (2012) 310-318.

[65] L. Zhou, E. Al-Zaini, A. A. Adesina, Fuel 103 (2013) 617-625.

[66] M. Rezayat and H. S. Ghaziaskar, Green Chem. 11 (2009) 710-715.

[67] X. Liao, Y. Zhu, S. G. Wang, Y. Li, Fuel Process. Technol. 90 (2009) 988-993.

[68] L. N. Silva, L. C. Valter, C. J. A. Mota, Catal. Commun. 11 (2010) 1036-1039.

[69] J. P. Konwar, P. Mäki-Arvela, P. Begum, N. Kumar, A. J. Thakur, J. P. Mikkola, R. C. Deka, D. Deka, J. Catal. 329 (2015) 237-247

[70] U. Chandrakala, R. B. N. Prasad, B. L. A. Prabhavathi Devi, Ind. Eng. Chem. Res. 53 (2014) 16164-16169.

[71] A. Hasabnis, S. Mahajani, Ind. Eng. Chem. Res. 49 (2010) 9058–9067.

[72] P. Ferreira, I.M. Fonseca, A.M. Ramos, J. Vital, J.E. Castanheiro, Catal. Commun. 10 (2009) 481-484.

[73] P. Ferreira, I.M. Fonseca b, A.M. Ramos, J. Vital, J.E. Castanheiro, Appl. Catal., B 91 (2009) 416-422.

[74] K. Jagadeeswaraiah, M. Balaraju, P.S. Sai Prasad, N. Lingaiah, Appl. Catal., A 386 (2010) 166-170.

[75] M. Balaraju, P. Nikhitha, K. Jagadeeswaraiah, K. Srilatha, P.S. Sai Prasad, N. Lingaiah, Fuel Process. Technol. 91 (2010) 249-253.

[76] M.S. Khayoon, B.H. Hameed, Appl. Catal., A 433–434 (2012) 152-161.

[77] C. E. Gonçalves, L. O. Laier, A. L. Cardoso, M. J. da Silva, Fuel Process. Technol. 102 (2012) 46-52.

[78] S. Zhu, Y. Zhu, X. Gao, T. Mo, Y. Zhu, Y. Li, Bioresour. Technol. 130 (2013) 45-51.

[79] S. Singh, A. Patel, Ind. Res. Chem. Res. 53 (2014) 14592-14600.
[80] M. Huang, X. Han, C. Hung, J. Lin, P. Wu, J. Wu, S. Liu, J. Catal. 320 (2014) 42-51.
[81] H. Rastegari, H. S. Ghaziaskar, M. Yalpani, Ind. Eng. Chem. Res. 54 (2015) 3279-3284.
[82] X. Liao, Y. Zhu, S. G. Wang, H. Chen, Y. Li, Appl. Catal., B 94 (2010) 64-70.
[83] P. Ferreira , I.M. Fonseca , A.M. Ramos , J. Vital , J.E. Castanheiro, Catal. Commun. 12 (2011) 573-576.
[84] X. Liu, H. Ma, Y. Wu, C. Wang, M. Yang, P. Yan, U. Welz-Biermann, Green Chem. 13 (2011) 697-701.
[85] S. Zhu, X. Gao, F. Dong, Y. Zhu, H. Zheng, Y. Li, J. Catal. 306 (2013) 155-163.
[86] M. S. Khayoon, S. Triwahyono, B. H. Hameed, A.A. Jalil, Chem. Eng. J. 243 (2014) 473-484.
[87] J. M. Rafi, A. Rajashekar, M. Srinivas, B. V. S. K. Rao, R. B. N. Prasad, N. Lingaiah, RSC Adv. 5 (2015) 44550-44556.
[88] https://en.wikipedia.org/wiki/Heteropoly_acid
[89] I. V. Kozhevnikov, Catal. Rev. Sci. Eng. 37 (1995) 311-352.
[90] H. Atia, U. Armbruster, A. Martin, Appl. Catal., A 393 (2011) 331-339.
[91] A. Corma, Chem. Rev. 95 (1995) 559-614.
[92] https://www.sigmaaldrich.com/content/dam/sigma-aldrich/docs/Aldrich/Instructions/ion_exchange_resins.pdf
[93] A. Chakrabarti, M. M. Sharma, React. Polym. 20 (1993) 1-45.
[94] https://commons.wikimedia.org/wiki/File:Ion_exchange_resin_beads.jpg
[95] https://en.wikipedia.org/wiki/Ion-exchange_resin
[96] S. D. Alexandratos, Ind. Eng. Chem. Res. 48 (2009) 388-398.
[97] P. Barbaro, F. Liguori, Chem. Rev. 109 (2009) 515–529.
[98] K. Suwannakarn, E. Lotero, J. G. Goodwin Jr., Catal. Lett. 114 (2007) 122-128.
[99] http://www.itcp.kit.edu/deutschmann/download/III_12_2009_UllmannEncycl_HetCatal_Turek_Deutschmann.pdf
[100] C. Perego, P. Villa, Catal. Today 34 (1997) 281-305.
[101] F. Pinna, Catal. Today, 41 (1998) 129-137.
[102] J. A. Schwarz, C. Contescu, A. Contescu, Chem. Rev. 95 (1995) 477-510.
[103] C.A. Emeis, J. Catal. 141 (1993) 347-354.
[104] D.M. Alonso, J.Q. Bond, D. Wang, J.A. Dumesic, Top. Catal. 54 (2011) 447-457.
[105] S. V. Gadekar, R. V. Naik, S. N. Kaul, J. Sci. Ind. Res. 68 (2009) 871-875.
[106] http://www.solvaychemicals.com/Chemicals%20Literature%20Documents/Polyglycerols/DOC 2800 general overview x3.pdf
[107] H. Sawada, J. Kawamoto, US Patent 3890983 (1975).

[108] K. Jerábek, L. Hanková, L. Holub, J. Mol. Catal. A: Chem. 333 (2010) 109-113.
[109] C. Buttersack, React. Polym. 10 (1989) 143-164.
[110] C. Buttersack, H. Widdecke, J. Klein, React. Polym. 5 (1987) 181-189.
[111] D. M. Alonso, J. Q. Bond, D. Wang, J. A. Dumesic, Top. Catal. 54 (2011) 447-457.
[112] M. F. Gomez, L.A. Arrua, M.C. Abello, J. Chem. Technol. Biotechnol. 79 (2004) 391-396.
[113] P. F. Siril, H. E. Cross, D. R. Brown, J. Mol. Catal. A: Chem. 279 (2008) 63-68.
[114] P. D. Cara, M. Pagliaro, A. Elmekawy, D. R. Brown, P. Verschuren, N. R. Shiju, G. Rothenberg, Catal. Sci. Technol. 3 (2013) 2057-2061.
[115] D. Gelosa, M. Ramaioli, G. Valente, M. Morbidelli, Ind. Eng. Chem. Res. 42 (2003) 6536-6544.
[116] S. -K. Hung, C. -C. Lee, H. -Y. Lee, C. -L. Lee, I. L. Chien, Ind. Eng. Chem. Res. 53 (2014) 11989-12002
[117] S. Kale, S. B. Umbarkar, M. K. Dongare, R. Eckelt, U. Armbruster, A. Martin, Appl. Catal., A 490 (2015) 10-16.
[118] H. M. Weiss, K. Touchette, J. Chem. Educ. 67 (1990) 707-708.
[119] S. Gao, S. L. Simon, Thermochim. Acta 589 (2014) 241-246.
[120] N. J. J. Dekker, J. A. A. Hoorn, S. Stegenga, F. Kapteijn, J. A. Moulijn, AIChE J. 38 (1992) 385-396.
[121] H. Guesmi, D. Berthomieu, B. Bromley, B. Coq, L. Kiwi-Minsker, PCCP 12 (2010) 2873-2878.
[122] L. Kiwi-Minsker, D. A. Bulushev, A. Renken, Catal. Today, 110 (2005) 191-198.
[123] E. P. Alves Rocha, F. B. Passos, F. C. Peixoto, Ind. Eng. Chem. Res. 53 (2014) 8726-8734.
[124] I. V. M. Barbosa, D. M. Merquior, F. C. Peixoto, Chem. Eng. Sci. 60 (2005) 5406-5413.
[125] A. O. Costa, L. S. Ferreira, F. B. Passos, M. P. Maia, F. C. Peixoto, Appl. Catal., A 445 (2012) 26-34.
[126] J. Kopyscinski, J. Choi, J. M. Hill, Appl., Catal. A, 445–446 (2012) 50-60.
[127] J. Kopyscinski, T. J. Schildhauer, F. Vogel, S. M. A. Biollaz, A. Wokaun, J. Catal. 271 (2010) 262-279.
[128] M. A. Goncalves, F. C. Peixoto, E. F. F. da Cunh, T. C. Ramalho, Chem. Phys. Lett., 609 (2014) 88-92.
[129] R. L. B. Rodrigues, M. Castier, F. C. Peixoto, Lat. Am. Appl. Res. 36 (2006) 229-233.
[130] G. Mestl, T. Ilkenhans, D. Spielbauer, M. Dieterle, O. Timpe, J. Kröhnert, F. C Jentoft, H. Knözinger, R. Schlögl, Appl. Catal., A 210 (2001) 13-34.
[131] T. M. McEvoy, K. J. Stevenson, Langmuir 21 (2005) 3521-3528.
[132] S. Damyanov, J. L. G. Fierro, Chem. Mater. 10 (1988) 871-879.
[133] N. Legagneux, J. M. Basset, A. Thomas, F. Lefebvre, A. Goget, J. Sa, C. Haedacre, Dalton Trans. 12 (2009) 2235-2240.
[134] S. -X. Guo, A. W. Mariotti, C. Schlipf, A. M. Bond, A. G. Wedd, Inorg. Chem. 45 (2006) 8563-8574

[135] T. H. Kang, J. H. Choi, Y. Bang, J. Yoo, J. H. Song, W. Joe, J. S. Choi, I. K. Song, J. Mol. Catal. A: Chem. 396(2015) 282-289.

[136] G. Busca, PCCP, 1 (1999) 723-736.

[137] R. Buzzoni, S. Bordiga, G. Ricchiardi, C. Lamberti, A. Zecchina, Langmuir 12 (1996) 930-940.

[138] A. G. Alejandre, P. Castillo, J. Ramírez, G. Ramis, G. Busca, Appl. Catal., A 216 (2001) 181-194.

[139] I. V. Kozhevnikov, Chem. Rev. 98 (1988) 171-198.

[140] S. Sato, K. Sagara, H. Furuta, F. Nazaki, J. Mol. Catal. A: Chem. 114 (1996) 209-216.

[141] B. B. Bardin, S. V. Bordawekar, M. Neurock, R. J. Davis, J. Phys. Chem. B 102 (1998) 10817-10825.

[142] H. Atia, U. Armbruster, A. Martin, J. Catal., 258 (2008) 71-82.

[143] J. Ren, Z. Li, S. Liu, Y. Xing, K. Xie, Catal. Lett. 124 (2008) 185-194.

[144] X. Gao, I. E. Wachs, Catal. Today 51 (1999) 233-254.

[145] I. Grohmann, W. Pilz, G. Walther, H. Kosslick, V. A. Tuan, Surf. Interface Anal. 22 (1994) 403-406.

[146] D.T. On, L.L. Noe, L. Bonneviot, Chem. Commun. (1996) 299-300

[147] L.L. Noc, D.T. On, S. Solomykina, B. Echchahed, F.Beland, C.C.D. Moulin, L. Bonneviot, Eleventh International Congress on Catalysis, Stud. Surf. Sci. Catal. 101 (1996) 611-620

[148] S. Bordiga, S. Coluccia, C. Lamberti, L. Marchese, A.Zecchina, F. Boscherini, F. Buffa, F. Genoni, G. Leofanti, G. Petrini, G. Vlaic, J. Phys. Chem. 98 (1994) 4125-4132.

[149] H. Nur, Mater. Sci. Eng., B, 133 (2006) 49-54.

[150] J. Saha, A. Mitra, A. Dandapat, G. De, Dalton Trans. 43 (2014) 521-5229.

[151] X. Gao, S. R. Bare, J. L. G. Fierro, M. A. Banares, I. E. Wachs, J. Phys. Chem. B 102 (1998) 5653-5666.

[152] G. N. Shao, R. Sheikh, A. Hilonga, J. E. Lee, Y. H. Park, H. T. Kim, Chem. Eng. J. 215-216 (2013) 600-607.

[153] A. Hilonga, J. K. Kim, P. B. Sarawade, H. T. Kim, Powder Technol. 199 (2010) 284-288.

[154] G. N. Shao, A. Hilonga, S. J. Jeon, J. E. Lee, G. Elineema, D. V. Quang, J. K. Kim, Powder Technol. 233 (2013) 123-130.

[155] S. Ren, X. Zhao, L. Zhao, M. Yuan, Y. Yu, Y. Guo, Z. Wang, J. Solid State Chem. 182 (2009) 312-316.

[156] A. Talebian-Kiakalaieh, N. A. S. Amin, Ind. Eng. Chem. Res. 54 (2015) 8113-8121.

[157] M. R. Nimlos, S. J. Blanksby, X. Qian, M. E. Himmel, D. K. Johnson, J. Phys. Chem. A 110 (2006) 6145-6156.

[158] L. Ma, J. Ji, F. Yu, N. Ai, H. Jiang, Microporous Mesoporous Mater. 165 (2013) 6-13.

[159] W. Y. Jung, S. H. Baek, J. S. Yang, K. T. Lim, M. S. Lee, G. D. Lee, S. S. Park, S. S. Hong, Catal. Today 131 (2008) 437-443.

[160] J. Yao, W. Zhan, X. Liu, Y. Guo, Y. Wang, Y. Guo, G. Lu, Microporous Mesoporous Mater. 148 (2012) 131-136

[161] Y. Han, H. Kim, J. Park, S. Lee, J. Kim, Int. J. Hydrogen Energy 37 (2012) 14240-14247.

[162] T. Blasco, A. Corma, M. T. Navarro, A. P. Pariente, J. Catal. 156 (1995) 65-74.

[163] M. Signoretto, E. Ghedini, V. Trevisan, C. L. Bianchi, M. Ongaro, G. cruciani, Appl. Catal., B, 95 (2010) 130-136.

7. Appendices

Appendix A:

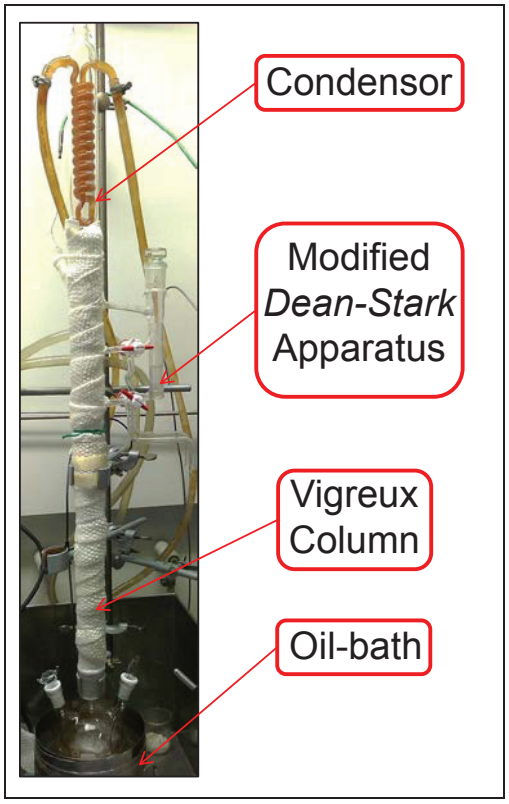

Figure A1. Liquid phase glycerol acetylation setup

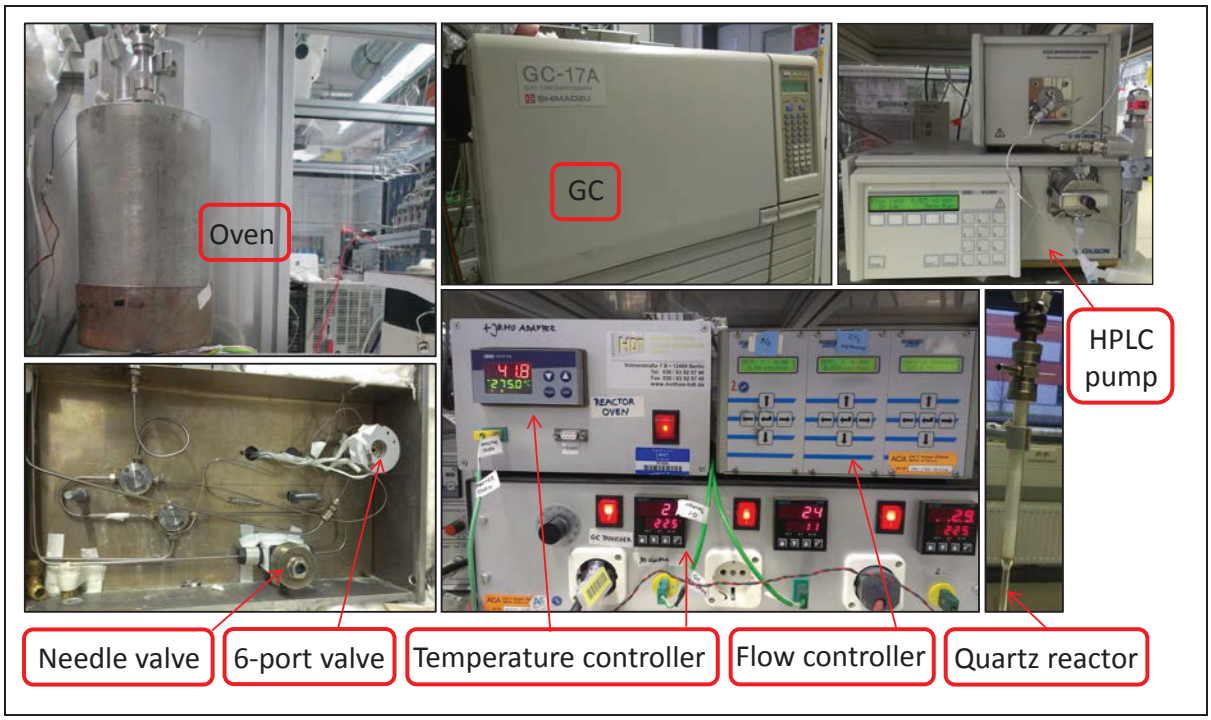

Figure A2. Gas phase glycerol acetylation setup

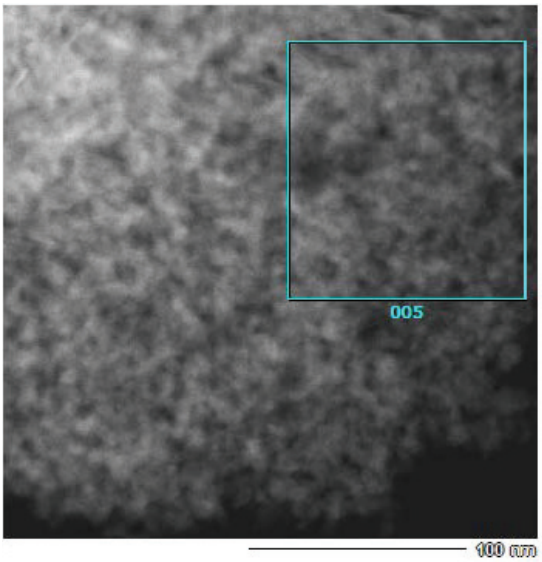

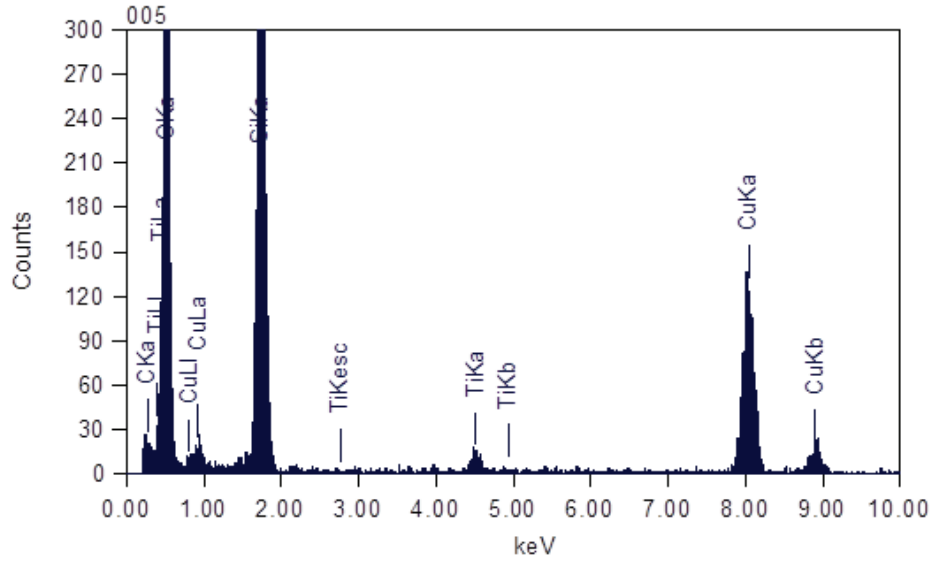

Thin Film Standardless Standardless Quantitative Analysis

Fitting Coefficient : 0.1358

Element	(keV)	Mass%	Counts	Sigma	Atom%	Compound	Mass%	Cation	K
C K*	(Excluded)								
O K*	(Excluded)								
Si K	(Ref.)	1.739	96.19	4035.15	2.09	97.73			1.0000
Ti K		4.508	3.81	120.99	0.40	2.27			1.3213
Cu K*	(Excluded)								
Total			100.00			100.00			

Figure A3. a) SiTi30 EDX measurement (box 005)

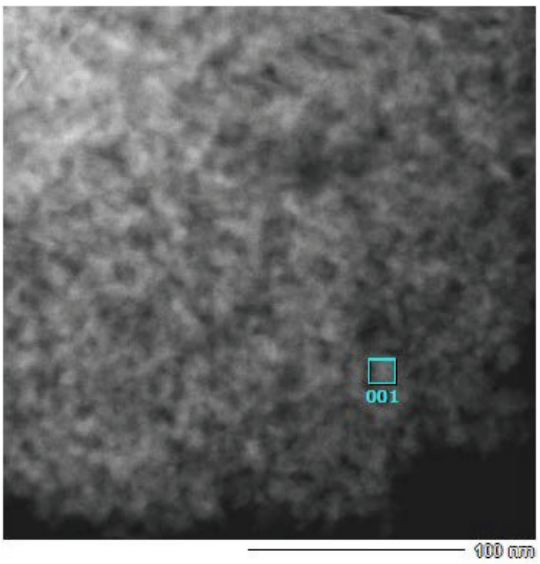

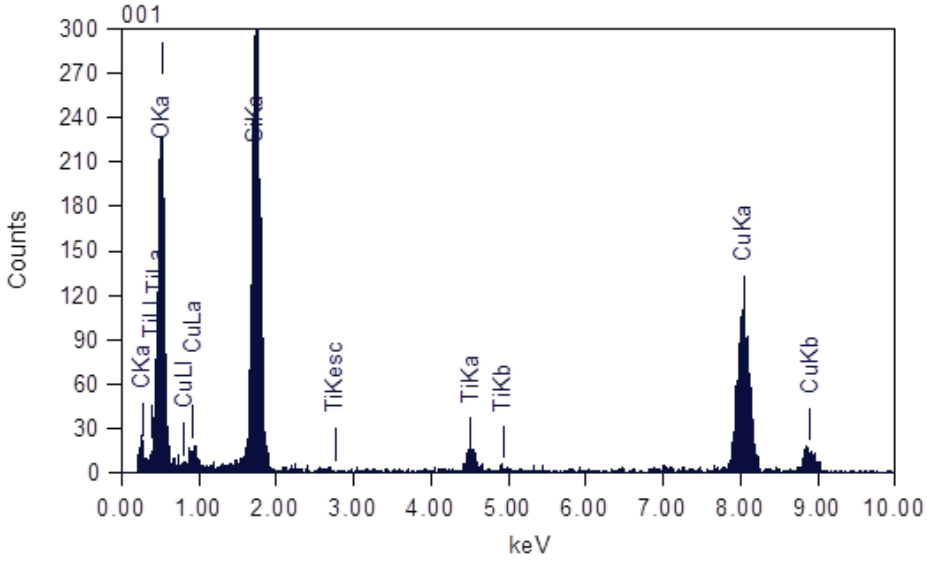

Thin Film Standardless Standardless Quantitative Analysis

Fitting Coefficient : 0.1219

Element	(keV)	Mass%	Counts	Sigma	Atom%	Compound	Mass%	Cation	K
C K*	(Excluded)								
O K*	(Excluded)								
Si K	(Ref.)	1.739	95.29	3067.95	1.89	97.18			1.0000
Ti K		4.508	4.71	114.64	0.35	2.82			1.3213
Cu K*	(Excluded)								
Total		100.00			100.00				

Figure A3. b) SiTi30 EDX measurement (box 001)

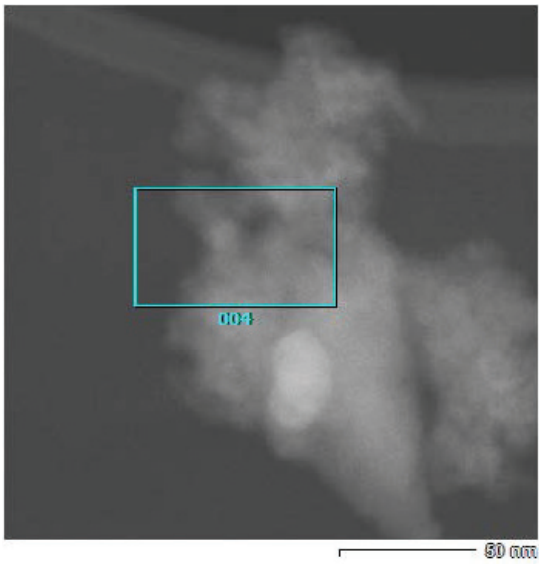

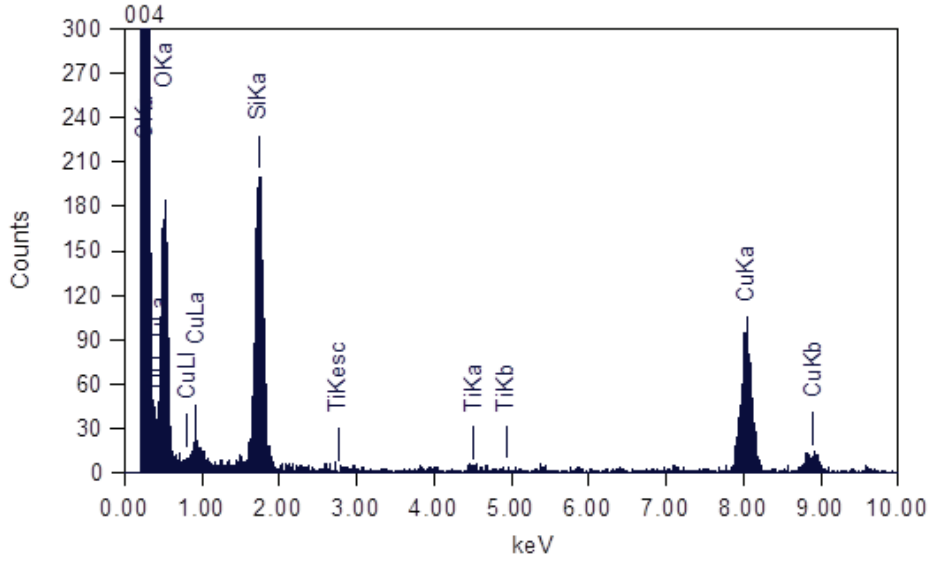

Thin Film Standardless Standardless Quantitative Analysis

Fitting Coefficient : 0.3158

Element	(keV)	Mass%	Counts	Sigma	Atom%	Compound	Mass%	Cation	K
C K*	(Excluded)								
O K*	(Excluded)								
Si K	(Ref.)	1.739	98.26	1814.97	3.30	98.97			1.0000
Ti K		4.508	1.74	24.28	0.56	1.03			1.3213
Cu K*	(Excluded)								
Total			100.00			100.00			

Figure A4. a) SiTi30-reg EDX measurement (box 004)

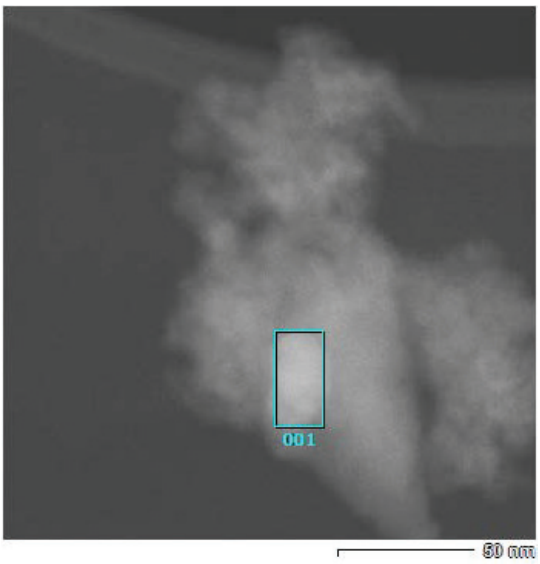

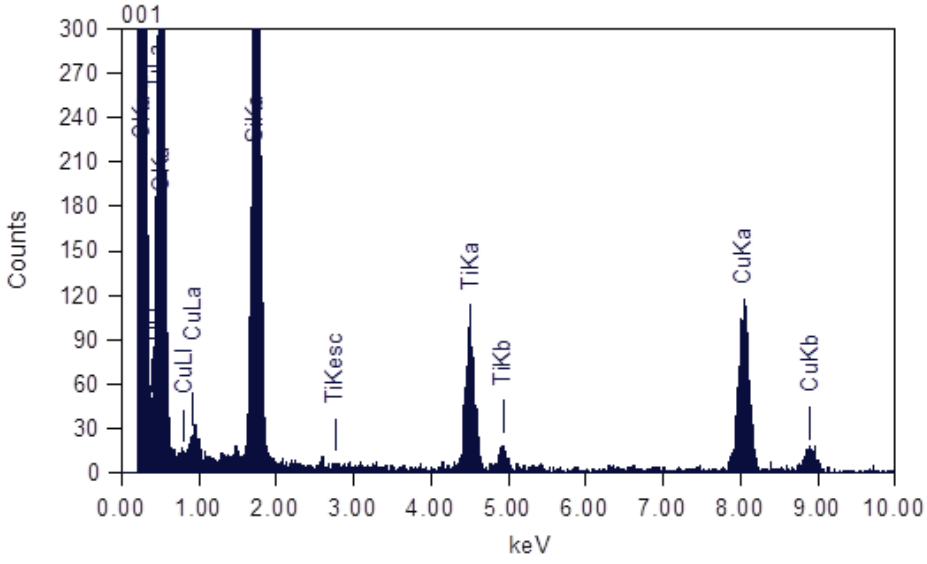

Thin Film Standardless Standardless Quantitative Analysis

Fitting Coefficient : 0.2727

Element	(keV)	Mass%	Counts	Sigma	Atom%	Compound	Mass%	Cation	K
C K*	(Excluded)								
O K*	(Excluded)								
Si K	(Ref.)	1.739	77.20	4272.34	1.64	85.23			1.0000
Ti K		4.508	22.80	955.17	0.77	14.77			1.3213
Cu K*	(Excluded)								

Figure A4. b) SiTi30-reg EDX measurement (box 001)

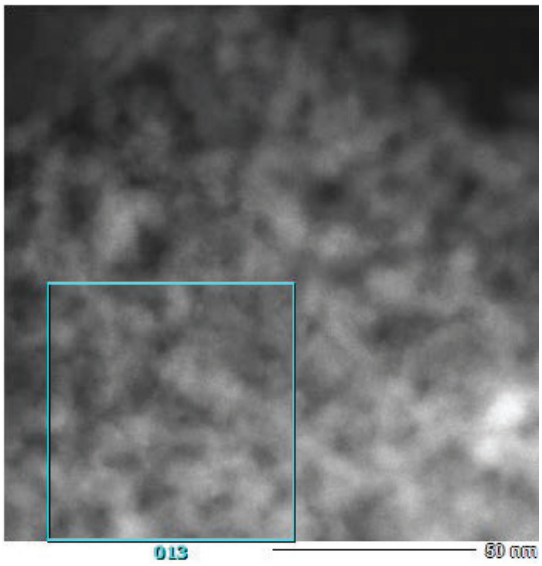

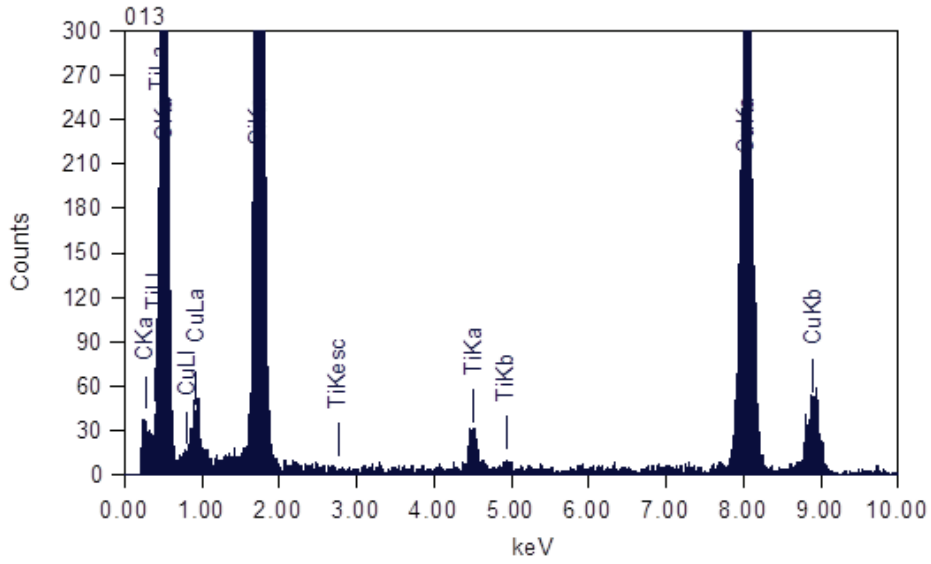

Thin Film Standardless Standardless Quantitative Analysis

Fitting Coefficient : 0.1063

Element	(keV)	Mass%	Counts	Sigma	Atom%	Compound	Mass%	Cation	K
H *	(Excluded)								
C K*	(Excluded)								
O K*	(Excluded)								
Si K	(Ref.)	1.739	95.39	7641.46	1.49	97.24			1.0000
Ti K		4.508	4.61	279.59	0.30	2.76			1.3213
Cu K*	(Excluded)								
Total			100.00			100.00			

Figure A5. a) Ti-SiO_2 EDX measurement (box 013)

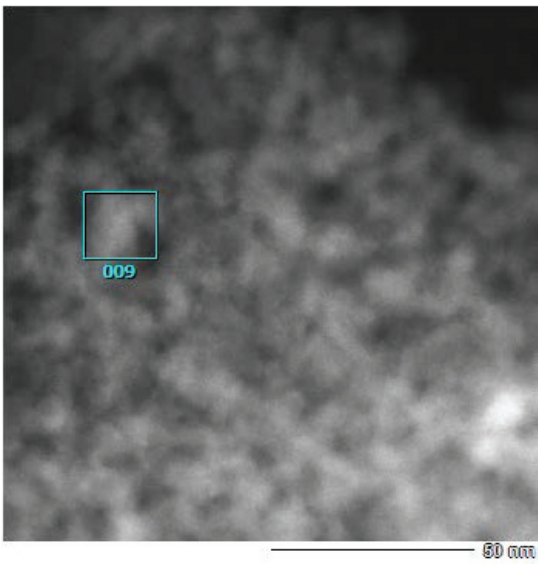

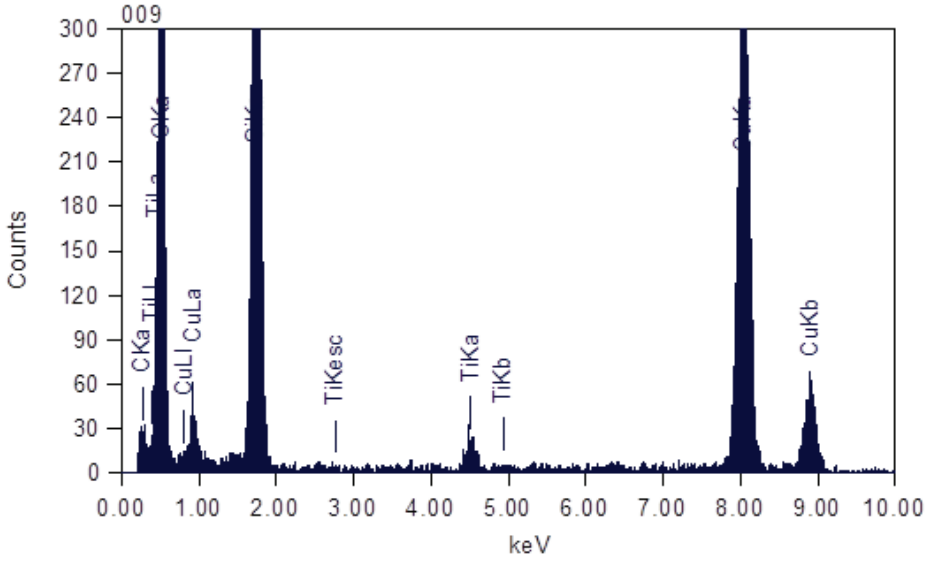

Thin Film Standardless Standardless Quantitative Analysis

Fitting Coefficient : 0.0901

Element	(keV)	Mass%	Counts	Sigma	Atom%	Compound	Mass%	Cation	K
C K*	(Excluded)								
O K*	(Excluded)								
Si K	(Ref.)	1.739	96.32	5759.89	1.73	97.81			1.0000
Ti K		4.508	3.68	166.68	0.34	2.19			1.3213
Cu K*	(Excluded)								
Total		100.00			100.00				

Figure A5. b) Ti-SiO_2 EDX measurement (box 009)

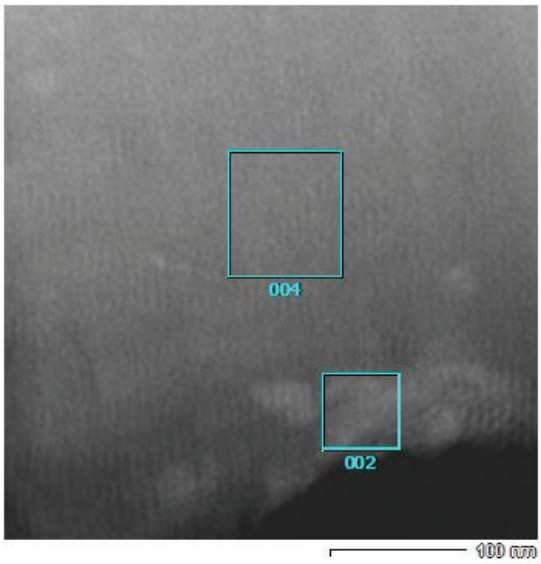

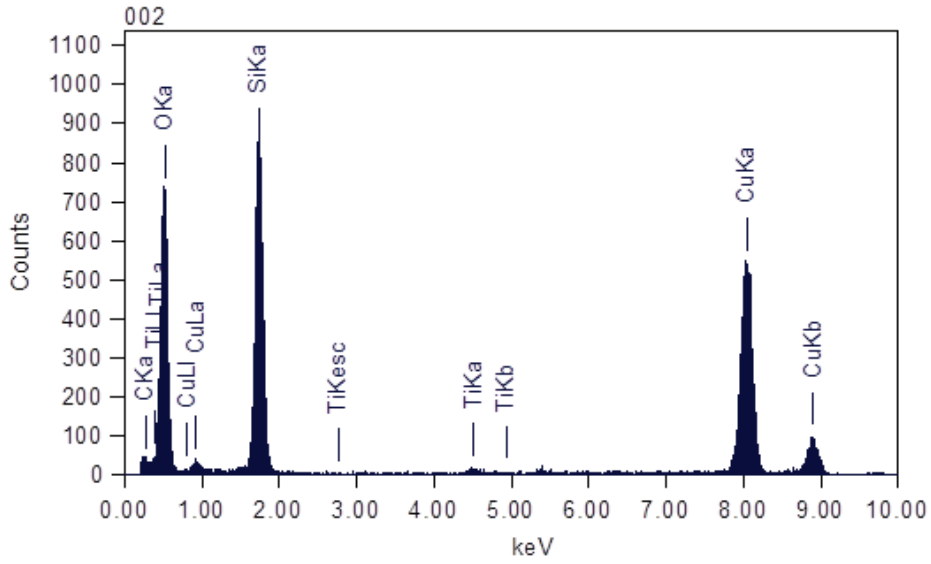

Thin Film Standardless Standardless Quantitative Analysis

Fitting Coefficient : 0.1139

Element	(keV)	Mass%	Counts	Sigma	Atom%	Compound	Mass%	Cation	K
C K*	(Excluded)								
O K*	(Excluded)								
Si K	(Ref.)	1.739	98.58	8122.44	1.51	99.16			1.0000
Ti K		4.508	1.42	88.38	0.20	0.84			1.3213
Cu K*	(Excluded)								
Total			100.00			100.00			

Figure A6. a) Ti-SBA-15 EDX measurement (box 004)

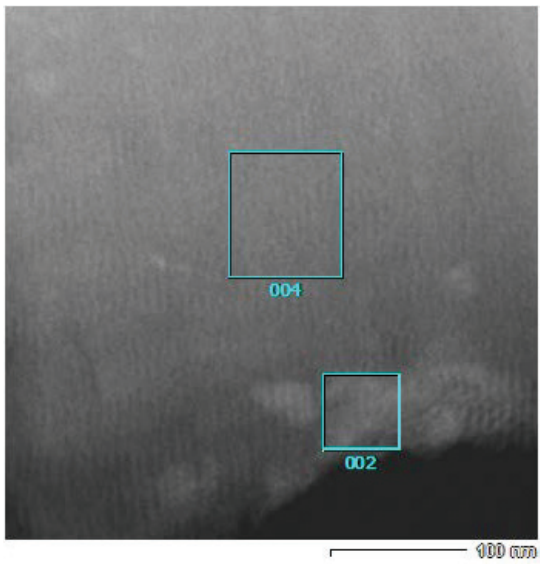

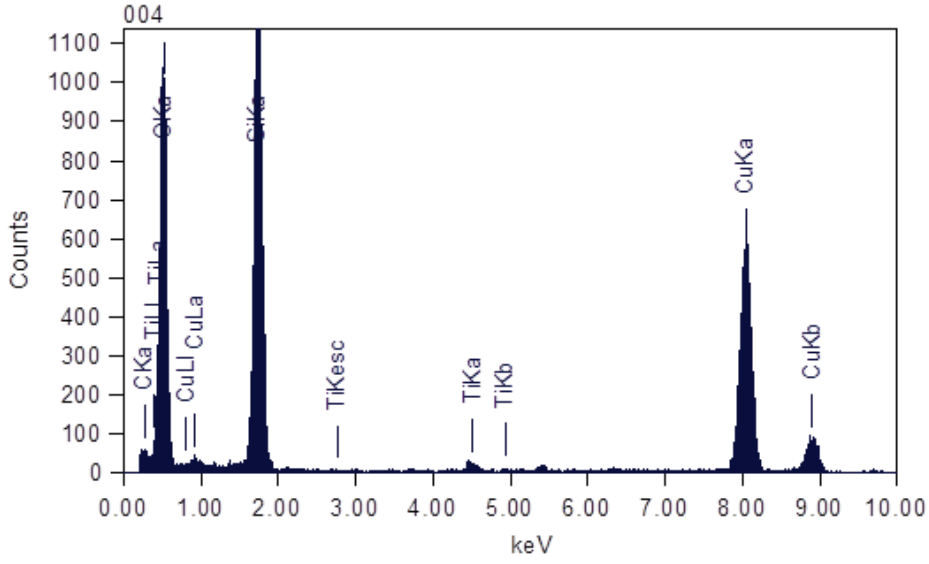

Thin Film Standardless Standardless Quantitative Analysis

Fitting Coefficient : 0.1155

Element	(keV)	Mass%	Counts	Sigma	Atom%	Compound	Mass%	Cation	K
C K*	(Excluded)								
O K*	(Excluded)								
Si K	(Ref.)	1.739	97.83	12020.28	1.24	98.71			1.0000
Ti K		4.508	2.17	201.84	0.18	1.29			1.3213
Cu K*	(Excluded)								
Total		100.00			100.00				

Figure A6. b) Ti-SBA-15 EDX measurement (box 002)

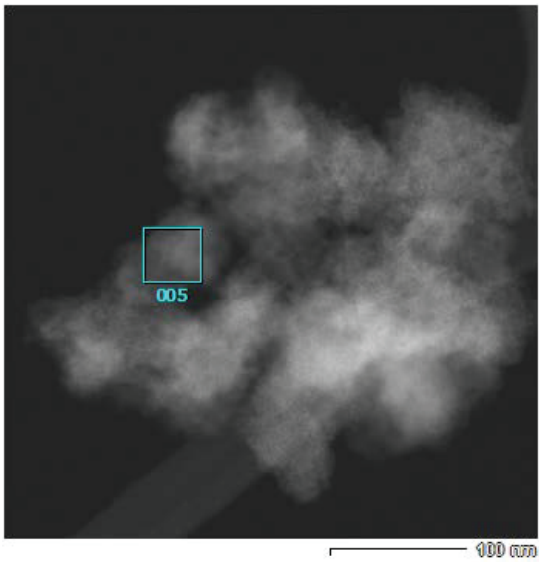

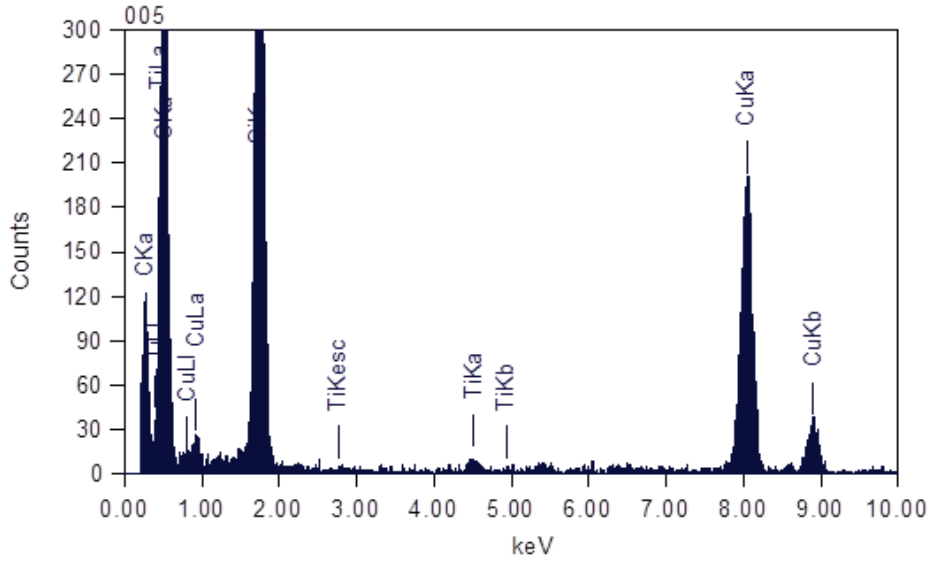

Thin Film Standardless Standardless Quantitative Analysis

Fitting Coefficient : 0.1193

Element	(keV)	Mass%	Counts	Sigma	Atom%	Compound	Mass%	Cation	K
C K*	(Excluded)								
O K*	(Excluded)								
Si K	(Ref.)	1.739	98.67	6250.02	48138160.00	99.22			1.0000
Ti K*		4.508	1.33	63.76	6420051.00	0.78			1.3213
Cu K*	(Excluded)								
Total		100.00			100.00				

Figure A7. a) Ti-MCM-41 EDX measurement (box 005)

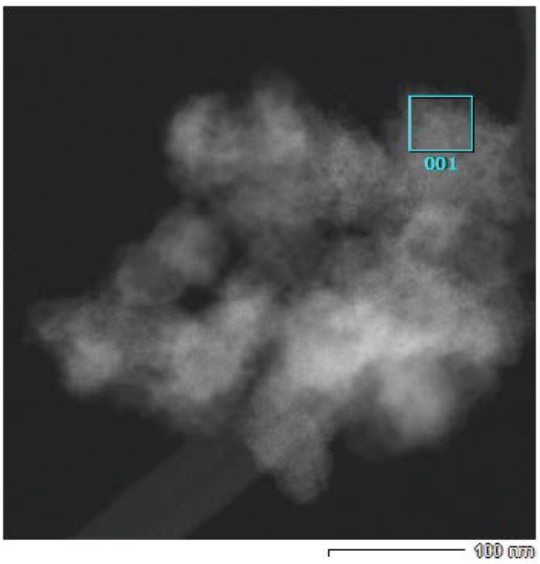

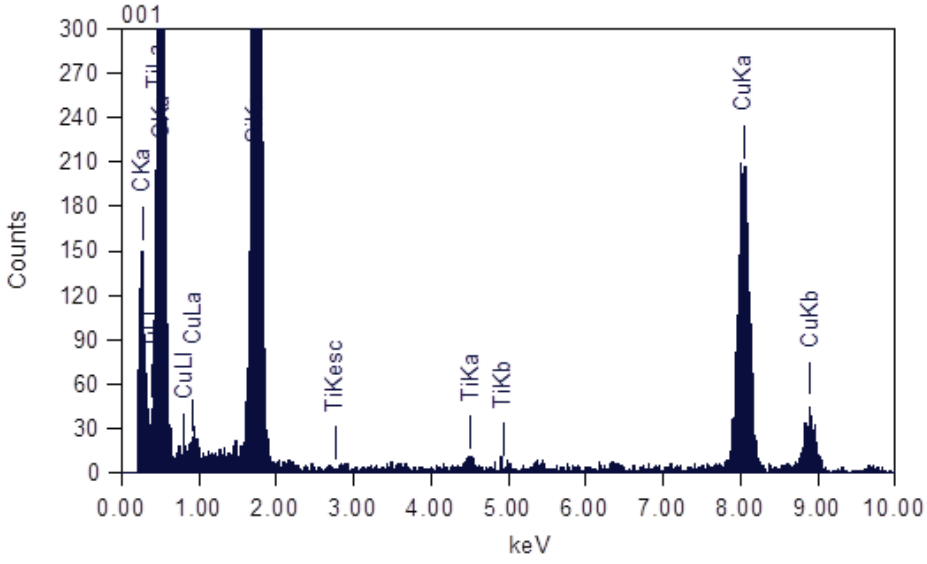

Thin Film Standardless Standardless Quantitative Analysis

Fitting Coefficient : 0.1520

Element	(keV)	Mass%	Counts	Sigma	Atom%	Compound	Mass%	Cation	K
C K*	(Excluded)								
O K*	(Excluded)								
Si K	(Ref.)	1.739	98.41	7291.99	1.60	99.06			1.0000
Ti K*		4.508	1.59	89.13	0.19	0.94			1.3213
Cu K*	(Excluded)								
Total		100.00			100.00				

Figure A7. b) Ti-MCM-41 EDX measurement (box 001)

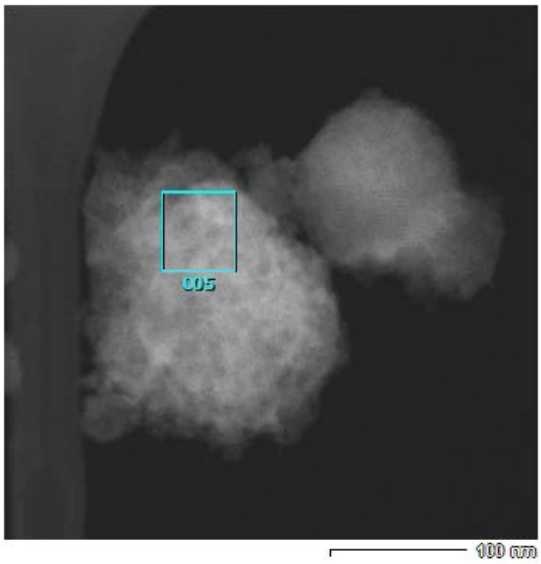

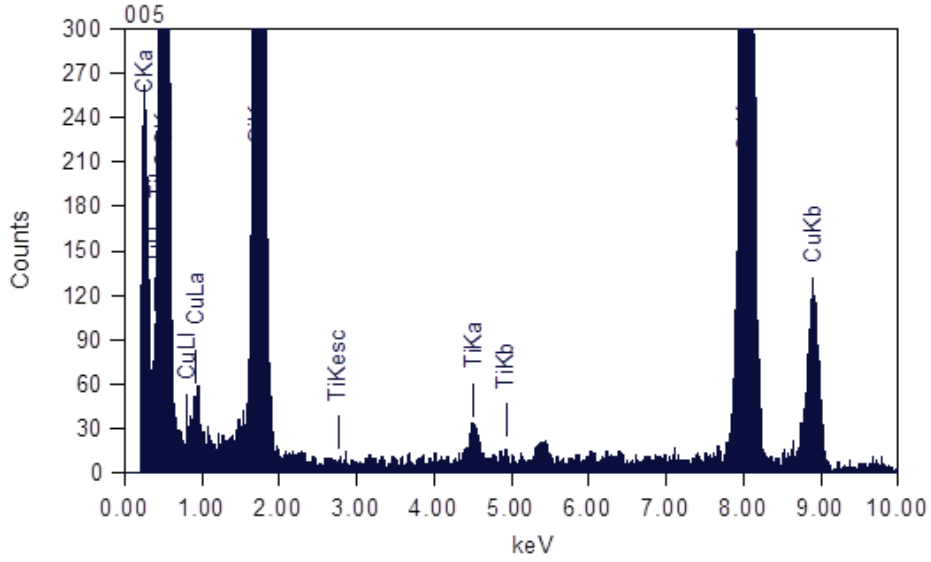

Thin Film Standardless Standardless Quantitative Analysis

Fitting Coefficient : 0.0996

Element	(keV)	Mass%	Counts	Sigma	Atom%	Compound	Mass%	Cation	K
C K*	(Excluded)								
O K*	(Excluded)								
Si K	(Ref.)	1.739	97.96	16395.28	0.84	98.79			1.0000
Ti K		4.508	2.04	258.02	0.11	1.21			1.3213
Cr K*	(Excluded)								
Cu K*	(Excluded)								
Total		100.00			100.00				

Figure A8. a) Ti-MCM-41-reg EDX measurement (box 005)

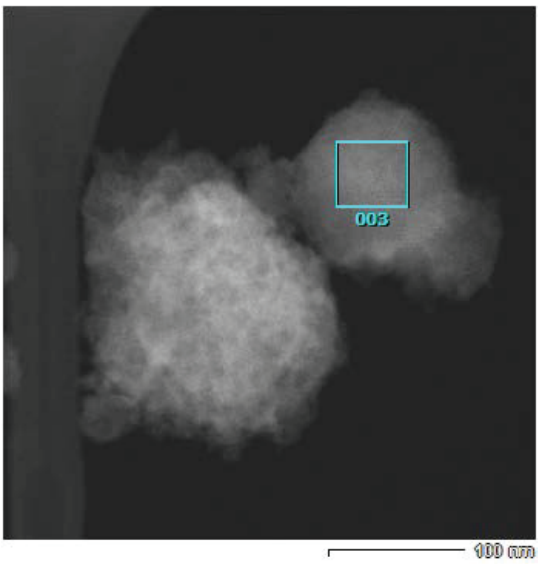

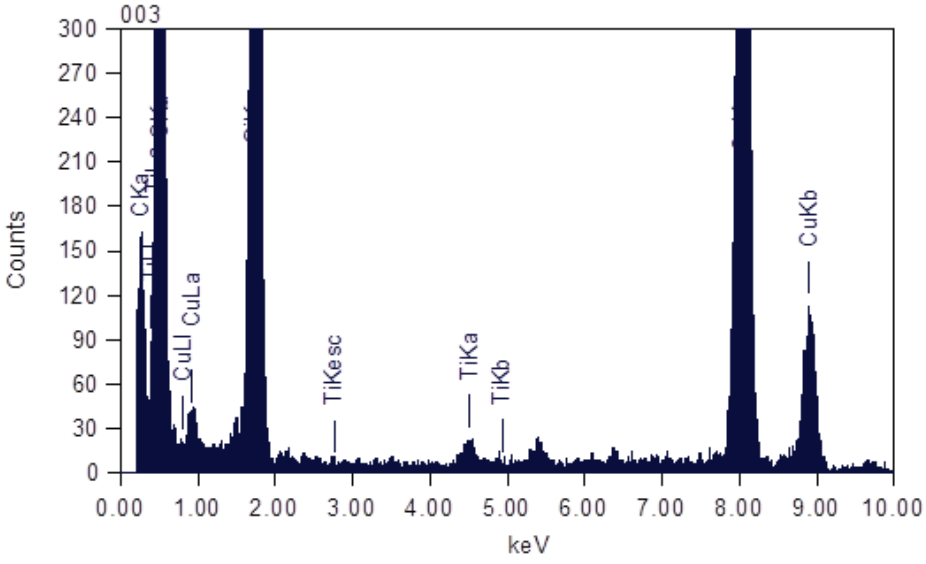

Thin Film Standardless Standardless Quantitative Analysis

Fitting Coefficient : 0.0874

Element	(keV)	Mass%	Counts	Sigma	Atom%	Compound	Mass%	Cation	K
C K*	(Excluded)								
O K*	(Excluded)								
Si K	(Ref.)	1.739	98.28	12580.32	1.20	98.98			1.0000
Ti K		4.508	1.72	166.91	0.16	1.02			1.3213
Cr K*	(Excluded)								
Cu K*	(Excluded)								
Total		100.00			100.00				

Figure A8. b) Ti-MCM-41-reg EDX measurement (box 001)

Appendices B:

List of Publications

S. Kale, S. B. Umbarkar, M. K. Dongare, R. Eckelt, U. Armbruster, A. Martin, "Selective formation of triacetin by glycerol acetylation using acidic ion-exchange resins as catalyst and toluene as an entrainer", Applied Catalysis A 490 (2015) 10 – 16.

S. S. Kale, U. Armbruster, R. Eckelt, U. Bentrup, S. B. Umbarkar, M. K. Dongare, A. Martin "Understanding the role of Keggin type heteropolyacid catalysts for glycerol acetylation using toluene as an entrainer", Applied Catalysis A (Under revision).

Conference Contribution

XII European Congress on Catalysis "Catalysis: Balancing the use of fossil and renewable resources", Aug 30 – Sept 4, 2015, Kazan, Russia

Sumeet Kale, Udo Armbruster, Shubhangi Umbarkar, Mohan Dongare, Reinhard Eckelt, Andreas Martin "Gas phase glycerol acetylation to fuel additive over solid acid catalysts" (Poster and Short Presentation)

10th Green Chemistry Conference - An international event, Barcelona, Spain, November 05-07, 2013,

Sumeet Kale, Udo Armbruster, Shubhangi Umbarkar, Mohan Dongare, Andreas Martin, "Esterification of glycerol with acetic acid for improved production of triacetin using toluene as an entrainer" (Oral Presentation)

LIKAT/CaSuS Workshop, Rostock, Germany, Sept. 16-18, 2013

Sumeet Kale, Udo Armbruster, Shubhangi Umbarkar, Mohan Dongare, Andreas Martin, "Esterification of glycerol with acetic acid for improved production of triacetin using toluene as an entrainer" (Poster presentation)

2nd Indo-German Symposium – Green Chemistry and Catalysis for Sustainable Development, Oct. 29-31, 2012, Mumbai, India.

Sumeet Kale, Udo Armbruster, Shubhangi Umbarkar, Mohan Dongare, Andreas Martin, "Acetylation of glycerol to synthesize bioadditives over solid acid catalysts" (Poster presentation)

15. Norddeutsches Doktoranden-Kolloquium der anorganischen Chemie, Sept. 24-25, 2012, Kiel, Germany

Sumeet Kale, Udo Armbruster, Shubhangi Umbarkar, Mohan Dongare, Andreas Martin, "Glycerol acetylation over solid acid catalyst" (Poster presentation).

Appendix C: Curriculum Vitae

Personal information

Full name	Sumeet S. Kale
Date of birth	19.07.1988
Gender	Male
Nationality	Indian
Email	sumeet.kale@catalysis.de, kalesumeet2006@gmail.com

Academic Education

03.2012 - present	Leibniz Institute for Catalysis at University of Rostock, Germany PhD student at the Department of Heterogeneous Catalytic Processes Supervisors: PD Dr. Andreas Martin, Dr. Ing. Udo Armbruster
06.2009 - 06.2011	University of Pune, Pune, India Master of Science (Organic Chemistry)
06.2006 - 06.2009	University of Pune, Pune, India Bachelor of Science (Chemistry)

Profession

07.2011 - 02.2012:	Project Assistant, National Chemical Laboratory (NCL), Pune Supervisors: Dr. Shubhangi B. Umbarkar